A Coupled Local Mode Investigation of Elastic Anisotropy in Shallow Water Environments: a study of anisotropy beyond VTI

Darin J. Soukup

Department of Earth and Space Sciences

University of Washington

63 Johnson Hall Box 351310

Seattle, WA 98195

Robert I. Odom *

Applied Physics Laboratory

University of Washington

1013 NE 40th Street

Seattle, WA 98105

Jeffrey Park

Department of Geology and Geophysics

POB 208109

Yale University

New Haven, CT 06520-8109

November 28, 2005

To be submitted to Journal of the Acoustical Society of America

*also at Department of Earth and Space Sciences, University of Washington, 63 Johnson Hall Box 351310, Seattle, WA 98195

REPORT DOCUMENTATION PAGE

Form Approved
OMB No. 0704-0188

1. REPORT DATE *(DD-MM-YYYY)*	2. REPORT TYPE	3. DATES COVERED *(From - To)*
28-11-2005	FINAL REPORT	01 JAN 2003 TO 31 MAR 2005

4. TITLE AND SUBTITLE

A Coupled Local Mode Investigation of Elastic Anisotropy in Shallow Water Environments: a study of anisotropy beyond VTI

5a. CONTRACT NUMBER

5b. GRANT NUMBER

N00014-03-1-0378

5c. PROGRAM ELEMENT NUMBER

6. AUTHOR(S)

Darin J. Soukup
Robert I. Odom

5d. PROJECT NUMBER

5e. TASK NUMBER

5f. WORK UNIT NUMBER

7. PERFORMING ORGANIZATION NAME(S) AND ADDRESS(ES)

Applied Physics Laboratory, University of Washington
1013 NE 40th Street
Seattle, WA 98105-6698

8. PERFORMING ORGANIZATION REPORT NUMBER

9. SPONSORING/MONITORING AGENCY NAME(S) AND ADDRESS(ES)

Office of Naval Research (ONR 321OA)
875 North Randolph Street, Suite 1425
Arlington, VA 22203-1995
Attn: Dr. Ellen Livingston

10. SPONSOR/MONITOR'S ACRONYM(S)

ONR 321OA

11. SPONSOR/MONITOR'S REPORT NUMBER(S)

12. DISTRIBUTION/AVAILABILITY STATEMENT

Approved for public release

13. SUPPLEMENTARY NOTES

None

14. ABSTRACT

This paper presents theoretical and numerical results for the coupled mode, shallow water seismo-acoustic wavefield in generally anisotropic, range-dependent media. General anisotropy affects the form of the elastic stiffness tensor, which directly affects the polarization of the local modes, the frequency and angular dispersion curves, and the coupling of the local modes in range-dependent media. The effects of anisotropy (1-D models) and the combination of anisotropy and lateral heterogeneity (2-D models) are examined. Perhaps surprisingly, horizontally polarized particle motion cannot be ignored when sediment anisotropy is present. Depending on the propagation direction relative to the symmetry axis orientation, even weak anisotropy may have a significant impact on seismo-acoustic wave propagation, exhibiting particle motion polarization in all three coordinate directions. Transversely isotropic (TI) media with a non-vertical symmetry axis allow both quasi-P-SV and quasi-SH modes to carry energy. The discrete modes for an anisotropic medium are best described as generalized P-SV-SH modes with polarizations in all three Cartesian coordinate directions. The superposition of these generalized P-SV-SH modes describe the seismo-acoustic signal and illustrate the importance of using an elastic treatment of the seafloor bottom/subbottom for low frequency shallow water seismo-acoustic wave propagation.

15. SUBJECT TERMS

ocean acoustics, modes, anisotropy, shallow water, coupled modes

16. SECURITY CLASSIFICATION OF:			17. LIMITATION OF ABSTRACT	18. NUMBER OF PAGES	19a. NAME OF RESPONSIBLE PERSON
a. REPORT	b. ABSTRACT	c. THIS PAGE			Robert I. Odom
U	U	U	UU		19b. TELEPHONE NUMBER *(Include area code)* 206 685-3788

Abstract

This paper presents theoretical and numerical results for the coupled local mode formalism of the seismo-acoustic wavefield in generally anisotropic range-dependent media. General anisotropy affects the form of the elastic stiffness tensor, which directly affects the polarization of the local modes, the frequency and angular dispersion curves, the coupling of the local modes in range-dependent media, and also introduces the effects of nearly degenerate modes. The effects of anisotropy and the combination of anisotropy and lateral heterogeneity are examined for 1-D and 2-D models, respectively. Horizontally polarized shear motion plays an important role in seismo-acoustic wave propagation in shallow water environments. The transverse particle motion cannot be ignored when anisotropy is present for low frequency modes having significant bottom interaction. The seismo-acoustic wavefield has polarizations in all three coordinate directions even in the absence of any scattering or heterogeneity. The magnitude of anisotropy as well as the direction of the symmetry axis can be of equal importance. Even weak anisotropy may have a significant impact on seismo-acoustic wave propagation, depending on the propagation direction in relation to the symmetry axis orientation of the anisotropy. Unlike isotropic and VTI media where acoustic signals are composed of P-SV modes alone (in the absence of any scattering), tilted TI media allow both quasi-P-SV and quasi-SH modes to carry seismo-acoustic energy. The discrete modes for an anisotropic medium are best described as generalized P-SV-SH modes with polarizations in all three Cartesian coordinate directions. The superposition of these generalized P-SV-SH modes describe the seismo-acoustic signal and reveal the importance of using an elastic treatment of the seafloor

bottom/subbottom for low frequency shallow water seismo-acoustic wave propagation.

1 Introduction

This work presents theoretical and numerical results for modeling seismo-acoustic wave propagation in 1-D homogeneous anisotropic and 2-D anisotropic range-dependent shallow water environments. There is an apparent trade-off between anisotropy and lateral heterogeneity, and it can be difficult to separate the two effects in a propagating signal. Mochizuki (1997) obtained analytical expressions concerning the trade-offs between anisotropy and heterogeneity by extending the Central Slice Theorem to the anisotropic case. The motivation of this work is to begin to unravel these two effects numerically and consider them separately within a coupled local mode framework.

Shallow water environments may be highly variable, with both lateral heterogeneity and anisotropy being almost ubiquitous in the seafloor bottom/subbottom regions. Some common causes of lateral heterogeneity in shallow water environments are marine sediment composition, non-planar boundaries, rough surfaces, strong density or velocity contrasts, and variation in water column depth and/or sediment cover thickness. Shallow water sediments exhibit considerable lateral heterogeneity over short ranges (Stoll *et. al.*, 1994). In addition to lateral heterogeneity, anisotropy is often an intrinsic property of marine sediments. Marine sediments exhibit anisotropy and high velocity gradients in shear velocity (Ewing *et. al.*, 1992). Anisotropy in material properties can lead to observed anisotropic effects in fluid flow(permeability), heat or electrical conductivity (resistivity), stress and strains, or elastic properties for example (Friedman and Jones, 2001). When considering acoustic propagation, the elastic properties of anisotropic marine sediments are of primary concern. Possible sources of elastic anisotropy in marine sediments are reported to be the alignment of

cracks and/or pores in the sediment structure, preferred orientation of mineral grains, and lamination as a result of compositional layering. (Carlson *et. al.*, 1982).

[Figure 1 about here.]

[Figure 2 about here.]

Marine sediments often have transversely isotropic elastic symmetry (TI) with the fast velocity directions in the plane parallel to the bedding plane and the slow velocity direction along the normal of the bedding plane as shown in figure ??. The slow velocity direction is parallel to an infinite fold symmetry axis $\hat{s}$, also shown in figure ??. This type of elastic anisotropy found in marine sediments is likely predominantly due to compositional layering (Carlson *et. al.*, 1982).

There exists a wide body of literature on the investigations of wave propagation in TI environments, and much recent work has been done investigating more generalized anisotropy. The majority of investigations have concentrated on TI elastically symmetric media with a vertical symmetry axis(VTI), where $\hat{s} = \hat{z}$ as in figure ??, or with a horizontal symmetry axis(HTI), where $\hat{s} = \cos\varphi\hat{x} + \sin\varphi\hat{y}$. Figure ?? and figure 2 show the fixed coordinate frame of reference. An example of a VTI medium is the horizontally layering of fine isotropic sediments, and an HTI medium can be produced by the introduction of vertical parallel cracks in isotropic sediments. Although VTI and HTI are completely adequate for many applications, there are many instances where a more general orientation of the symmetry axis $\hat{s}$ is needed, and should be considered to complement the existing body of VTI and HTI work. Simply having VTI or HTI layered sediments with non-horizontal bedding planes

provides an example of a TI medium with a non-vertical and non-horizontal tilted symmetry axis. Anisotropic variations other than azimuthal may also be considered, where the anisotropic symmetry axis $\hat{s}$ is allowed to tilt in both azimuth and elevation. Martin *et. al.* (1997), Thomson *et. al.* (1997), and Zhu and Dorman (2000) provide complementary results to the work presented in this paper. In addition, Martin *et. al.* (1997) provides an excellent summary of work relevant to the topic of anisotropy and coupled modes.

The work presented in this dissertation employs a modal representation of the seismo-acoustic signal. An acoustic signal may be composed of acoustic modes, hybrid acoustic-crustal modes also known as seismo-acoustic modes, and crustal modes. An acoustic mode carries its energy in the water column and has very little interaction with the bottom/subbottom. A crustal mode propagates its energy in the sediment and basement layers. A hybrid acoustic-crustal mode has significant energy in both the water column and the underlying sediment and basement layers. Neglecting any seafloor bottom/subbottom elastic properties may be a reasonable approach for problems involving high frequencies where the depth of the water column is much greater than the wavelength of the acoustic signal of interest. For these problems the acoustic signal may be entirely contained within the water column and may not interact with the seafloor. However, for low frequencies and shallow water environments the bottom interaction of the acoustic signal becomes significant, and affects the propagation of the acoustic signal. An acoustic wavefield will interact with the bottom/subbottom at some portion if not the entire length of the propagation path. Therefore, the characteristics of the acoustic signal are influenced by interactions with the seafloor and seabed. Energy from the acoustic wavefield can be scattered, radiated into

the bottom, or absorbed by attenuation, resulting in a signal that is more accurately described as seismo-acoustic. The seismo-acoustic signal then is composed of both acoustic modes and hybrid acoustic-crustal modes. In this work the focus remains predominantly on acoustic and seismo-acoustic modes (hybrid acoustic-crustal modes) with energy within the fluid layer. Odom *et. al.* (1997) investigate the effects of VTI elastic symmetry on local modes and on the coupling of local modes, focusing on sediment modes. Their model has been modified to facilitate the study of acoustic and seismo-acoustic modes in a generally anisotropic medium. The work of Odom *et. al.* (1997) is extended by including a more generalized description of anisotropy found in marine sediments. A modal formalism and coupled local mode formalism are used to examine the seismo-acoustic wave propagation in 1-D and 2-D anisotropic models respectively. The coupled local mode formalism is not necessary for wave propagation in a 1-D homogeneous plane layered anisotropic structure. However, the coupled local mode formalism is an appropriate method for the 2-D range-dependent anisotropic wave propagation problem. Therefore the method of modes is also applied when the wave propagation problem reduces to a 1-D homogeneous plane layered anisotropic structure. The effect of symmetry axis rotations on the propagating modes are investigated.

The body of the paper centers around two distinct models. The first model describes general anisotropy for a 1-D homogeneous plane layered structure. The effects of anisotropy, entirely independent of any range-dependence are considered. The second model focuses on the effects of anisotropy in combination with a 2-D range-dependent medium. Anisotropic effects on mode coupling, induced by lateral heterogeneity are considered.

Section 2 discusses anisotropy and wave propagation for a 1-D homoge-

neous anisotropic plane-layered structure. A brief description of the modal formalism of Maupin(1988) as applied to the 1-D anisotropic structure is contained in section 3.1. An introduction to TI elastic symmetry and nomenclature is found in section 2.1 and section 2.2 demonstrates the usefulness of the Bond transformation in obtaining a generalized elastic stiffness tensor. Numerical calculations are discussed in section 3 for the 1-D homogeneous anisotropic plane layered structure. The anisotropic model/profile is described in section 3.2 and slowness curves are considered in section 3.3. Section 3.4 covers angular and frequency dispersion curves while section 3.5 provides the resulting generalized eigenfunctions. The combined effects of anisotropy and lateral heterogeneity are presented in section 4, beginning in section 4.1 with a brief discussion on the coupled local mode formalism of Maupin (1988) for a 2-D anisotropic range-dependent structure. The description of the 2-D anisotropic range-dependent structure and its velocity/density profile is found in section 4.2 and a discussion on coupled local modes, including local mode coupling matrices, eigenfunctions, and dispersion curves is presented in section 4.3. The summary, conclusions and discussion of results are contained in section 5.

A variety of useful relations, such as theory, and concepts concerning anisotropy have been collected and presented in the appendices. Appendix A expands on the elastic stiffness tensor and matrix notation, while Appendix B provides further insight on the differential operator $\mathbf{A}$ from the equations of motion. Appendix C defines the coupling matrix $\mathbf{B}_{qr}$ and Appendix D defines some possible forms of anisotropy parameterization. Appendix E elaborates on the specifics of the Bond transform for a TI medium. The notation used along with definitions of variables or parameters can be found in

the List of Symbols. Symmetry planes and wave polarizations are considered in Appendix G for TI elastic symmetry.

2 Anisotropy Background

A study of a 1-D homogeneous plane-layered structure, with the absence of any range-dependence is presented. By assuming anisotropic sediments, the elastic properties of the sediment layers are allowed to vary with propagation direction. Specifically, energy propagating along different directions within the sediment layers will result in the wave propagating at different velocities. These anisotropic sediments are assumed to have TI elastic symmetry with an arbitrarily oriented symmetry axis ($\hat{s}$). The effect of anisotropy on propagating modes, including changes in phase and group velocities, and eigenfunction polarizations are investigated.

2.1 Transversely Isotropic Elastic Symmetry

Nomenclature for anisotropy has not been standardized in the literature. This poses a problem that Crampin (1989) and Winterstein(1990) recognized over a decade ago. Because transverse isotropy is used with multiple meanings in the current literature, any possible confusion is attempted to be eliminated by explicitly stating the nomenclature used in this work.

For the purposes of this dissertation, a general anisotropic medium is defined by an elastic stiffness tensor belonging to the transversely isotropic elastic symmetry system. The nomenclature of Winterstein (1990) is used, where TI refers to a medium with transversely isotropic elastic symmetry having an infinite-fold symmetry axis. A medium retains its TI elastic symmetry

regardless of the orientation of the symmetry axis or any physical rotation of the media. A TI medium with a vertical, horizontal, or arbitrarily tilted symmetry axis is labeled VTI, HTI, and TTI respectively.

The term "transverse" in transverse isotropy refers to any direction which is perpendicular to the symmetry axis of the medium and not to a fixed coordinate direction. As noted by Winterstein (1990), TI has occasionally been used to refer to a VTI medium. In addition, hexagonal symmetry has often been used interchangeably with the TI symmetry in the wave propagation communities. The hexagonal symmetry class is a subset of the TI symmetry system. Both TI and hexagonally symmetric media have the same strain-energy functions, and the elastic equation of motion will be exactly the same for both media. Elastically, a hexagonally symmetric and TI symmetric medium look exactly the same, but compositionally or structurally they are quite different. It is likely that a real earth structure would belong to the transverse isotropy symmetry class, and according to Winterstein (1990), sediments are unlikely to be structurally hexagonally symmetric. Elastically, TI and hexagonal symmetries have the exact same degree of symmetry, since both require five elastic constants. However, structurally TI has a higher degree of symmetry and is closer in symmetry to isotropy than the hexagonal symmetry. This is a result of TI having an infinite-fold symmetry axis, the hexagonal symmetry only has a six-fold symmetry.

TI is an elastic symmetry system distinguished by a unique form of the elastic stiffness tensor. The elastic stiffness tensor has five independent constants that define the individual coefficients. Each coefficient is a linear combination of these five independent constants, and these five independent constants can be parameterized into several forms. They may be expressed

as velocities, elastic moduli, or even a combination of ratios of velocities and elastic moduli (see Appendix D). In comparison, an isotropic material is parameterized by only two elastic moduli. Although the elastic symmetry has been limited to transverse isotropy for this work, the theory and some portions of the code can incorporate more general anisotropy (up to 21 independent elastic moduli). The elastic stiffness matrix ${}^{a}\mathbf{C}$ for a VTI medium is:

$$ {}^{a}\mathbf{C} = \begin{bmatrix} A & H & F & 0 & 0 & 0 \\ H & A & F & 0 & 0 & 0 \\ F & F & C & 0 & 0 & 0 \\ 0 & 0 & 0 & L & 0 & 0 \\ 0 & 0 & 0 & 0 & L & 0 \\ 0 & 0 & 0 & 0 & 0 & N \end{bmatrix} \qquad \text{where } H = A - 2N \tag{1} $$

The A, C, F, L, N and $H = A - 2N$ represent the VTI elastic moduli in Love (1944) notation. The 6×6 abbreviated subscript matrix ${}^{a}\mathbf{C}$ contains all of the information of the elastic stiffness tensor, C_{iklj} (see Appendix A).

The form or appearance of the elastic stiffness matrix is similar to an orthorhombic symmetric medium. They share the same filled-in elements and the same zero elements. The TI medium has a higher degree of symmetry than the orthorhombic medium, which has nine independent constants. The VTI medium in equation 1 may be thought of having the appearance of a quasi-orthorhombic medium. Such similarities with other symmetry systems are helpful when the elastic stiffness matrix ${}^{a}C_{IJ}$ is rotated to more general orientations.

The elastic moduli A, C, F, L, N from the above VTI medium in equation (1) can be related to velocities for compressional and shear plane-waves in the medium. The following describe the wave velocities for horizontally

transmitted plane waves within the xy-plane.

$$\alpha_H \equiv \sqrt{\frac{A}{\rho}} \quad \text{compressional waves} \tag{2}$$

$$\beta_H \equiv \sqrt{\frac{N}{\rho}} \quad \text{horizontally polarized shear waves} \tag{3}$$

$$\beta_V \equiv \sqrt{\frac{L}{\rho}} \quad \text{vertically polarized shear waves} \tag{4}$$

A vertically transmitted plane wave parallel to the z-axis have the velocities

$$\alpha_V \equiv \sqrt{\frac{C}{\rho}} \quad \text{compressional waves} \tag{5}$$

$$\beta_V \equiv \sqrt{\frac{L}{\rho}} \quad \text{shear waves} \tag{6}$$

The elastic constant F is not typically defined in terms of a plane wave velocity. Muyzert and Snieder (2000) relate the elastic parameter F to a velocity of a wave propagating in a vertical plane between a source and receiver, and assign a velocity γ to the elastic parameter. Muyzert and Snieder (2000) indicate that Anderson (1961) relates this velocity γ to a wave with an incidence angle of 45° with the vertical axis.

$$\gamma \equiv \sqrt{\frac{F}{\rho}} \quad \text{velocity within the vertical xz-plane} \tag{7}$$

where $\gamma^2 = \alpha^2 - 2\beta^2$ in an isotropic medium.

The α and β represent the compressional and shear velocities, respectively, and the subscripts H and V denote the horizontal and vertical displacement directions. When $A = C = \lambda + 2\mu$, $L = N = \mu$, and $F = \lambda$, the medium is isotropic and rotationally independent.

2.2 Bond Transformation

Using the Bond transform for tilting a structure's symmetry axis has been suggested by Crampin (1981) and Winterstein (1990) and actually implemented for acoustic body waves by Auld (1990) and recently by Zhu and Dorman (2000) and Okaya and McEvilly (2003). The Bond transformation is applied in the study of global modes and coupled local modes(section 4) to obtain a general rotation of the elastic stiffness matrix with TI symmetry.

A formalism similar to Crampin (1981) is used where the propagation direction is assumed to always coincide along a fixed coordinate direction, the x-axis. The elastic stiffness tensor is rotated in order to consider anisotropy with various symmetry axis orientations. This is equivalent to keeping the elastic stiffness tensor fixed and varying the direction of propagation. The first method is preferred because the theory does not need to be modified for each directional change, only the elements of the elastic stiffness tensor need to be changed. A physical reasonableness to the modeling should be retained. Randomly perturbing various elements of C_{IJ} can lead to a non-physical elastic stiffness matrix. By starting with a real physical model, the reasonableness of the model is maintained regardless of any rotation of the medium. Odom *et. al.* (1996) provides a good summary of the conditions which constrain the elastic moduli of a TI elastically symmetric medium. Another advantage of the Bond Transformation is working with a 6×6 matrix with only 36 individual elements rather than a fourth order tensor with 81 individual elements. Complex tensor transformations are replaced with simple matrix multiplication to transform the elastic stiffness matrix to any arbitrary orientation.

Rotating the elastic stiffness matrix ${}^{a}C_{IJ}$ essentially changes the form of

the elastic stiffness tensor, how the matrix or tensor is populated changes. This directly affects the solution of the equation of motion as the elements of ${}^{a}C_{IJ}$ change. The elastic stiffness matrix is a function of the spherical coordinate angles θ and φ when ${}^{a}C_{IJ} = {}^{a}C_{IJ}(\theta, \varphi)$

For an isotropic medium, the direction of propagation does not matter. All planes are symmetry planes and all directions are symmetry axis directions. The elements of the elastic stiffness tensor do not change with any rotation of the medium. For an anisotropic medium, the velocity of plane waves vary with propagation direction through the medium. The elements of the elastic stiffness tensor change with any rotation of the medium. For a TI elastically medium, five independent elastic moduli along with two polar coordinates relating the symmetry axis and the propagation direction are needed to adequately describe the velocity of plane wave through the medium. The elements of C_{iklj} are linear combinations of the five independent constants, being functions of the polar angles θ and ϕ.

While the elastic stiffness matrix may be rotated, the physical boundaries, discontinuities and the boundary conditions of the 1-D structure remain fixed. The procedure for implementing the Bond transformation is to rotate the elastic stiffness matrix with respect to a fixed set of coordinate axes. In general three angles ψ, θ, φ are needed to transform the elastic stiffness matrix ${}^{a}C_{ij}$ to any arbitrary orientation. The rotations are taken first about the z-axis, next about the y-axis, and finally about the z-axis again. ψ is an angle in the xy-plane and corresponds to the first rotation about the z-axis. The angle θ is defined in the xz-plane and corresponds to the second rotation about the y-axis. The final angle φ is also defined in the xy-plane which corresponds to the third rotation about the vertical axis. When the starting medium is VTI,

only rotations through the angles θ and φ need to be considered. In figure ?? the Bond transformation is visually demonstrated. The elastic stiffness matrix representing the elastic constants within the layer can be rotated to any arbitrary orientation, as shown by the blocks on the right of the figure.

The spherical coordinates of the symmetry axis directions, $\hat{s} = \hat{s}(\theta, \varphi)$can be projected onto a unit sphere. When tilting the symmetry axis, the symmetry axis traces lines of constant elevation on the unit sphere as φ is varied and remains θ fixed. Similarly, keeping φ fixed at some value and varying the value of θ traces lines of constant azimuth. The lines of constant elevation represent changes in azimuthal anisotropy and the lines of constant azimuth representation changes in elevational anisotropy. These are shown as red arcs in figure 4.

Applying the Bond Transformation to the unrotated elastic moduli within ${}^{a}\mathbf{C}''$:

$$ {}^{a}\mathbf{C}' = [\mathbf{M}^{y}][{}^{a}\mathbf{C}''][\mathbf{M}^{y}]^{T} \qquad \text{Bond transformation about y-axis} \qquad (8) $$

$$ {}^{a}\mathbf{C} = [\mathbf{M}^{z}][{}^{a}\mathbf{C}'][\mathbf{M}^{z}]^{T} \qquad \text{Bond transformation about z-axis} \qquad (9) $$

$\mathbf{M}^{y}$ and $\mathbf{M}^{z}$ are transformation matrices (e.g. Auld, 1990) about the y-axis and z-axis respectively, and are defined for an elastic stiffness tensor with TI symmetry in the Appendix E.

Substituting equation (8) into equation (9) and using the matrix multiplication property $[\mathbf{M}^{z}\mathbf{M}^{y}]^{T} = [\mathbf{M}^{y}]^{T}[\mathbf{M}^{z}]^{T}$ to obtain:

$$ {}^{a}\mathbf{C} = [\mathbf{R}][{}^{a}\mathbf{C}''][\mathbf{R}]^{T} \qquad \text{where } \mathbf{R} = \mathbf{M}^{z}\mathbf{M}^{y} \qquad (10) $$

The individual elements of the elastic-stiffness tensor can be found by the

following relation for a medium with TI elastic symmetry.

$$\begin{aligned} {}^{a}C_{IJ} &= A(R_{i1}R_{j1} + R_{i2}R_{j2}) + H(R_{i1}R_{j2} + R_{i2}R_{j1}) \\ &+ F(R_{i1}R_{j3} + R_{i2}R_{j3} + R_{i3}R_{j1} + R_{i3}R_{j2}) + CR_{i3}R_{j3} \\ &+ L(R_{i4}R_{j4} + R_{i5}R_{j5}) + NR_{i6}R_{j6} \end{aligned} \tag{11}$$

The elements of ${}^{a}C_{IJ}$ or C_{iklj} are dependent upon the orientation of the symmetry axis through the elements of $\mathbf{R}$. A rotation of the symmetry axis changes the value of any given element in C_{IJ}, where the specific elements of C_{IJ} remain linear combinations of A, C, F, L, N as demonstrated by equation(11). The tractable, analytic form for the rotated elastic stiffness matrix found in equation (11) is due to the large number of elements with zero-values for a VTI medium.

The sensitivity of the ${}^{a}C_{IJ}$ elements rotation can be determined by taking the derivative of equation (11) with respect to θ and φ. The derivative with respect to a generic angle Δ is:

$$\frac{\partial({}^{a}\mathbf{C})}{\partial\Delta} = \frac{\partial({}^{a}C_{IJ})}{\partial\Delta} \qquad \text{where } \Delta = \theta \text{ or } \varphi \tag{12}$$

The angular sensitivity of a TI symmetric medium with an arbitrarily

tilted symmetry axis may be express as:

$$\begin{aligned}
\frac{\partial({}^{a}C_{IJ})}{\partial\Delta} &= A\left(\frac{\partial R_{i1}}{\partial\Delta}R_{j1}+R_{i1}\frac{\partial R_{j1}}{\partial\Delta}+\frac{\partial R_{i2}}{\partial\Delta}R_{j2}+R_{i2}\frac{\partial R_{j2}}{\partial\Delta}\right)\\
&+ H\left(\frac{\partial R_{i1}}{\partial\Delta}R_{j2}+R_{i1}\frac{\partial R_{j2}}{\partial\Delta}+\frac{\partial R_{i2}}{\partial\Delta}R_{j1}+R_{i2}\frac{\partial R_{j1}}{\partial\Delta}\right)\\
&+ F\left(\frac{\partial R_{i1}}{\partial\Delta}R_{j3}+R_{i1}\frac{\partial R_{j3}}{\partial\Delta}+\frac{\partial R_{i2}}{\partial\Delta}R_{j3}+R_{i2}\frac{\partial R_{j3}}{\partial\Delta}\right.\\
&\quad \left.\frac{\partial R_{i3}}{\partial\Delta}R_{j1}+R_{i3}\frac{\partial R_{j1}}{\partial\Delta}+\frac{\partial R_{i3}}{\partial\Delta}R_{j2}+R_{i3}\frac{\partial R_{j2}}{\partial\Delta}\right)\\
&+ C\left(\frac{\partial R_{i3}}{\partial\Delta}R_{j3}+R_{i3}\frac{\partial R_{j3}}{\partial\Delta}\right)\\
&+ L\left(\frac{\partial R_{i4}}{\partial\Delta}R_{j4}+R_{i4}\frac{\partial R_{j4}}{\partial\Delta}+\frac{\partial R_{i5}}{\partial\Delta}R_{j5})+R_{i5}\frac{\partial R_{j5}}{\partial\Delta}\right)\\
&+ N\left(\frac{\partial R_{i6}}{\partial\Delta}R_{j6}+R_{j6}\frac{\partial R_{i6}}{\partial\Delta}\right) \qquad (13)
\end{aligned}$$

[Figure 3 about here.]

Each element of the ${}^{a}C_{IJ}$ matrix may be evaluated through equation (11) and equation (13). Figure 3 plots the a_{11}^{C} element and its angular sensitivity as function of θ and φ.

Auld (1990) provides a more complete treatment of the Bond transformation and additional details are included in Appendix D. Appendeix G contains a useful and instructional tutorial on symmetry planes and wave polarizations for a TI medium. The appearance of a lower degree of symmetry when the TI symmetry axis rotated has been determined independently, but similarly to Okaya and McEvilly (2003). Whereas they determined that rotations about the y-axis result in a monoclinic form of the elastic stiffness matrix, the rotations in Appendix G show that rotations where the symmetry axis remains in any of the coordinate planes results in a monoclinic form of the elastic stiffness matrix.

3 1-D Plane-Layered Anisotropic Structure Calculations

A phase velocity ordering is used for all of the modes when considering the eigenfunctions, dispersion curves, and coupling matrices. The modes are ordered from smallest phase velocity to the largest phase velocity, where the lowest order mode has the lowest phase velocity and the highest ordered mode has the highest phase velocity. Note that the phase velocity ordering scheme is independent of polarizations of the particular modes, therefore the phase velocity ordering is still used when the P-SV and SH modes propagate independently. This is slightly different than Odom *et. al.* (1996), and Park and Odom (1998) where only the P-SV modes were included in the phase velocity ordering of the modes, and the SH modes were not included. The mode finding code developed by Park (1996) calculates the eigenvalues and eigenfunctions, which is an extension of the Chen (1993) algorithm. The ANIPROP code (Park, 1996) has been modified to include fluid layers and used to generate eigenvalues and eigenfunctions for each given model. The fluid/solid reflection and transmission coefficients were determined using the method of Mallick and Frazer (1991), when adding the fluid layers to ANIPROP. The effect of tilted TI symmetry on eigenfunctions is studies, as well as their and their respective phase and group velocities. Consider the tilting of the symmetry axis along lines of constant azimuth and constant elevation as shown in figure 4.

[Figure 4 about here.]

The model, described in the next section is characterized by propagating acoustic modes which have phase velocities within the range of $1500m/s$ and

$2000m/s$ for frequencies between 10.0Hz and 100.0Hz. The corresponding wavelengths at 50.0Hz would be $\lambda = 30m$ and $\lambda = 40m$ respectively. The computations were carried out on a desktop PC with dual 400MHz processors.

[Table 1 about here.]

3.1 Modal Formalism for Plane Layered Anisotropic Structure

A modal representation of the Green's function for the 1-D seismo- acoustic wave propagation problem is employed, with the expression of the wavefield as a superposition of global modes. The global modes are defined as the eigenfunctions (displacement and tractions) of a 1-D homogeneous anisotropic structure. The homogeneous plane-layered medium is infinite in the xy-plane, and the global modes are the eigenfunctions appropriate for the entire domain and path of propagation. The initial mode excitation may be determined by an appropriate source term.

The modal representation of the wavefield is a convenient method of solving the non-separable first order coupled equations of motion. The modes also provide a natural way of observing hos sources and material parameters affect the wavefield. However, some limitations exist. The computation time for calculating the modes and therefore the wavefield becomes larger as the number of layers and or frequency of the model increases. This can be inconvenient for very detailed analyses.

[Figure 5 about here.]

The modal formalism based on Maupin's (1988) theory is presented for a 1-D plane layered seismo-acoustic environment with general anisotropy as shown in figure 5. This modal approach to the equations of motion has the advantage of allowing the physics of propagation to be examined on a mode by mode basis and is formally exact. The modal theory arises out of the equations of motion and is a convenient first order theory. Additional and complimentary work with coupled-modes are given by Odom (1986), Maupin (1988), Odom *et. al.*(1996),and Park and Odom (1998, 1999). The theory for the 1-D plane layered wave propagation problem contains two critical steps: i) expressing the equation of motion as a first order differential equation and ii) solving the wave-equation with a superposition of global modes. For this chapter the application of the modes is limited to deterministic anisotropic structures. In addition, only the discrete modes are considered, while the continuum modes and their contribution are neglected. Attenuation is also ignored, although the theory remains valid for the inclusion of attenuation, since complex quantities have been accounted for throughout the theory. Weak attenuation could easily be included as a perturbation.

As previously shown in figure ?? and 2, a Cartesian coordinate system is assumed with wave propagation progressing in the horizontal direction parallel to the x-axis. The y-axis, the transverse direction, is the geometric symmetry axis for the 1-D medium along which material properties remain constant. This direction corresponds to the motion of a pure horizontally polarized shear wave. The z-axis is the vertical direction, positive downwards, and corresponds to the direction of motion of a pure vertically polarized shear wave.

The Einstein summation convention is assumed unless otherwise noted.

The theory development uses both Woodhouse(1974) and abbreviated subscript notation (e.g. Auld, 1990), also known as Voigt notation (e.g. Nye, 1957), for representing the fourth order elastic stiffness tensor, C_{iklj}. The Woodhouse notation is used primarily to represent a general anisotropic medium in the modal theory and the coupled local mode theory (section 4), and the abbreviated subscript notation is convenient for rotating the elastic stiffness matrix through the Bond transformation. In order to avoid some confusion, a superscript notation has been introduced. The superscripts w and a imply Woodhouse and abbreviated subscript notations respectively (i.e. ${}^{w}\mathbf{C}$ or ${}^{a}\mathbf{C}$). The indices of the fourth order elastic stiffness tensor are $iklj$ rather than the conventional $ijkl$ in order to facilitate the mapping between tensor notation and the matrix notation of Woodhouse (1974). In addition, lower case indices vary over ranges of $i, k, l, j = 1, 2, 3$ while upper case indices vary over ranges of $I, J = 1, 2, 3, 4, 5, 6$. A more detailed account of elastic stiffness tensor and matrix representations are located in Appendix A.

$\mathbf{C}$	$=$	C_{iklj}	fourth order elastic stiffness tensor
${}^{a}\mathbf{C}$	$=$	${}^{a}C_{IJ}$	6×6 abbreviated subscript elastic stiffness matrix
${}^{w}\mathbf{C}$	$=$	$({}^{w}C_{ij})_{kl}$	9×9 Woodhouse elastic stiffness matrix

The 3-component displacement field vector $\mathbf{w} = (\mathrm{w}_1, \mathrm{w}_2, \mathrm{w}_3)$ is assumed to be in harmonic form and involves a double Fourier transform over y and t of the displacement field $\mathbf{w}(x, y, z, t)$:

$$\mathbf{w}(x, z, k_y, \omega) = \int_{-\infty}^{+\infty} \int_{-\infty}^{+\infty} \mathbf{w}(x, y, z, t) \exp(-ik_y y + i\omega t) dy dt \qquad (14)$$

Note that the physics convention of the Fourier Transform has been used,

the same as Aki and Richards (1980). The double Fourier transform has a mixed sign convention consistent for wave propagation problems. In contrast, Maupin(1988) used the engineering convention of the Fourier Transform. Therefore, the right going wavefields in this work have a phase factor in the form:

$$\exp(ik_x x - i\omega t) \tag{15}$$

Throughout this work, all references to the displacement, traction, and stress-displacement vectors incorporated the double Fourier transform. The 3-component tractions can be expressed as:

$$\mathbf{t}_i = {}^{w}C_{ij}\frac{\partial \mathbf{w}}{\partial x_j} \tag{16}$$

where the elastic stiffness matrix, ${}^{w}C_{ij}$, is in Woodhouse (1974) notation. Each traction vector relates to stress elements in the form $\mathbf{t}_i = (\tau_{i1},\ \tau_{i2},\ \tau_{i3})$ for $i = 1, 2, 3$.

The equations of motion have the same general form for both fluid and solid media. The equations of motion are found in Appendix F in equation (86). The For solid media a 6-component displacement-stress vector $\mathbf{u} = (\mathbf{w}, \mathbf{t})^T$ can be introduced, where $\mathbf{t} = \mathbf{t}_1$. For fluid media, a 2-component displacement-stress vector may be defined as $\mathbf{u} = (\mathrm{w}, \mathrm{t})^T$ where $\mathrm{w} = \mathrm{w}_1$ and $\mathrm{t} = \tau_{ii}$ (no summation). The equation of motion for the 1-D plane-layered structure shown in figure 5 can now be expressed as:

$$\frac{\partial \mathbf{u}}{\partial x} = \mathbf{A}\mathbf{u} - \mathbf{F} \tag{17}$$

and the boundary conditions as:

$$\begin{aligned} [\tau_{ii}]_m &= [\mathrm{w}_3]_m = 0 \\ [\mathbf{t}_3]_n &= [\mathbf{w}]_n = 0 \end{aligned} \tag{18}$$

where the m^{th} subscript is for fluid-fluid and fluid-solid interfaces and the n^{th} subscript is for solid-solid interfaces. A free-slip boundary condition is imposed on the horizontal displacements at the fluid-solid interfaces. The solid-solid interfaces are assumed to be welded contacts where the displacement vector $\mathbf{w}$ and the traction vector $\mathbf{t}_3$ are continuous across the interfaces. For fluid-fluid interfaces and fluid-solid interfaces the displacements, w_3, and the vertical stress, τ_{33}, are assumed to be continuous across the interfaces. Following the notation of Maupin(1988), the square brackets with a subscript (e.g. $[quantity]_{n,m}$) in equation (18) and the following equations represent the evaluation of a quantity across the interface m or n. The quantity may be continuous or discontinuous and the evaluation is taken from the bottom of the interface to the top of the interface. For example, a discontinuity in the elastic stiffness matrix across the nth interface would be expressed as:

$$[{}^{a}C_{ij}]_n = {}^{a}C_{ij}\Big|_{n^+} - {}^{a}C_{ij}\Big|_{n^-} \tag{19}$$

The differential operator $\mathbf{A}$, described in Maupin (1988), from equation (17) and the boundary conditions from equation (18) contain the physics of the 1-D problem for the plane layered homogeneous anisotropic structure. Implicit in the $\mathbf{A}$ operator is the elastic stiffness matrix ${}^{w}\mathbf{C}$ which represents a TI elastically symmetric medium with an arbitrary symmetry axis. The orientation of the symmetry axis is defined by the two angles θ and φ as in figure 2 and figure 4. To obtain a general rotation of the elastic stiffness matrix with TI symmetry, the Bond transformation is utilized. The elements of the $\mathbf{A}$ operator may be real or complex. Attenuation may be included as complex values when the medium becomes visco-elastic. Although attenuation effects are currently neglected, the complex form of the elements of the $\mathbf{A}$ operator are retained. The generalized form of the operator $\mathbf{A}$ in equation

(??) of Appendix ?? does not need to be complex, but the form used by Maupin (1988) remains complex due to the explicit derivative with respect to the y-coordinate. The form of **A** can be found in Appendix B for a fluid medium, a general solid anisotropic medium, as well as for specific tilted TI orientations where meaningful analytical results can be obtained. **F** from equation (17) is the sum of an external source $\mathbf{F}^S$.

$$\mathbf{F} = \mathbf{F}^S = \begin{pmatrix} \mathbf{0} \\ \mathbf{f}^S \end{pmatrix} \tag{20}$$

A modal description of the wavefield is assumed, and the reader is remined that the modal representation of the wavefield is formally exact. The modes are independent solutions for the equations of motion and are functions only of depth. The initial wavefield, **u** is expressed as a superposition of global modes $\mathbf{u}^r = (\mathbf{w}^r, \mathbf{r}^t)^T$ weighted by source excitation amplitude coefficients c_r^0. The horizontal wave number is $k^r(\xi)$ and x_s denotes the source position.

$$\mathbf{u} = (\mathbf{w}, \mathbf{t})^T = \sum_r c_r^0 \exp\left(i \int_{x_s}^{x} k^r(\xi)\, d\xi\right) \mathbf{u}^r(z) \tag{21}$$

The modal description of the wavefield in equation (21) is for the discrete modes only, and the continuum modes have been neglected. The seismo-acoustic signal propagating within the 1-D plane-layered waveguide will experience geometrical spreading as the signal propagates along the x-direction. The modes of the homogeneous plane-layered medium are also energy normalized.

$$\left(\frac{2}{\pi k^r (x - x_s)}\right)^{\frac{1}{2}} \qquad \text{geometrical spreading term} \tag{22}$$

$$\left(\frac{1}{8 v_c^r U^r I^r}\right)^{\frac{1}{2}} \qquad \text{energy normalization term} \tag{23}$$

where v_c^r, U^r, and I^r are the phase velocity, group velocity, and energy integral of the mode r respectively as defined by Aki and Richards (1980).

Note that no assumptions have yet been made about the nature of the symmetry of the elastic layers in the modal theory. The theory describes propagation where the elastic regions have general triclinic anisotropy - a medium described by 21 independent elastic moduli. One consequence of restricting wave propagation to the x-direction is the reduction in the number of elastic elements from the elastic stiffness tensor C_{iklj} needed to describe the medium. For the 3-D propagation problem, all 21 elements of the elastic stiffness tensor would be needed and included in the differential operator **A**. For the 2-D propagation problem with propagation along the x-direction in a medium with triclinic symmetry, the total number of elastic elements needed from C_{iklj} is 15. These fifteen elements of the elastic stiffness matrix remain linear combinations of the original 21 independent elastic moduli when ${}^{a}C_{IJ}$ has been rotated.

$$
{}^{a}\mathbf{C} = \left[\begin{array}{c|c|cccc}
C_{11} & & C_{13} & C_{14} & C_{15} & C_{16} \\
\hline
 & & & & & \\
\hline
C_{31} & & C_{33} & C_{34} & C_{35} & C_{36} \\
C_{41} & & C_{43} & C_{44} & C_{45} & C_{46} \\
C_{51} & & C_{53} & C_{54} & C_{55} & C_{56} \\
C_{61} & & C_{63} & C_{64} & C_{65} & C_{66}
\end{array}\right] \tag{24}
$$

The second row and the second column of the elastic stiffness matrix in abbreviated subscript notation are not used in the 2-D wave propagation theory within the xz-plane. Using the symmetry relationships for the elastic stiffness tensor, the 15 elements of the abbreviated elastic stiffness matrix

needed are:

$$\begin{aligned} &{}^{a}C_{11}, {}^{a}C_{13}, {}^{a}C_{14}, {}^{a}C_{15}, {}^{a}C_{16} \\ &{}^{a}C_{33}, {}^{a}C_{34}, {}^{a}C_{35}, {}^{a}C_{36}, {}^{a}C_{44} \\ &{}^{a}C_{45}, {}^{a}C_{46}, {}^{a}C_{55}, {}^{a}C_{56}, {}^{a}C_{66} \end{aligned} \tag{25}$$

The propagating seismo-acoustic signal will only be sensitive to these 15 elements of the elastic stiffness matrix, regardless of whether the elastic stiffness matrix is rotated or not. Essentially, the 2-D description excludes any sensitivity to the elements in the 2^{nd} row and 2^{nd} column of the elastic stiffness matrix. Zhu and Dorman (2000) also report a dependence of 15 elements for the elastic stiffness tensor for a general TI medium.

Every term in the differential operator **A** which contains elastic moduli also contains the elements of ${}^{w}C_{11}$. It is reasonable to expect that the equations of motion and therefore the modes are sensitive to the changes in these elastic elements.

$${}^{a}C_{11}, {}^{a}C_{15}, {}^{a}C_{16}, {}^{a}C_{55}, {}^{a}C_{56}, {}^{a}C_{66} \tag{26}$$

3.2 Anisotropic Model

Nine parameters are necessary to describe each elastic layer. The necessary parameters include the thickness of the layer, the density, the five elastic moduli, and the two polar angles for the symmetry axis. The elastic moduli A, C, F, L, N describe the intrinsic elastic symmetry of the layer, the polar angles describe the orientation of the symmetry, and the thickness describes the boundaries of the layer.

It is assumed that all anisotropic layers have the same symmetry axis orientation. The elastic properties are constant within each layer, where

each layer may have its own degree of anisotropy, except the last layer which is defined as a uniform isotropic halfspace.

A sediment model that is representative of a typical marine sediment profile has been chosen. A typical sediment structure with TI anisotropy has its symmetry axis normal to the bedding planes. The density for typical sediments range from $1.90-2.49 g/cm^3$, while compressional speeds vary from $1.87-4.87 km/s$ and the degree of velocity variation due to anisotropy varies from 1-13% (Carlson *et al.*) The degree of anisotropy typically increases with depth, where sediments with bedding exhibit a higher degree of anisotropy than unbedded sediments. The global modes are determined for a 1-D plane layered medium with the velocity/density profile shown in figure 6.

[Figure 6 about here.]

The model is a variation of the Berge *et. al.* (1991) profile, and similar to the model used by Odom *et. al.* (1996) and Park and Odom (1998). The velocity and density profile is based upon a data set acquire *in situ* near the New Jersey coast from Berge *et. al.* (1991), with the addition of a deeper water column and an oceanic crustal component. The model consists of an isovelocity fluid layer, five thin anisotropic sediment layers and seven thin isotropic layers, a higher velocity subbottom layer, and a uniform isotropic halfspace as a basement layer. The model has a water column depth of 100m. The low shear speed sediments have a total thickness of 27.5m and overlay higher speed sediments 372.5m thick. The degree of anisotropy varies from 11% to 15% for the shear velocities. The compressional speeds of all the layers are isotropic. Figure 6 shows the velocity/density profile, while table 2 provides the parameter values for the model structure.

[Table 2 about here.]

Table 2 indicates that the elastic symmetry is actually a reduced version of the TI elastic symmetry. In all of the layers $A = C$, leaving only four independent elastic moduli. This effectively places all of the anisotropy in the difference between the shear moduli N and L. The anisotropy is purely shear in nature, where the compressional velocity is isotropic and the shear velocity is transversely isotropic. Berge *et. al.*'s (1991) experiment was insensitive to compressional wave anisotropy.

The Berge *et. al.* (1991) data set is altered further by allowing the symmetry axis of the TI layers to vary. With the modified Berge *et. al.* model as a starting VTI medium, the symmetry axis is rotated for all the anisotropic layers by using the Bond transformation as discussed previously.

3.3 Slowness Curves

Slowness curves reveal the nature of anisotropy in the direction of propagation. The slowness curves show the inverse of the velocities of three mutually orthogonal plane-waves propagating in an anisotropic medium: quasi-P, quasi-SV, and quasi-SH. Velocities and therefore slownesses of the medium are determined numerically solving the Christoffel equation 27 (e.g. Auld 1990).

$$\begin{aligned} (k^2\gamma_{ij} - \rho\omega^2\delta_{ij})v_j &= 0 \\ |k^2\gamma_{ij} - \rho\omega^2\delta_{ij}| &= 0 \end{aligned} \tag{27}$$

Solving the characteristic equation could be attempted analytically, which involves a cubic polynomial. Although there exists an analytical solution to the general cubic equation (first published by the Italian mathematician Girolamo Cardano in 1545, english translation published by M.I.T. Press,

1968), it is not very insightful for the general elastic stiffness tensor. The characteristic equation to be solved is:

$$
\begin{aligned}
- & \left(\frac{\rho\omega^2}{k^2}\right)^3 + (\gamma_{11}+\gamma_{22}+\gamma_{33})\left(\frac{\rho\omega^2}{k^2}\right)^2 + (\gamma_{23}\gamma_{32}+\gamma_{12}\gamma_{21} \\
+ & \gamma_{13}\gamma_{31}-\gamma_{11}\gamma_{22}-\gamma_{11}\gamma_{33}-\gamma_{22}\gamma_{33})\left(\frac{\rho\omega^2}{k^2}\right) \\
+ & \gamma_{11}\gamma_{22}\gamma_{33}-\gamma_{11}\gamma_{23}\gamma_{32}-\gamma_{12}\gamma_{21}\gamma_{33}+\gamma_{13}\gamma_{21}\gamma_{32} \\
+ & \gamma_{12}\gamma_{23}\gamma_{31}-\gamma_{13}\gamma_{22}\gamma_{31}=0 \qquad (28)
\end{aligned}
$$

Slowness curves may be considered where the symmetry axis remains along a fixed direction and the propagation direction is allowed to vary. The slowness curves for the first anisotropic sediment layer, as described by line 2 of table 2 are shown in Figure 7. The slowness curves show plane-wave propagation in the xy, xz, and yz-planes.

[Figure 7 about here.]

Figure 7 shows the slowness curves for the xy, xz, and yz propagating planes for symmetry axes aligned with the $\hat{z}$, $\hat{x}$, and $\hat{y}$ axes respectively. The quasi-P plane waves are entirely isotropic in nature, being rotationally invariant and all anisotropy is only in the shear velocities. For a modal description of a seismo-acoustic wavefield in a waveguide, the P and SV polarizations are always coupled together as P-SV modes. Therefore, any variation in the SV plane-wave velocity will affect the P-SV propagating modes, even without any variation in the P plane-wave velocities.

[Figure 8 about here.]

Figure 8 shows the slowness curves for the xz propagation plane for 36 symmetry axes orientations within the first quadrant. The intervals of θ and

φ are 0°, 20°, 40°, 50°, 70°, and 90°. The horizontal axis of the figure is the φ axis, where rows represent changes in the azimuthal angle φ. The vertical axis of the figure is the θ axis, where columns represent changes in the elevational angle θ. Note that all of the slowness curves in the fifth row are degenerate along the z-axis. These are slowness curves for propagation in the xz-plane at $\theta = 70°$ and $\varphi = 0°, 20°, 40°, 50°, 70°, 90°$. The two shear velocities remain degenerate for propagation along the z-axis for all variations of φ. When the shear velocities are degenerate along the z-axis, then the modes separate into two subfamilies of P-SV and SH modes that propagate independently. This is the same mechanism for a VTI medium, where the degenerate shear velocities along the vertical direction allow the SH and P-SV modes propagate independently.

The line singularites for a TI medium is dependent upon the the specific values of the elastic moduli A, C, F, L, N. Every different TI model may have a line singularity at a different value of elevation θ. The TI medium used in this dissertation has a line singularity at approximately 70° elevation. When $\theta = 70°$, the line singularity nearly intersects the z-axis. The shear plane-wave velocities may become degenerate, but the polarization of the two shear waves still remain orthogonal.

There are instances where the plane waves (body waves) become degenerate. This only occurs for the shear waves. The degeneracies of the shear plane waves occur at singularities in the phase velocity sheet. For a VTI medium, line singularities occur at θ approximately 70° and 110°, and kiss singularities occur at $\theta = 0°$ and $\theta = 180°$. A kiss singularity occurs where two phase-velocity sheets touch tangentially at isolated points. A line singularity occurs where two phase-velocity sheets intersect. The phase-velocity

sheets intersect in the plane perpendicular to the symmetry axis $\hat{s}$. A kiss singularity always occurs in a medium with transverse isotropic elastic symmetry. The kiss singularity occurs where the phase-velocity sheet intersects the symmetry axis $\hat{s}$. The slowness surfaces for VTI media have singularities. The P-wave slowness sheet doesn't have any singularities, and is a perfect sphere. The two shear wave slowness sheets have two kiss singularities and two line singularities (Crampin; 1981,1984,1989,1991). Crampin (1989,1991) contain 3-D schematics that graphically distinguish between the different types of singularities.

3.4 Angular and Frequency Dispersion Curves

A dispersion curve shows how the velocities of a set of modes change with the variation of a particular independent variable. The phase or group velocities of the modes trace out branches as the independent parameter is varied. The dispersion curves are functions of ω, θ, and φ which are defined as the frequency, angle of symmetry axis $\hat{s}$ tilt in the vertical plane θ, and angle of symmetry axis $\hat{s}$ tilt in the horizontal plane φ.

[Figure 9 about here.]

Fixing the symmetry axis orientation by keeping θ and φ constant while varying ω results in a standard frequency dispersion curve. For a 1-D model, the frequency dispersion curve in figure 9 shows how the number of acoustic modes and the phase velocity of the model varies with frequency. The frequency dispersion curve produces vertical branches in phase or group velocity. The frequency dispersion curve for the general TI medium looks very much like the frequency dispersion curves for isotropic or VTI media. In both

frequency dispersion curves of figure 9, notice the "solotone" effect, where the spacing of the eigenvalues cluster to form apparent "solotone" branches, the dark bands in the figures. The modes that contribute to the "solotone" branches are the modes sensitive only to the isotropic portion of the model, and are therefore labeled as "invariant acoustic modes". The "solotone" effect is due to discontinuities in the density and elastic moduli of the model. The solotone effect is a direct result of the inclusion of an elastic bottom structure for the sediments and basement layers. This effect has been documented by Lapwood(1975), Kennett *et. al.*(1983), and Alenitsyn(1998). The "solotone" branches are not a result of any anisotropy in the model, however the invariant modes that contribute to the "solotone" branches play an important role in angular dispersion curves. This solotone effect is frequency dependent. The number of modes in the 1500m/s-2000m/s range increases with frequency, and the number of acoustic/invariant modes become more numerous as the frequency increases. Another feature worth noting in the frequency dispersion curves occurs for the eigenvalues at higher frequencies. Figure 9(b) reveals modes that are closely spaced together and experience a braiding effect, where the two eigenvalues appear to become intertwined, even though they do not cross. This effect is not seen for the VTI case in figure 9(a) where the quasi-P-SV and quasi-SH modes propagate independently.

Fixing the value of ω and θ while varying φ creates an azimuthal angular dispersion curve. Keeping ω and φ constant while varying θ creates an elevational angular dispersion curve. The phase and group velocities of the modes are first computed for a beginning symmetry axis orientation $\hat{s}(\theta, \varphi)$. The symmetry axis $\hat{s}$ in the angular dispersion curves is then allowed follow lines of constant elevation or constant azimuth on a unit sphere as described

in figure 4.

[Figure 10 about here.]

The VTI and TTI models appear similar, when observing the frequency dispersion curves in figure 9. The differences between the models become much more evident in the angular dispersion curves. An angular dispersion curve with variations in θ or φ produce horizontal branches of phase or group velocities. Figure 10 displays azimuthal angular dispersion curves on the top (figures 10(a) and 10(b)) and elevational angular dispersion curves on the bottom (figures 10(c) and 10(d)). The left most figures (figures 10(a) and 10(c)) are the phase velocity angular dispersion curves and the figures on the right (figures 10(b) and 10(d)) are the group velocity angular dispersion curves. Note that a rectangular grid is used rather than a polar grid for the angular dispersion curves. The velocities are displayed on the vertical axis, and the angle variations are on the horizontal axis. A visual inspection of the angular dispersion curves reveals that a complexity exists when considering anisotropy. The dispersion branches show many instances where the branches approach one another. The phase velocities appear to attract and repel one another as the tilt angle varies for the 1-D model. It is evident that the the greatest changes in phase and group velocities occur for the elevational angular dispersion curves (changes in θ).

The eigenvalues do not remain evenly spaced. Near 0° the variations are small and the curvature of the dispersion branches are nearly flat. For azimuthal variations in φ there are less converging and diverging of the dispersion branches and the spacing of the eigenvalues remain more even. Take note of the horizontal branches that occur at 1511m/s, 1550m/s, 1625m/s, and 1904m/s at 50.0Hz, which have been highlighted in red in figure 10(c).

These are the dispersion branches for the invariant acoustic modes at 50.0Hz. The phase velocities for the invariant acoustic modes for other frequencies are found in table 3.

The phase velocity of these modes scarcely change for any variations of the symmetry axis direction, in either the azimuthal or elevational dispersion curves. These modes are the same invariant acoustic modes that participate in the "solotone" effect in the frequency dispersion curves. The frequency "solotone" effect precisely predicts the invariant modes that sample the isotropic part of the model which are not sensitive to any tilt of the symmetry axis. Because of the constancy of these modes, they allow for an "angular solotone" effect to occur when another mode branch sensitive to tilt angle approaches. These modes that are affected by the tilt of the symmetry axis are labeled "sensitive modes". The phase branches do not actually intersect, but as the sensitive mode approaches the invariant mode, their characteristics switch. The invariant mode branch takes on the character of the sensitive mode branch and the sensitive mode branch takes the character of the invariant mode branch. When the P-SV and SH modes coalesce into a single family of quasi-P-SV and quasi-SH modes or P-SV-SH modes, then any neighboring phase velocity branch may approach the invariant acoustic mode branches and switch characteristics.

[Table 3 about here.]

An example of this can be seen in figure 17 of the eigenfunction section 3.5, which will be discussed in further detail later. Two sensitive mode branches can also approach one another. The branches do not actually cross, but they effectively take on the characteristics of the other mode. It appears that when two mode branches that are sensitive to the tilt of the symmetry axis,

that they are modes of different wave types. A quasi-P-SV mode approaches a quasi-SH mode or vice versa. When the P-SV and SH modes propagate independently, then only the P-SV modes will approach the invariant acoustic modes and switch characteristics.

The angular dispersion curves are sampled discretely, so the near crossing of the branches may lack some strong curvature in the narrow angular ranges. A degeneracy in the mode eigenvalues (phase velocities) occurs when $c_r = c_q$ or $k_r = k_q$. The two modes combine into a single composite mode which is mutually orthogonal to all of the other modes in the basis set. The result is still a set of mutually orthogonal modes, but the number of modes is reduced as the two modes combine into a single mode. As two modes become nearly degenerate, the phase and group velocities and mode shapes move toward a single phase and group velocity and mode shape. When the eigenvalues become nearly degenerate, then the branches either pinch close together, or indicate an apparent crossing. An actual crossing of the dispersion branches does not need to occur in order for the mode order sequence to change. The phase velocity branches appear to cross, but they never actually cross because of the numerical method imposed by the ANIPROP code. Park(1996) applies an approximate plane wave solution when the reflectivity matrix is nearly defective. The reflection matrix is formally defective when two eigenvalues are repeated, and only one eigenfunction is shared for the duplicated eigenvalues. The treatment of the defective matrix is necessary for numerical stability in ANIPROP, as two eigenvalues become degenerate or nearly degenerate. In the real earth, the modes likely never cross because heterogeneity and roughness would destroy the degeneracy. Polarization of the modes ,whether predominantly P-SV or SH, cannot be inferred directly

by a visual inspection of the curves, apart from the invariant acoustic modes.

Similar findings to Martin *et. al.* (1997) and Thomson (1997) have been observed, where the group velocity branches cross, but they do not necessarily correspond to crossings of plane-waves in the slowness diagrams. Their phase and group velocity dispersion curves show many of the same features as the angular dispersion curves. Martin *et. al.* (1997) report the crossing of the phase velocities in azimuthal angular dispersion curves. Several obvservations include the pinching together of the phase velocity branches, apparent crossings of the phase velocity branches, as well as changes in the mode order sequence. Mode ordering can change for variations in θ or φ. The change in the sequence of the modes occurs for both types of angular dispersion curves, azimuthal and elevation. The branches approach very closely without actually touching.

The angular dispersion branches of the modes are symmetrical over a 180° range, with the mirror symmetry plane occurring at 90°. This is true for changes in θ or φ. For propagation in the xz-plane, the P-SV angular dispersion branches are symmetrical over a 90° range and the mirror symmetry occurring at 45°. The SH angular dispersion branches are not symmetrical over the range of $0° - 90°$ in the xz-plane.

The group velocity angular dispersion curves are helpful in revealing how quickly the velocity of the energy of a mode changes with the rotation of the symmetry axis. The invariant acoustic modes have particularly stable group velocities for changes in θ or φ. The group velocity of the invariant acoustic modes only tend to change when near degeneracies occur and the mode characteristics are being switched with another mode. Other modes reveal group velocity changes as the symmetry axis sweeps across constant

lines of azimuth or elevation. The group velocities are particularly sensitive to changes in the characteristics of the modes due to apparent branch crossings in the phase velocities. The group velocities change rapidly when another mode approaches. These changes occur over an angular range that correspond to the near crossings of the phase velocity branches.

The higher group velocities belong to the invariant acoustic modes. These are similar to the "banded" modes discussed in Thomson(1997). When the sensitive modes transition into an invariant mode, the group velocities of both modes converge, and then cross. The sensitive mode's group velocity then resumes the invariant's place, and the invariant mode becomes a sensitive mode with a lower group velocity.

It is usually easier to interpret the azimuthal angular dispersion curves than the elevation angular dispersion curves as in figure 10. However, additional insight into the mode branch sensitivity to the tilt of the symmetry axis $\hat{s}$ may be gained when the velocity data for an entire set of elevation angular dispersion curves is stacked.

[Figure 11 about here.]

Figure 11 shows the stacked elevation angular dispersion curves for several frequencies. The number of modes and character of the curves is frequency dependent. The width of the envelopes tells us the sensitivity of the modes to changes in azimuth at a particular angle θ. At 50.0Hz when θ is near $0°$ the envelope is narrow and the phase branches are only slightly dispersed. This is true of the branches near $70°$ as well. The envelope has the largest width in the θ range from $5° - 30°, 45° - 65°$, and $75° - 90°$ for Figure 11(e) at 50.0Hz.

3.5 Generalized Modes for Anisotropic Media

The focus for this section is on the effect anisotropy has on the modes - eigenfunctions. The concept of generalized modes of Crampin (1981) is used to described modes with particle motion in all three coordinate directions. Any lateral heterogeneity is neglected for now, but will be included in section 4. In addition the crustal modes are ignored, and only the modes which contribute primarily to an acoustic or seismo-acoustic signal are considered. These are the discrete modes within the phase velocity range of 1500m/s - 2000m/s. From the angular dispersion curves it has been demonstrated that changes in the orientation of the symmetry axis can have a dramatic impact on the eigenvalues of the propagating modes. How these variations in the modal eigenvalues affect the characteristics of the eigenfunctions are now considered.

The most distinctive feature of acoustic wave propagation in anisotropic media is 3-D polarization of the particle motion. The polarization of the modes depends on the angle between the propagation direction and the symmetry axis direction of the anisotropic media. The properties of the elastic stiffness matrix determine the degree with which the modes share particle motion polarizations. Crampin (1981) notes that the two independent wave types, P-SV and SH, of isotropy coalesce into a single family of generalized modes with three dimensional elliptical motion for general anisotropy. The once pure P-SV modes acquire SH motion and the once pure SH modes acquire P-SV motion. This results in quasi-P-SV and quasi-SH modes or generalized P-SV-SH modes, which possess polarizations into all three coordinate directions.

The eigenfunctions are generally complex in value. Anytime the sin-

gle generalized family of modes for anisotropic media separate into two independent family of modes, the components of the eigenfunctions become purely real or purely imaginary. When a medium exhibits more generalized anisotropy, the eigenfunctions may have both real and imaginary components in the three polarization directions. The imaginary components represent a phase delay in the time domain.

As discussed in Appendix (G), the form of the elastic stiffness tensor affects the eigenvalues of the modal basis in the seismo-acoustic waveguide. Special symmetry axis orientations exist where P-SV and SH motions propagate independently in TI symmetric media. In an isotropic medium, the pure P-SV and pure SH modes do not share the same particle motion polarizations. The medium is completely rotationally symmetric. For a TI elastically symmetric medium, the P-SV particle motions and the SH particle motions propagate independently when the symmetry axis $\hat{s}$ lies within the sagittal plane or along one of the three coordinate axes, as summarized by table 4. The sagittal plane is defined as the vertical plane containing the propagation direction. Since the propagation direction is assumed to be parallel to the x-axis, the sagittal plane is parallel to the xz-plane.

[Table 4 about here.]

A visual interpretation of the eigenfunctions at 50.0Hz in figure 12 reveals the P-SV modes have polarizations only in the xz-plane, and the SH modes have polarization in the y-direction. The pure SH modes are all rather similar to one another, with no particle motion in the fluid, and the largest amplitudes in the thin anisotropic sediments. The shape of P-SV and SH eigenfunctions are similar to the propagating modes for an equivalent isotropic medium. Schoenberge and Costa (1991) found that SH waves in a stratified

monoclinic medium can be modeled using an equivalent stratified isotropic medium for propagation in the plane of symmetry. In instances where the P-SV and SH modes propagate independently, it may not be entirely necessary to implement anisotropic modeling. When the P-SV and SH particle motions propagate independently in a plane layered homogeneous medium (i.e. the absence of scattering), only the P-SV modes are necessary to represent the seismo- acoustic wavefield.

[Figure 12 about here.]

The SH modes (e.g. 12(b)) are purely sediment and crustal modes when they propagate independently.

As shown in figure 13 the mode shape of mode 9 does not vary dramatically when the symmetry axis $\hat{s}$ is aligned with any of the three coordinate axes. This is typical of any of the modes when the symmetry axis $\hat{s}$ is aligned parallel to one of the coordinate axes.

[Figure 13 about here.]

The P-SV and SH motions are also separable when $\theta = 70°$. These symmetry axis orientations correspond to one of the line singularities in the TI elastically symmetric medium. The eigenfunctions are complex, but otherwise very similar to those in figure 12.

[Figure 14 about here.]

As seen in figures 12 and 14, there is no SH motion in the fluid layers. Even in the generalized eigenfunctions, motion is suppressed in the y-direction because the fluid layer can not support any shear stress. However, y-displacements in the generalized eigenfunctions do become evident in the bottom/subbottom layers for a tilted symmetry axis.

For more general tilt of the symmetry axis away from the sagittal plane or coordinate axes, the ${}^{a}C_{IJ}$ has the form of a quasi-triclinic elastic stiffness matrix. For these general geometries, the modes of the waveguide belong to the generalized eigenfunctions. They have polarization in all three coordinate directions, as seen in figure 14. The modes can be classified as predominantly quasi-P-SV or predominantly quasi-SH for most symmetry axis orientations. Energy begins to appear in the SH component of the quasi-P-SV modes as shown in figure 14(a). A similar effect for the quasi-SH eigenfunctions is shown in figure 14(b). As the symmetry axis is tilted away from the vertical the quasi-SH eigenfunctions gain particle directions in the x and z-directions. However, some symmetry axis orientations exist where it is impossible to label a mode as predominantly quasi-P-SV or predominantly quasi-SH. These modes can be more accurately described as composite P-SV-SH modes. As seen in figure 14(c)the amplitudes in the vertical, y and x directions are similar magnitudes for the P-SV-SH modes. The quasi-P-SV, quasi-SH, and P-SV-SH modes possess both P-SV and SH particle motion characteristics. This is a direct result of treating the sediments and bottom/subbottom as elastic.

The quasi-P-SV, quasi-SH, and P-SV-SH modes for when the symmetry axis $\hat{s}(\theta, \varphi) = \hat{s}(80°, 20°)$ are shown in figure 19. The x, y, and z components of displacement are in figures 19(a), 19(b), and 19(c) respectively. Notice that the amplitudes of the modes are about the same magnitude in the three coordinate directions. The x- and z-components resemble hybrid acoustic-sediment particle motions, and the y-components resemble the displacements of sediment modes.

[Figure 15 about here.]

Some of the modes have the majority of their energy in the water column and the isotropic portions of the model. They have relatively little particle motion in the anisotropic sediment regions of the model. These invariant modes are predominantly quasi-P-SV acoustic modes with very little particle motion in the y-direction. Because these eigenfunctions are dominated by the isotropic features of the model, they are only slightly affected by any tilt of the symmetry axis within the anisotropic sediments. They closely resemble the P-SV acoustic modes for isotropy and symmetry axis orientations where P-SV and SH mode propagate independently. An example of an invariant acoustic mode is shown in figure 15. These are the same modes that participate in the frequency and angular solotone effects observed in the dispersion curves. The acoustic modes are more sensitive to the anisotropy at lower frequencies. As the frequency increases, the acoustic modes' phase and group velocities become more invariant, indicating they become less sensitive to the anisotropy. These acoustic modes then become the invariant acoustic modes seen in the dispersion curves that participate in the "solotone" effect. An example of the frequency dependence of an acoustic mode is shown in figure 16. The figure shows the second acoustic mode for when $\hat{s} = \hat{z}$. The x-component and z-component particle motions are shown in figures 16(a) 16(b) respectively.

[Figure 16 about here.]

In order to satisfy the boundary conditions between a fluid and anisotropic solid for the equations of motion, the particle motion in the y-direction must be included. The modes in figure 14 clearly show that as the symmetry axis $\hat{s}$ tilts away from the vertical, the P-SV particle motion is no longer independent of the SH motion. Quasi-SH, quasi-P-SV and P-SV-SH modes

are needed for and accurate representation the seismo-acoustic wavefield.

For the dispersion curve in figure 10 near degeneracies occurred for P-SV modes, even when the SH modes propagate independently. These degeneracies are due entirely to the solotone effect, where the phase and group velocities of the invariant acoustic modes are almost stationary.

[Figure 17 about here.]

Near degeneracies seen in figure 10 affect the characteristics of the modes. Even though the dispersion curves do not cross, the characteristics of the modes switch. This is seen in the dispersion branches when a sensitive mode becomes an invariant mode. Figure 17 shows how the characteristics of the modes changes as the angle θ varies. Figures 17(a), 17(b), and 17(c) show the displacements for the x, y, and z-directions respectively. The mode begins as a predominantly quasi-SH mode and transforms into a predominantly quasi-P-SV as the angle θ varies. The characteristics of the quasi-SH mode are taken on by the quasi-P-SV mode and the characteristics of quasi-P-SV mode are taken on by mode the quasi-SH mode. The identity of the mode in figure 17 is exchanged as it closely approaches the quasi-P-SV mode. As the modes approach near degeneracy, the eigenfunctions of both modes transition towards composite modes with characteristics of both modes. There can exist two P-SV-SH modes that closely resemble each other as the modes become nearly degenerate.

The mode order sequence does not remain fixed for increases in frequency or changes in symmetry axis orientations. The sense of mode ordering is somewhat lost when the two sets of mode polarizations coalesce into a single set of generalized P-SV-SH modes. The sequence of the mode ordering is not completely clear as the symmetry axis is tilted. The switching of modes is a

complex function of the phase and group velocity relationships with the phase velocities approaching one another and where the group velocities actually cross. For TI elastic symmetry, the mode ordering of the eigenfunctions does not necessarily stay fixed as the symmetry angle is tilted. The mode ordering changes when two modes approach one another. The mode order sequence tends to remain the same for the eigenfunctions at lower frequencies. The eigenvalues are spaced further apart and near degeneracies do not occur. As the frequency increases, the eigenvalues become more closely spaced, as is evident in the the dispersion figures 9 and 10. Near degeneracies have a higher occurrence as the frequency increases, and the modes switch characteristics more often. Although it may be insightful to keep track of individual modes and their characteristics as they transition from quasi-P-SV to quasi-SH or vice versa, it really is not necessary. The modal formalism of section 3.1 does not require all of the modes to be individually identified as P-SV, SH quasi P-SV, quasi SH or P-SV-SH. All that is needed is to be sure and include all of the modes important to the seismo-acoustics waves composition.

[Figure 18 about here.]

[Figure 19 about here.]

The modes of the shallow water waveguide may be directly excited by any number of source types. When the PSV and SH modes propagate independently, then the polarization of the acoustic modes are more source dependent represented by figure 18. An explosive source will excite only PSV motion (x and z-displacements). The displacements for the x, y, and z-directions excited by an explosive source are shown in figures 18(a), 18(b), and 18(c) respectively. Moment tensor sources can also be of interest for some acoustic

wave propagation problems, such as T-wave excitation (Park *et. al.*, 2001). A pure double couple in the xy-plane will only excite SH motion as displayed in figures 18(d), 18(e), and 18(f). The excitation of the P-SV and SH modes can be compared to the excitation of quasi-P-SV, quasi-SH, and P-SV-SH modes. Using an explosive source, energy becomes evident in the x, y, and z-displacement directions in figures 19(a), 19(a), and 19(a) respectively. The significance is that the wavefield will contain y-displacements in the absence of any heterogeneity or scattering. Using a double-couple source contained in the horizontal plane, excitation of x, y, and z-displacements again becomes evident as shown in figures 19(d), 19(e), and 19(f) modes. Here, a shear source is able to excite modes which contribute to a seismo-acoustic wavefield. Because of the 3-D polarization of the modes, they may be excited by a wide range of sources.

The generalized mode structure is significant for shallow water media. With the bottom interacting modes, acoustic energy can leave the water column. It can then be attenuated by the low shear velocity sediments, and redistributed to other predominantly sediment modes. In addition, energy from other sources or signals, such as noise, from the sediment and bottom layers can enter the water column through these bottom interacting modes. With the anisotropic bottom interacting modes, there exists a greater opportunity for the energy to become redistributed and leave or enter the water column. This is due to the three component nature of the eigenfunctions, the displacement and the tractions. Therefore, in the presence of anisotropy, attenuation of bottom interacting modes would be underestimated if isotropy is assumed.

G

4 Anisotropy and Geometrical Heterogeneity

It is helpful to separate the effects of anisotropy and the effects of heterogeneity in a complicated medium. In sections 2 and 3 the effect of anisotropy in the absence of heterogeneity was investigated. Now consider the effect of lateral heterogeneity on the coupling of local modes for isotropic, VTI, and TTI media. The local modes are defined as the eigenfunctions of a 1-D model that is the local equivalent of the range-dependent model at a fixed position x_i. The local modes are weighted by range-dependent amplitude coefficients, which can be determined by solving an evolution equation. This evolution equation depends on the coupling matrix $\mathbf{B}_{qr}$ which contains all of the physics for the redistribution of energy between coupled local modes. $\mathbf{B}_{qr}$ contains the elastic moduli of the model, lateral derivatives of the elastic moduli, the local eigenfunctions, and the vertical derivatives of the local eigenfunctions.

Building upon the previous discussions concerning homogeneous plane-layered anisotropic media, now consider 2-D wave propagation effects for a range-dependent model. The local modes are orthogonal, but any lateral heterogeneity breaks the orthogonality of the modes, and allows them to couple, where energy is redistributed between the modes.

4.1 Coupled Local Mode Formalism for Anisotropic Range-Dependent Media

The theory presented for the 1-D homogeneous anisotropic plane-layered half-space of section 3.1 can be extended. The method of coupled local modes is applied to the 2-D range-dependent seismo-acoustic wave propagation prob-

lem. Any introduction of lateral heterogeneity leads to two additional steps in solving the equations of motion. As for the previous homogeneous anisotropic plane-layered medium, the equations of motion can be expressed as a first order differential equation and the solution of the coupled first order equations are expressed in terms of the basis of local modes. In addition, the interface boundary conditions must be transformed into equivalent localized volume forces, and an evolution equation for the amplitude coefficients which describes the coupling between modes in a range-dependent medium must be obtained. The specific deterministic anisotropic structure of the medium is assumed to be known for the model.

The modal theory in Section 3.1 is extended by following the the coupled local mode formalism of Maupin (1988). The boundary conditions for geometrical heterogeneity along interfaces may be expressed as:

$$[\mathbf{t}(\hat{n})_3]_n = [\mathbf{w}(\hat{n})]_n = 0, \qquad \text{for the } n^{th} \text{ interface} \tag{29}$$

The local coupled mode formalism also assumes that all tractions vanish at the free surface, imposes a free-slip boundary at any fluid-solid interfaces, and enforces a radiation condition at infinity. In addition, the displacement and tractions are considered continuous across interface normals.

Consider an effective volume force term $\mathbf{F}^T$ arising from traction discontinuities along interfaces.

$$\mathbf{F} = \mathbf{F}^S + \mathbf{F}^T = \begin{pmatrix} \mathbf{0} \\ \mathbf{f}^S \end{pmatrix} + \begin{pmatrix} \mathbf{0} \\ [\mathbf{t}]_n \, \delta\left(z - h_n(x)\right) \end{pmatrix}$$

This additional effective volume force will be found in the coupling terms of the local modes. The interfaces between fluid layers are considered planar, and do not contribute an equivalent volume force.

As before a modal description of the wavefield is assumed, where the local modes are independent solutions for the non-separable equation of motion. The wavefield, $\mathbf{u}$ is expressed as a superposition of local modes $\mathbf{u}^r(z;x)$ weighted by range-dependent amplitude coefficients $c_r(x)$.

$$\mathbf{u} = (\mathbf{w}, \mathbf{t})^T = \sum_r c_r(x) \, \exp\left(i \int_{x_s}^{x} k^r(\xi) \, d\xi \right) \, \mathbf{u}^r(z;x) \tag{30}$$

where $k^r(\xi)$ is the local horizontal wave number, and x_s denotes the source position.

Substituting the Ansatz (30) into the equation of motion (17), taking the scalar product with respect to local mode $\mathbf{u}^q$, and then evaluating the scalar product integrals results in an evolution equation for the amplitude coefficients $c_r(x)$.

$$\frac{\partial c_q}{\partial x} = B_{qr} c_r \tag{31}$$

where the coupling matrix $\mathbf{B}_{qr}$ is defined as:

$$\mathbf{B}_{qr} = \left(- \left\langle \mathbf{u}^q, \frac{\partial \mathbf{u}^r}{\partial x} \right\rangle + i \sum_n \dot{h}_n \mathbf{w}^{q*} \left[\mathbf{t}^r \right]_n \right) \exp\left(i \int_0^x (k^q - k^r) d\xi \right) \tag{32}$$

and the Hermitian scalar product is defined as:

$$\langle \mathbf{u}^q, \mathbf{u}^r \rangle = i \int_0^\infty (\mathbf{w}^{*q} \mathbf{t}^r - \mathbf{t}^{*q} \mathbf{w}^r) \, dz \tag{33}$$

The range-dependent amplitude coefficients are determined from the solution of equation (??). The combined effects of heterogeneity and anisotropy on the eigenfunctions are studied through the coupling matrix $\mathbf{B}_{qr}$. For a deterministic medium, $\mathbf{B}_{qr}$ is a mode coupling matrix which essentially determines how much of the modal energy from local mode q is redistributed

into local mode r. The coupling matrix contains an inner product which introduces volume terms and interface terms. It contains the local eigenfunctions, their vertical derivatives, and the material properties as well as any lateral heterogeneities. The range-dependent amplitude coefficients are determined from the solution of equation (31). $\mathbf{B}_{qr}$ would be a diagonal matrix, describing the only self-modal coupling, for a homogeneous plane-layered medium. The modes are all mutually orthogonal, preventing any redistribution of energy between the modes. Some heterogeneity needs to exist for the coupling matrix $\mathbf{B}_{qr}$ to contain off diagonal terms that leads to mode coupling. The heterogeneity could be sloping or rough interfaces, volume variations, or both. A full expanded form of the coupling matrix $\mathbf{B}_{qr}$ can be found in Appendix C.

The deterministic coupling matrix of Maupin (1988) contains both boundary interface terms and volume terms. The volume terms contain lateral derivatives of matrices containing elastic moduli. When we assume that the material properties are constant within each layer of the model, then any derivative of these constants is zero. All volume terms in the coupling matrix $\mathbf{B}_{qr}$ become zero, and we are then left with only the interface terms of the $\mathbf{B}_{qr}$ matrix. Therefore in the absence of material property variations we obtain:

$$\begin{aligned}
\mathbf{B}_{qr} &= \frac{1}{k^q - k^r}\left(\sum_n \dot{h}_n\left[-\mathbf{w}^{q*}\rho\omega^2\mathbf{w}^r - \frac{\partial \mathbf{w}^{q*}}{\partial z}Q_{33}\frac{\partial \mathbf{w}^r}{\partial z} + \mathbf{w}^{q*}Q_{22}\mathbf{w}^r p^2\right.\right. \\
&\quad \left.\left. -\frac{\partial \mathbf{w}^{q*}}{\partial z}(C_{31}C_{11}^{-1})\mathbf{t}^r - \mathbf{t}^{q*}(C_{11}^{-1}C_{13})\frac{\partial \mathbf{w}^r}{\partial z} + \mathbf{t}^{q*}C_{11}^{-1}\mathbf{t}^r\right]_n\right. \\
&\quad - \dot{h}\left(-\frac{\partial t_{33}^{q*}}{\partial z}\frac{1}{\rho\omega^2}\frac{\partial t_{33}^r}{\partial z} - t_{33}^{q*}\left(\frac{1}{\lambda} - \frac{p^2}{\rho\omega^2}\right)t_{33}^r + w_1^{q*}\rho\omega^2 w_1^r\right)_{h(x)^-} \\
&\quad \left. - i\dot{h}\left((k^q - k^r)(w_1^{q*}t_{33}^r + t_{33}^{q*}w_1^r)\right)_{h(x)^+}\right) \exp\left(i\int_0^x (k^q - k^r)d\xi\right) \qquad (34)
\end{aligned}$$

where the ${}^{w}Q_{ij}$ matrix is defined as:

$$ {}^{w}Q_{ij} = {}^{w}C_{ij} - ({}^{w}C_{i1})({}^{w}C_{11}^{-1})({}^{w}C_{1j}) \tag{35} $$

4.2 Anisotropic Laterally Heterogeneous Media

The local eigenfunctions and mode coupling for two classes of models are analyzed: where the symmetry axis $\hat{s}$ is defined by a fixed θ and variable φ and where the $\hat{s}$ is defined by a fixed φ and variable θ. Finally, the coupling matrices of the models are compared and studied to reveal modal energy redistribution in the presence of range-dependence. The VTI model will be the standard for comparing the various rotations of the general anisotropic medium belonging to the TI symmetry class.

The shallow 2-D water environment has a bottom/subbottom with complex elastic properties that vary in both direction and location. Figure 20 shows a representation of a 2-D range-dependent model. The thin anisotropic sediments are modeled as in Sections 2 and 3.

[Figure 20 about here.]

When investigating the effects of anisotropy in a 2-D range-dependent seismo-acoustic environment, 1-D profiles are generated that are the local equivalent of the range-dependent model shown in figure 20. At a particular point, x_i of the 2-D range-dependent model a 1-D profile is created with the same elastic properties and depth dependence as the 2-D model. For example, the density and elastic moduli of the 2-D model are described in

the 1-D profile as:

$$\rho(x_i; z) = \rho(z)$$

$$A(x_i; z) = A(z)$$

$$C(x_i; z) = C(z)$$

$$F(x_i; z) = F(z)$$

$$L(x_i; z) = L(z)$$

$$N(x_i; z) = N(z)$$

The model is range-dependent with elastic sediments and bottom layers. The anisotropy belongs to the transversely isotropic elastic symmetry class, and is only in the thin sediment layers. All other layers remain isotropic. The elastic parameters are known and assumed to be deterministic in nature, while ignoring any small scale variations that would be evident in a real earth structure.

For the 1-D profile, the same model as shown in figure 5 and table 2 is used. The 1-D vertical profiles are the plane layered homogeneous anisotropic halfspace considered previously in Sections 2 and 3.

4.3 Deterministic Interface Coupling Matrices

The coupling matrix $\mathbf{B}_{qr}$ essentially determines how much of local mode r is redistributed into mode q. For isotropy, when the symmetry axis $\hat{s}$ is within the sagittal plane, or $\hat{s}$ is aligned to one of the coordinate axes, the SH and P-SV particle motions propagate independently. Any mode coupling is dominated by nearest neighbor interactions between modes of the same wave type. If the modes involved in the $\mathbf{B}_{qr}$ matrix are strictly different wavetypes with completely separate polarizations, then the coupling between

the different wavetypes will be zero. Only SH/SH and P-SV/P-SV coupling is observed between the modes. Figure 21 shows the $\mathbf{B}_{qr}$ coupling matrices for pure P-SV and SH modes at 20.0Hz, 30.0Hz, 40.0Hz, and 50.0Hz.

[Figure 21 about here.]

The white elements in the coupling matrices represent zero values. Note that the diagonal elements, which represents the self-coupling of a mode or the phase of the mode, have also been set to zero. It appears that the coupling between modes may not be dominated by nearest-neighbor interactions, but in fact the modes are only coupling with their respective wave types and the coupling is strongest for the nearest mode of the same wave type. Absolutely no coupling occurs between the SH and P-SV local modes. If the P-SV and SH modes are separated and then grouped first by modal wavetype, and second ordered by phase velocity, then the nearest-neighbor coupling of Odom *et. al.* (1996) is observed.

As the symmetry axis is tilted, coupling can occur between any generalized mode regardless of mode wavetypes, as shown in figure 22. The quasi-P-SV, quasi-SH, and generalized P-SV-SH modes may have energy in all three coordinate directions, allowing the modes to be available for a wide redistribution of energy whenever lateral heterogeneity is present. The mode coupling may be dominated by nearest-neighbor interactions or by non-nearest-neighbor interactions. The strength of the coupling depends on the closeness of the phase velocities of the modes and the degree of similarity of the polarizations. However, the 3-D particle motion of the local modes allow coupling between all of the modes, whether of similar or dissimilar polarization.

[Figure 22 about here.]

Figure 22 shows the $\mathbf{B}_{qr}$ coupling matrices for a symmetry axis orientation where $\hat{s}(\theta, \varphi) = \hat{s}(10°, 20°)$ Notice that all of the modes couple to some degree.

The invariant acoustic modes have polarizations predominantly in the sagittal plane. The invariant modes appear at higher frequencies in isotropic, VTI, and TTI media. They are essentially insensitive to most tilt of the symmetry axis $\hat{s}$ within thin anisotropic sediment layers. These modes couple weakly with any predominantly quasi-SH modes when lateral heterogeneity is present. In contrast, the invariant acoustic modes may couple strongly with any quasi-P-SV, generalized P-SV-SH, or quasi-SH modes with significant particle motion polarizations in the sagittal plane.

Near degeneracies play an important role in the coupling of local modes. Since the $\mathbf{B}_{qr}$ matrix is directly dependent upon the phase velocities of the two modes, as well as the eigenfunctions of the modes,it is important to consider what happens as the eigenvalues become degenerate. Many near degeneracies in the modal phase velocities can be seen in Figure 10(c) between $10° - 20°$ and $70° - 80°$.

$$\mathbf{B}_{qr} = \frac{1}{\Delta k}\mathbf{B}_{qr}{}' \tag{36}$$

As the difference between the mode phase velocities becomes smaller, the contribution to the coupling matrix $\mathbf{B}_{qr}$ may become larger.

$$\frac{1}{k^q - k^r} = \frac{c^q c^r}{\omega(c^r - c^q)} \tag{37}$$

The coupling of the two modes are expected to become very large as they approach a near degenerate state. The $\mathbf{B}_{qr}$ coupling matrix may be dominated by such interaction of closely spaced modes. The coupling at near degeneracies is not infinite, but the closely spaced phase velocities, and

therefore the closely spaced wavenumbers of the two discrete modes, can dominate the coupling term between the modes, as shown in figure 23(a). When the nearest-neighbor contributions are removed as in figure 23(b), then the $\mathbf{B}_{qr}$ coupling matrix is similar to the one in figure 22(d). As the modal phase velocities converge, the polarizations of the modes become more alike.

[Figure 23 about here.]

In contrast, when the spacing of two eigenvalues is large, then the coupling between two modes is weak. In addition, If two eigenfunctions have rather dissimilar polarizations, then the coupling may also be weak, if the wave numbers of the two modes are not in close proximity to one another. An example of when the polarizations are completely dissimilar is when pure P-SV and SH local modes propagate independently, as observed in figure 21. In general, eigenfunctions with different polarizations will tend to couple more weakly than eigenfunctions that have similar polarizations. The strongest coupling occurs between modes of similar polarizations. For an isotropic case only P-SV modes may have similar polarizations with other P-SV modes, and only SH modes may have similar polarizations with other SH modes. For the more general anisotropic case, any two modes with particle motions in all three polarization directions and closely space eigenvalues will exhibit strong coupling.

[Table 5 about here.]

Table 5 summarizes the combinations of of wave types that will couple for a TTI medium.

When the symmetry axis $\hat{s}$ allows for a quasi-triclinic *form* of the elastic stiffness tensor all the modes are excited regardless of the source type, and all the modes are involved in the coupling, although some modes contribution is much smaller than others. The coupling matrix $\mathbf{B}_{qr}$ results suggest that the combination of a tilted symmetry axis and lateral heterogeneity is rather efficient at scattering a seismo-acoustic signal.

Figure 24 shows the $\mathbf{B}_{qr}$ coupling matrices for four moment tensor sources, which is of interest for T-wave excitation. The figure clearly shows which modes are excited when the source modes are pure P-SV and SH modes with separate polarizations. The explosive source in figure 24(a) clearly shows that the SH modes are excluded entirely as they are not excited at all. A double couple source in the xz-plane produces a similar coupling matrix to the explosive source, where again the SH modes are not directly excited, as shown in figure 24(c). The double couple sources in the xy-plane and the yz-plane only excite the SH modes, as shown in figures 24(b) and 24(d) respectively.

[Figure 24 about here.]

4.4 Stochastic Interface Coupling Matrices

Park and Odom (1999) have successfully included both deterministic bathymetry terms and rough boundary interface terms for isotropic and transverse isotropy media into the coupled mode equations. The formulation for the scattering coupling matrix $\mathbf{S}_{qr}$ presented by Park and Odom (1999) is valid for more general anisotropy symmetries, such as those already discussed previously. The terms of the coupling matrix can be cast in a form that that only includes the displacement $\mathbf{w}$, the traction vector $\mathbf{t}$, and their respective derivatives.

This gives uniformity, where all of the coupling matrices may be expressed in terms of the stress-displacement vector $\mathbf{u} = (\mathbf{w}, \mathbf{t})^T$ and is derivatives.

The evolution equation for coupling due to stochastic rough interfaces come from the dissertation of Minkyu Park (1997):

$$\begin{aligned}
\frac{\partial d_q}{\partial x} &= \sum_r \left(\left(< \mathbf{u}^q, \frac{\partial \mathbf{u}^r}{\partial x} > + i \sum_n \dot{h}_n^0 \left[\mathbf{w}^{q*} \cdot \mathbf{t}^r \right]_n \right) \exp\left(i \int_0^x (k^r - k^q) d\xi \right) \right) d_r \\
&\quad + \sum_r \mathbf{D}_{qr} c_r + \sum_r \mathbf{E}_{qr} \frac{\partial c_r}{\partial x} \\
&= \sum_r \mathbf{B}_{qr} d_r + \sum_r \mathbf{D}_{qr} c_r + \sum_r \sum_s \mathbf{E}_{qs} \mathbf{B}_{sr} c_r \\
&= \sum_r \mathbf{B}_{qr} d_r + \sum_r \mathbf{S}_{qr} c_r \qquad (38)
\end{aligned}$$

The $\mathbf{B}_{qr}$ matrix is defined the same as in section ?? and Appendix C. The matrices $\mathbf{D}_{\alpha\beta}$ and $\mathbf{E}_{\alpha\beta}$ are defined as:

$$\begin{aligned}
\mathbf{D}_{qr} &= i \sum_n \gamma_n \frac{1}{\sqrt{1 + \left(\dot{h}_n^0 \right)^2}} \left(\left[\mathbf{w}^{q*} \cdot \frac{\partial \mathbf{t}^r(\hat{\mathbf{n}}_o)}{\partial z} \right]_n - i k^r \dot{h}_n^0 \left[\mathbf{w}^{q*} \cdot \mathbf{t}^r(\hat{\mathbf{n}}_o) \right]_n \right. \\
&\quad + \left(\dot{h}_n^0 \right)^2 \left[\mathbf{w}^{q*} \cdot \frac{\partial \mathbf{t}^r(\hat{\mathbf{n}}_o)}{\partial z} \right]_n + \frac{\dot{h}_n^0 \ddot{h}_n^0}{1 + \left(\dot{h}_n^0 \right)^2} \left[\mathbf{w}^{q*} \cdot \mathbf{t}^r(\hat{\mathbf{n}}_o) \right]_n \\
&\quad \left. + \frac{\dot{h}_n^0 \ddot{h}_n^0}{\sqrt{1 + \left(\dot{h}_n^0 \right)^2}} \left[\mathbf{w}^{q*} \cdot \mathbf{t}^r(\hat{\mathbf{x}}) \right]_n \right) \exp\left(i \int_0^x (k^r - k^q) d\xi \right), \qquad (39) \\
\mathbf{E}_{qr} &= -i \sum_n \gamma_n \frac{\dot{h}_n^0}{\sqrt{1 + \left(\dot{h}_n^0 \right)^2}} \left[\mathbf{w}^{q*} \cdot \mathbf{t}^r(\hat{\mathbf{n}}_o) \right]_n \exp\left(i \int_0^x (k^r - k^q) d\xi \right) \qquad (40)
\end{aligned}$$

Note the sign correction for the fourth term of the $\mathbf{D}_{qr}$ matrix. After some

algebra, the matrices can be expressed as:

$$\mathbf{D}_{qr} = i\sum_n \gamma_n \left(\left[\mathbf{w}^{q*} \cdot \frac{\partial \mathbf{t}_3^r}{\partial z} \right]_n - \dot{h}_n^0 \left[\mathbf{w}^{q*} \cdot \frac{\partial \mathbf{t}_1^r}{\partial z} \right]_n \right.$$

$$\left. + ik^r \frac{\left(\dot{h}_n^0\right)^2}{1+\left(\dot{h}_n^0\right)^2} \left[\mathbf{w}^{q*} \cdot \mathbf{t}_1^r\right]_n + \frac{\dot{h}_n^0 \ddot{h}_n^0}{(1+\left(\dot{h}_n^0\right)^2)^2} \left[\mathbf{w}^{q*} \cdot \mathbf{t}_1^r\right]_n \right) \quad (41)$$

$$\times \exp\left(i \int_0^x (k^r - k^q) d\xi \right), \quad (42)$$

$$\mathbf{E}_{qr} = i\sum_n \gamma_n \frac{(\dot{h}_n^0)^2}{1+\left(\dot{h}_n^0\right)^2} \left[\mathbf{w}^{q*} \cdot \mathbf{t}_1^r\right]_n \exp\left(i \int_0^x (k^r - k^q) d\xi \right), \quad (43)$$

The derivative of the traction vector $\mathbf{t}_3$ can be determined from the original equations of motion. The vertical derivatives of the tractions $\mathbf{t}_3$ and $\mathbf{t}_1$ can be expressed as:

$$\frac{\partial \mathbf{t}_3}{\partial z} = -\rho\omega^2 \mathbf{w} - \frac{\partial \mathbf{t}_1}{\partial x} \quad (44)$$

where it has been assumed that all propagation is restricted to the xz-plane, and all derivatives in the y-coordinate direction are zero.

Figures 25 and 26 present the scattering coupling matrix $\mathbf{S}_{qr}$ for a VTI medium and TTI where $\hat{s}(\theta, \varphi) = (10°, 20°)$ respectively.

[Figure 25 about here.]

The rows and columns of $\mathbf{S}_{qr}$ represent the primary and scattered modes respectively. Figure 25 is similar to those presented by Park and Odom (1999), except that SH modes have been included into the mode sets. Figure 26 represents the extension of the work presented by Odom and Park (1999) to a more general case of anisotropy, where the symmetry axis of the TI elastically symmetric medium may have any arbitrary orientation. The symmetry axis, $\hat{s}(\theta, \varphi) = (10°, 20°)$, is not to far from vertical. Some of

the scattered modes are preferentially excited, while others are less excited. Scattered modes 2, 4, and 5 from Figure 26(c), represented by columns 2, 4, and 5 respectively, are excited to a much smaller degree than scattered modes 0, 3, 4, 7, 9, and 11. At the frequency of 40.0Hz (Figure 26(c)), it can be seen that the primary modes 1, 4, 6, 7, 9, and 12, represented by rows 1, 4, 6, 7, 9, and 12 contribute the most to resulting scattered wavefield. What is interesting is the characteristics of these modes. The primary modes 0, 3, and 11 are "invariant" acoustic modes, with the majority of their energy in the isotropic portion of the model. They do not contribute to the scattered wavefield as strongly as the more "sensitive" modes. This implies that the energy will remain coherent longer in these modes that the "sensitive" modes. However, these same "invariant" modes from the scattered wavefield receive more energy than the "sensitive" type modes. This implies that rough interface boundaries tend to preferentially redistribute energy from "sensitive" modes to "invariant" modes. This may indicate that energy from seismic sources below that water column would be preferentially scattered into "invariant" acoustic modes, which would remain coherent longer. Such mechanism could help explain T--wave generation.

[Figure 26 about here.]

5 Summary and Conclusions

The form of the elastic stiffness matrix, and its symmetry in relation to the propagation direction affects the wave propagation in the seismo-acoustic waveguide. The form of the elastic stiffness tensor determines whether the local modes coalesce into a set of quasi-P-SV, quasi-SH, and generalized P-

SV-SH modes or into P-SV and SH modes which propagate independently. This distinction greatly affects the polarization of the propagating signal. Since it usually cannot be prearrange to record a seismo-acoustic signal in a symmetry plane, tilted anisotropy cannot be completely ignored. Horizontal shear motion is often ignored or neglected in the modeling of acoustic signals. The majority of attention has been placed on the P-SV motion. However, any description of seismo-acoustic signal propagation which ignores SH motion in these environments would be incomplete. All three coordinate particle motion polarizations must be included into the seismo-acoustic wavefield.

Conversion of acoustic energy into horizontally polarized shear motion can be expected at fluid/solid boundaries where lateral heterogeneity or anisotropy exists in the solid layer. As a result, one consequence of the presence of anisotropy is that the seismo-acoustic signals can have a significant portion of their energy in horizontally polarized shear motion (SH and quasi-SH) even in the absence of any range-dependence. This is in contrast to an isotropic or VTI elastic medium, where all acoustic energy propagates independently of any horizontally polarized shear motion. In the absence of any scattering, all particle motion for an acoustic signal would be restricted to the sagittal plane. For general anisotropy the compressional motion(quasi-P), vertically polarized shear motion (quasi-SV) and horizontally polarized shear motion (quasi-SH) no longer propagate independently. Horizontally polarized shear motion experiences more attenuation than compressional motion, where intrinsic SH attenuation is approximately 2-3 times larger than compressional wave attenuation, or even larger in low shear speed sediments. Because shear motions experience higher attenuation than compressional motion, this could be an important loss mechanism for acoustic signals with

significant seafloor interaction. The SH motion could have a profound effect on the propagation of the acoustic signal. The signal may experience more energy loss than an equivalent signal propagating in an isotropic model or only fluid layers. Hughes (1990) observed high propagation loss in thin sediment layers over hard bottoms. Some of this type of loss may result from acoustic energy being converted to quasi-SH modes.

The elements of the $\mathbf{B}_{qr}$ coupling matrices have given insight into the degree of energy distribution among the modes due to heterogeneity in the presence of anisotropy. It has also become clear that a generalized set of P-SV-SH modes is required to correctly model seismo-acoustic signals where tilted anisotropy is present. Since there no longer exists a clear distinction between pure P-SV and SH modes, all modes can carry energy for the seismo-acoustic signal. The implication is that all of the modes are intricately coupled for even weak anisotropy. There are more modes available in anisotropic media for the redistribution of energy. The combination of lateral heterogeneity and anisotropy is very effective at scattering the wavefield. Any lateral heterogeneity can cause the modes to couple, and the coupling tends to become stronger as the phase velocities associated with the local modes converge to similar values. In contrast the isotropic and transversely isotropic modes transfer energy only to a few nearest-neighbor modes of the same wavetype (e.g. modes having the same polarizations). In nearest neighbor energy transfer, lower order modes couple to the nearest lower order modes and higher order modes transfer energy to the nearest higher order mode. With the introduction of even modest amounts of anisotropy, it becomes possible for higher order modes to directly transfer energy into lower order modes without cascading down through multiple nearest neighbor

interactions.

An investigation has been carried out on how the anisotropic elastic stiffness tensor affects eigenfunctions, phase and group velocity dispersion curves as a function of frequency or symmetry axis orientation (angular dispersion curve), and energy transfer between modes. The magnitude of anisotropy as well as the direction of the symmetry axis have been observed to be of equal importance. Any rotation of the symmetry axis away from vertical (e.g. non-horizontal bedding planes) will cause energy to be transferred between the modes, even if lateral variation is weak. Heterogeneity is very efficient at redistributing energy among modes in anisotropic media. The combination of lateral heterogeneity and anisotropy appears to be effective at scattering a signal, and energy is redistributed broadly among all of the propagating modes. It has been demonstrated that an elastic treatment of the bottom and subbottom of the shallow water environment at low frequencies is necessary for understanding the propagation of the seismo-acoustic energy for tilted anisotropy.

ACKNOWLEDGMENTS

This research supported by the Office of Naval Research and the Applied Physics Laboratory, University of Washington. Thanks to P. Wessel and W.H.F Smith for the availability GMT mapping software.

REFERENCES

Alenitsyn, A., 1998. Double wave of Stoneley type on the interface of a stratified fluid layer and an elastic solid half-space, *J. Acoust. Soc. Am.*, **103**, 795-800.

Aki, K. and Richards, P.G., 1980. *Quantitative Seismology, Vol. I*, W. H. Freeman and Company, New York, New York.

Auld, B.A., 1990. *Acoustic Fields and Waves in Solids*, Vol. I, 2nd ed., Krieger, Malabar, FL.

Backus, G.E., 1962. Long-Wave Elastic Anisotropy Produced by Horizontal Layering *J. Geophys. Research*, **67**, 4427-4440.

Backus, G.E., 1965. Possible Forms of Seismic Anisotropy of the Uppermost Mantle under Oceans *J. Geophys. Research*, **70**, 3429-3439.

Berge, P.A., Mallick, S., Fryer, G.J., Barstow, N., Carter, J.A., Sutton, G.H., and Ewing, J.I., 1991. In *situ* measurement of transverse isotropy in shallow-water marine sediments, *Geophys. J. Int.*, **104**, 241-254.

Budden, K.G., F.R.S and M. Eve, 1975. Degenerate modes in the Earth-ionosphere waveguide, *Proc. R. Soc. Lond. A.*, **342**, 175-190.

Burridge, R. and Knopoff, L., 1964. Body-force equivalents for seismic dislocations, *Bull. seism. Soc. Am.*, **54**, 1875-1888.

Carlson, R.L., Schafternaar, C.H., and Moore, R.P.,, 1984. Causes of compressional-wave anisotropy in carbonate-bearing, deep-sea sediments, *Geophysics.*, **49**, 525-532.

Chen, X., 1993. A systematic and efficient method of computing normal modes for multilayered halfspace, *Geophys. J. Int.*, **115**, 391-409.

Chiaruttini, C., Costa, G., and Panza, G.F.,, 1985. Wave propagation in multilayered media: the effect of waveguides in oceanic and continental Earth models, *J. Geophys.*, **58**, 189-196.

Crampin, S., 1981. A review of wave motion in anisotropic and cracked elastic-media, *Wave Motion*, **3**, 343-391.

Crampin, S., 1984. An introduction to wave propagation in anisotropic media, *Geophys. J. R. Astr. Soc.*, **760**, 17-28.

Crampin, S., 1989. Suggestions for a consistent terminology for seismic anisotropy, *Geophys. Prospecting*, **37**, 753-777.

Crampin, S., 1991. Effects of point singularities on shear-wave propagation in sedimentary basins, *Geophys. J. Int.*, **107**, 531-543.

Ewing J., Carter J.A., Sutton G.H., and Barstow N., 1992. Shallow-water sediment properties derived from high-frequency shear and interface waves *J. Acoust. Soc. Am.*, **97**, 4739-4762.

Friedman, S.P., and Jones, S.B., 2001. Measurement and approximate path analysis of the pore-scale-induced anisotropy factor of an unsaturated porous medium, *Water Resources Research*, **37**, 2929-2942.

Hughes, S.J., Ellis, D.D., Chapman, D.M.F., and Staal, P.R., 1990. Low-frequency acoustic propagation loss in shallow water over hard-rock seabeds covered by a thin layer of elastic-solid sediment, *J. Acoust. Soc. Am.*, **88**, 283-297.

Kennett, B.L.N. and Clarke, T.J., 1983. Seismic waves in a stratified half-space –IV: P-SV wave decoupling and surface wave dispersion, *Geophys. J. R. Astr. Soc.*, **72**, 633-645.

Kennett, B.L.N., 1983. *Seismic wave propagation in stratified media*, Cambridge University Press, New York.

Lapwood, E.R., 1975. The Effect of Discontinuities in Density and Rigidity on Torsional Eigenfrequencies of the Earth, *Geophys. J. R. Astr. Soc.*, **40**, 453-464.

Love, A.E.H, 1944. *A Treatise on the Mathematical Theory of Elasticity*, Dover, New York, New York.

Mallick, S. and Frazer, L.N., 1991. Reflection/transmission coefficients and azimuthal anisotropy in marine seismic studies, *Geophys. J. Int.*, **105**, 241-252.

Martin, B.E., and Thomson, C.J., 1997. Modelling surface waves in anisotropic structures II: Examples, *Phys. Earth Planet. Inter.*, **103**, 253-297.

Maupin, V., 1988. Surface waves across 2-D structures: a method based on coupled local modes, *Geophys. J.*, **93**, 173-185.

Maupin, V., 1989. Surface waves in weakly anisotropic structures: on the use of ordinary or quasi-degenerate perturbation methods, *Geophys. J.*, **98**, 553-563.

Mochizuki, E., 1997. Nonuniqueness of Two-Dimensional Anisotropic Tomography, *Bull. seism. Soc. Am.*, **87**, 261-264.

Muyzert, E., and Snieder, R., 2000. An alternative parameterization for surface waves in a transverse isotropic medium, *Phys. Earth Planet. Inter.*, **118**, 125-133.

Nye, J.F., 1957. *Physical Properties of Crystals*, Oxford University Press, London.

Odom, R.I., Park, M., Mercer, J.A., Crosson, R.S. & Paik, P., 1996. Effects of transverse isotropy on modes and mode coupling in shallow water, *J. Acoust. Soc. Am.*, **100**, 2079-2092.

Okaya, D.A. and McEvilly, T.V., 2003. Elastic wave propagation in anisotropic crustal material possessing arbitrary internal tilt, *Geophys. J. Int.*, **153**, 344-358.

Park, J., 1996. Surface waves in layered anisotropic structures, *Geophys. J. Int.*, **126**, 173-183.

Park, M. and Odom, R.I., 1998. Effects of elastic heterogeneities and anisotropy on mode coupling and signals in shallow water, *J. Acoust. Soc. Am.*, **104**, 747-757.

Park, M. and Odom, R.I., 1999. The effect of stochastic rough interfaces on coupled-mode elastic waves, *Geophys. J. Int.*, **136**, 123-143.

Park, M., Odom, R.I., and Soukup, D., 2001. Modal scattering: a key to understanding oceanic T-waves, *Geophys. Res. Lett.*, **29**, 401-404.

Park, M., 1997. Effects of anisotropy and lateral heterogeneities on elastic waves and mode coupling in shallow water, Ph.D. disseration, University of Washington.

Romanowicz, B. and Snieder, R., 1988. A new formalism for the effect of lateral heterogeneity on normal modes and surface waves - II. General anisotropic perturbation, *Geophys. J.*, **93**, 91-99.

Saito, M., 1988. DISPER80: A Subroutine Package for the Calculation of Seismic Normal-Mode Solutions, in *SEISMOLOGICAL ALGORITHMS: Computational Methods and Computer Programs*, pp. 293-319, ed. Doornbos, D., Academic, San Diego, California.

Schoenberg, M. and Costa, J., 1991. The insensitivity of reflected SH waves to anisotropy in an underlying layered medium, *Geophys. Prospecting*, **39**, 985-1003.

Shearer, P.M. and Orcutt, J.A., 1986. Compressional and shear wave anisotropy in the oceanic lithosphere - the Ngendei seismic refraction experiment, *Geophys. J. R. Astr. Soc.*, **87**, 967-1003.

Stoll, R.D., Bryan G.M., and Bautista, E.O., 1994. Measuring lateral variability of sediment geoacoustic properties, *J. Acoust. Soc. Am.*, **96**, 427-438.

Takeuchi, H. & Saito, M., 1972. Seismic surface waves, in *Seismology: Surface waves and earthquake oscillations* (methods in computational physics, Vol. 11), pp. 217-295, ed. Bolt, B.A., Academic Press, New York.

Thomsen, L., 1986. Weak elastic anisotropy, *Geophysics.*, **51**, 1954-1966.

Thomson, C.J., 1997. Modelling surface waves in anisotropic structures I: Theory, *Phys. Earth Planet. Inter.*, **103**, 195-203.

Tromp, J., 1994. A coupled local-mode analysis of surface-wave propagation in a laterally heterogeneous waveguide, *Geophys. J. Int.*, **117**, 153-161.

Wessel, P. and Smith, W. H. F., 1991. Free software helps map and display data, *EOS Trans. AGU*, **72**, 441

Winterstein, D.F., 1990. Velocity anisotropy terminology for geophysicists, *Geophysics.*, **55**, 1070-1088.

Zhu, J., and Dorman, J., 2000. Two-dimensional, three-component wave propagation in a transversely isotropic medium with arbitrary-orientation–finite-element modeling *Geophysics.*, **65**, 934-942.

A Elastic Stiffness Tensor and Matrix Notation

The fourth order elastic stiffness tensor C_{iklj} has symmetries that allow the 21 independent elements to be expressed in more compact matrix notations. The elastic stiffness tensor obeys the following symmetry:

$$C_{iklj} = C_{kilj} = C_{ikjl} = C_{ljik}.$$

which reduces the 81 components of C_{iklj} to at most 21 independent components.

The indices of the fourth order elastic stiffness tensor are $iklj$ rather than the conventional $ijkl$ in order to facilitate the mapping between tensor notation and the matrix notation of Woodhouse (1974). Woodhouse's notation (1974) and abbreviated subscript notation (e.g. Auld, 1990) describe the exact same elastic parameters from the elastic stiffness tensor C_{iklj}. However, the Woodhouse matrix and the abbreviated subscript matrix are not equivalent.

$\mathbf{C}$	$=$	C_{iklj}	fourth order elastic stiffness tensor
${}^{a}\mathbf{C}$	$=$	${}^{a}C_{IJ}$	6×6 abbreviated subscript elastic stiffness matrix
${}^{w}\mathbf{C}$	$=$	$({}^{w}C_{ij})_{kl}$	9×9 Woodhouse elastic stiffness matrix
${}^{w}C_{ij}$			3×3 Woodhouse submatrix

Lower case suffixes such as $iklj$ have values that range from $i, k, l, j = 1, 2, 3$. Upper case suffixes such as IJ have values that range from $I, J = 1, 2, 3, 4, 5, 6$. The individual elements of the elastic stiffness tensor can be put into a matrix format by using an abbreviated subscript notation, also known as Voigt notation (Nye, 1957) or matrix notation. Table $A.1$ below describes how to transfer between traditional fourth order tensor notation

and the abbreviated subscript notation for the individual elements of C_{iklj} and C_{IJ}.

[Table 6 about here.]

The four suffixes $iklj$ are replaced with two suffixes IJ. Considering the Woodhouse elastic stiffness matrix first, which is composed of nine submatrices:

$$ {}^{w}\mathbf{C} = ({}^{w}C_{ij})_{kl} = \begin{bmatrix} ({}^{w}C_{11})_{kl} & ({}^{w}C_{12})_{kl} & ({}^{w}C_{13})_{kl} \\ ({}^{w}C_{21})_{kl} & ({}^{w}C_{22})_{kl} & ({}^{w}C_{23})_{kl} \\ ({}^{w}C_{31})_{kl} & ({}^{w}C_{32})_{kl} & ({}^{w}C_{33})_{kl} \end{bmatrix} \tag{45} $$

The 9×9 Woodhouse matrix is a symmetric matrix, and there are only six unique submatrices, where:

$$ {}^{w}C_{ij} = {}^{w}C_{ij}{}^{T} = {}^{w}C_{ji} = {}^{w}C_{ji}{}^{T} \tag{46} $$

The elements of the Woodhouse submatrices ${}^{w}\mathbf{C}_{ij}$ expressed in traditional fourth order subscript notation, composing the 9×9 Woodhouse matrix:

$$ {}^{w}\mathbf{C} = \left[\begin{array}{ccc:ccc:ccc} C_{1111} & C_{1121} & C_{1131} & C_{1112} & C_{1122} & C_{1132} & C_{1113} & C_{1123} & C_{1133} \\ C_{1211} & C_{1221} & C_{1231} & C_{1212} & C_{1222} & C_{1232} & C_{1213} & C_{1223} & C_{1233} \\ C_{1311} & C_{1321} & C_{1331} & C_{1312} & C_{1322} & C_{1332} & C_{1313} & C_{1323} & C_{1333} \\ \hdashline C_{2111} & C_{2121} & C_{2131} & C_{2112} & C_{2122} & C_{2132} & C_{2113} & C_{2123} & C_{2133} \\ C_{2211} & C_{2221} & C_{2231} & C_{2212} & C_{2222} & C_{2232} & C_{2213} & C_{2223} & C_{2233} \\ C_{2311} & C_{2321} & C_{2331} & C_{2312} & C_{2322} & C_{2332} & C_{2313} & C_{2323} & C_{2333} \\ \hdashline C_{3111} & C_{3121} & C_{3131} & C_{3112} & C_{3122} & C_{3132} & C_{3113} & C_{3123} & C_{3133} \\ C_{3211} & C_{3221} & C_{3231} & C_{3212} & C_{3222} & C_{3232} & C_{3213} & C_{3223} & C_{3233} \\ C_{3311} & C_{3321} & C_{3331} & C_{3312} & C_{3322} & C_{3332} & C_{3313} & C_{3323} & C_{3333} \end{array}\right] \tag{47} $$

The elements of the Woodhouse submatrices as expressed in abbreviated subscript notation, composing the 9×9 Woodhouse matrix:

$$
{}^{w}\mathbf{C} = \left[\begin{array}{ccc:ccc:ccc}
C_{11} & C_{16} & C_{15} & C_{16} & C_{12} & C_{14} & C_{15} & C_{14} & C_{13} \\
C_{61} & C_{66} & C_{65} & C_{66} & C_{62} & C_{64} & C_{65} & C_{64} & C_{63} \\
C_{51} & C_{56} & C_{55} & C_{56} & C_{52} & C_{54} & C_{55} & C_{54} & C_{53} \\
\hdashline
C_{61} & C_{66} & C_{65} & C_{66} & C_{62} & C_{64} & C_{65} & C_{64} & C_{63} \\
C_{21} & C_{26} & C_{25} & C_{26} & C_{22} & C_{24} & C_{25} & C_{24} & C_{23} \\
C_{41} & C_{46} & C_{45} & C_{46} & C_{42} & C_{44} & C_{45} & C_{44} & C_{43} \\
\hdashline
C_{51} & C_{56} & C_{55} & C_{56} & C_{52} & C_{54} & C_{55} & C_{54} & C_{53} \\
C_{41} & C_{46} & C_{45} & C_{46} & C_{42} & C_{44} & C_{45} & C_{44} & C_{43} \\
C_{31} & C_{36} & C_{35} & C_{36} & C_{32} & C_{34} & C_{35} & C_{34} & C_{33}
\end{array}\right] \tag{48}
$$

The above forms of the ${}^{w}\mathbf{C}$ are valid for any triclinic anisotropic medium with 21 independent constants, as well as for any medium with a higher degree of symmetry, such as TI. Substituting the Love notation (1944) elastic constants into the Woodhouse matrix for a TI elastically symmetric medium.

For $\hat{s}(\theta, \varphi) = \hat{s}(0°, 0°) = \hat{z}$

$$
{}^{w}\mathbf{C} = \left[\begin{array}{ccc:ccc:ccc}
A & 0 & 0 & 0 & H & 0 & 0 & 0 & F \\
0 & N & 0 & N & 0 & 0 & 0 & 0 & 0 \\
0 & 0 & L & 0 & 0 & 0 & L & 0 & 0 \\
\hdashline
0 & N & 0 & N & 0 & 0 & 0 & 0 & 0 \\
H & 0 & 0 & 0 & A & 0 & 0 & 0 & F \\
0 & 0 & 0 & 0 & 0 & L & 0 & L & 0 \\
\hdashline
0 & 0 & L & 0 & 0 & 0 & L & 0 & 0 \\
0 & 0 & 0 & 0 & 0 & L & 0 & L & 0 \\
F & 0 & 0 & 0 & F & 0 & 0 & 0 & C
\end{array}\right] \tag{49}
$$

For $\hat{s}(\theta,\varphi) = \hat{s}(90°, 0°) = \hat{x}$

$$
{}^{w}\mathbf{C} = \left[\begin{array}{ccc:ccc:ccc}
C & 0 & 0 & 0 & F & 0 & 0 & 0 & F \\
0 & L & 0 & L & 0 & 0 & 0 & 0 & 0 \\
0 & 0 & L & 0 & 0 & 0 & L & 0 & 0 \\
\hdashline
0 & L & 0 & L & 0 & 0 & 0 & 0 & 0 \\
F & 0 & 0 & 0 & A & 0 & 0 & 0 & H \\
0 & 0 & 0 & 0 & 0 & N & 0 & N & 0 \\
\hdashline
0 & 0 & L & 0 & 0 & 0 & L & 0 & 0 \\
0 & 0 & 0 & 0 & 0 & N & 0 & N & 0 \\
F & 0 & 0 & 0 & H & 0 & 0 & 0 & A
\end{array}\right] \tag{50}
$$

For $\hat{s}(\theta,\varphi) = \hat{s}(90°, 90°) = \hat{y}$

$$
{}^{w}\mathbf{C} = \left[\begin{array}{ccc:ccc:ccc}
A & 0 & 0 & 0 & F & 0 & 0 & 0 & H \\
0 & L & 0 & L & 0 & 0 & 0 & 0 & 0 \\
0 & 0 & N & 0 & 0 & 0 & N & 0 & 0 \\
\hdashline
0 & L & 0 & L & 0 & 0 & 0 & 0 & 0 \\
F & 0 & 0 & 0 & C & 0 & 0 & 0 & F \\
0 & 0 & 0 & 0 & 0 & L & 0 & L & 0 \\
\hdashline
0 & 0 & N & 0 & 0 & 0 & N & 0 & 0 \\
0 & 0 & 0 & 0 & 0 & L & 0 & L & 0 \\
H & 0 & 0 & 0 & F & 0 & 0 & 0 & A
\end{array}\right] \tag{51}
$$

The 6×6 abbreviated subscript matrix is also a symmetric matrix, with the possibility of 21 unique and independent elements where:

$$
{}^{a}C_{IJ} = {}^{a}C_{IJ}{}^{T} = {}^{a}C_{JI} = {}^{a}C_{JI}{}^{T}. \tag{52}
$$

Any additional symmetry would reduce the number of independent elements. The elements of the abbreviated subscript elastic stiffness matrix expressed

in traditional fourth order tensor notation for a general triclinic medium.

$$ {}^{a}\mathbf{C} = \begin{bmatrix} C_{1111} & C_{1122} & C_{1133} & C_{1123} & C_{1113} & C_{1112} \\ C_{2211} & C_{2222} & C_{2233} & C_{2223} & C_{2213} & C_{2212} \\ C_{3311} & C_{3322} & C_{3333} & C_{3323} & C_{3313} & C_{3312} \\ C_{2311} & C_{2322} & C_{2333} & C_{2323} & C_{2313} & C_{2312} \\ C_{1311} & C_{1322} & C_{1333} & C_{1323} & C_{1313} & C_{1312} \\ C_{1211} & C_{1222} & C_{1233} & C_{1223} & C_{1213} & C_{1212} \end{bmatrix} \tag{53} $$

The abbreviated subscript elastic stiffness matrix with the elements expressed in abbreviated subscript notation.

$$ {}^{a}\mathbf{C} = \begin{bmatrix} C_{11} & C_{12} & C_{13} & C_{14} & C_{15} & C_{16} \\ C_{21} & C_{22} & C_{23} & C_{24} & C_{25} & C_{26} \\ C_{31} & C_{32} & C_{33} & C_{34} & C_{35} & C_{36} \\ C_{41} & C_{42} & C_{43} & C_{44} & C_{45} & C_{46} \\ C_{51} & C_{52} & C_{53} & C_{54} & C_{55} & C_{56} \\ C_{61} & C_{62} & C_{63} & C_{64} & C_{65} & C_{66} \end{bmatrix} \tag{54} $$

Consider a TI elastically symmetric medium as used in the main text of the paper. The elastic moduli are expressed in Love notation (1944).

For $\hat{s}(\theta, \varphi) = \hat{s}(0°, 0°) = \hat{z}$

$$ {}^{a}\mathbf{C} = \begin{bmatrix} A & H & F & 0 & 0 & 0 \\ H & A & F & 0 & 0 & 0 \\ F & F & C & 0 & 0 & 0 \\ 0 & 0 & 0 & L & 0 & 0 \\ 0 & 0 & 0 & 0 & L & 0 \\ 0 & 0 & 0 & 0 & 0 & N \end{bmatrix} \qquad \text{where } H = A - 2N \tag{55} $$

For $\hat{s}(\theta,\varphi) = \hat{s}(90°, 0°) = \hat{x}$

$$ {}^{a}\mathbf{C} = \begin{bmatrix} C & F & F & 0 & 0 & 0 \\ F & A & H & 0 & 0 & 0 \\ F & H & A & 0 & 0 & 0 \\ 0 & 0 & 0 & N & 0 & 0 \\ 0 & 0 & 0 & 0 & L & 0 \\ 0 & 0 & 0 & 0 & 0 & L \end{bmatrix} \qquad \text{where } H = A - 2N \tag{56} $$

For $\hat{s}(\theta,\varphi) = \hat{s}(90°, 90°) = \hat{y}$

$$ {}^{a}\mathbf{C} = \begin{bmatrix} A & F & H & 0 & 0 & 0 \\ F & C & F & 0 & 0 & 0 \\ H & F & A & 0 & 0 & 0 \\ 0 & 0 & 0 & L & 0 & 0 \\ 0 & 0 & 0 & 0 & N & 0 \\ 0 & 0 & 0 & 0 & 0 & L \end{bmatrix} \qquad \text{where } H = A - 2N \tag{57} $$

The individual elements for a TI medium with an arbitrary symmetry axis $\hat{s}(\theta,\phi)$ can be determined by equation (11) from the main text. The elements of ${}^{a}\mathbf{C}$ will be linear combinations of the elastic moduli A, C, F, L, N.

B Differential Operator A

The differential operator **A** from the equation of motion (17) in the main text and in equation (98) below is described in greater detail.

$$\frac{\partial \mathbf{u}}{\partial x} = \mathbf{A}\mathbf{u} - \mathbf{F} \tag{58}$$

where **u** is the stress-displacement vector, **A** is a differential operator which contains the combinations of the elastic stress matrix ${}^{w}C_{ij}$ and its derivatives, and **F** is an external force.

The operator lacks any horizontal derivatives and the only derivatives are vertical derivatives of the elastic moduli, horizontal slowness, and eigenfunctions. For a fluid medium or a solid anisotropic structure, the differential operator **A** may be expressed in terms of sub-operators:

$$\mathbf{A} = \begin{pmatrix} A^{11} & A^{12} \\ A^{21} & A^{22} \end{pmatrix} \tag{59}$$

For a solid triclinic anisotropic medium, the sub-operators are:

$$\begin{aligned} A^{11} &= \left(-({}^{w}C_{11}^{-1})({}^{w}C_{13})\frac{\partial}{\partial z} + ({}^{w}C_{11}^{-1})({}^{w}C_{12})ip \right), \\ A^{12} &= \left({}^{w}C_{11}^{-1}\right), \\ A^{21} &= \left(-\rho\omega^2 - \frac{\partial}{\partial z}({}^{w}Q_{33}\frac{\partial}{\partial z}) + ip\,{}^{w}Q_{23}\frac{\partial}{\partial z} + \frac{\partial}{\partial z}({}^{w}Q_{32}ip) + p^2({}^{w}Q_{22}) \right), \\ A^{22} &= \left(-\frac{\partial}{\partial z}({}^{w}C_{31})({}^{w}C_{11}^{-1}) + ip({}^{w}C_{21})({}^{w}C_{11}^{-1}) \right), \end{aligned} \tag{60}$$

where the ${}^{w}Q_{ij}$ matrix is defined as:

$${}^{w}Q_{ij} = {}^{w}C_{ij} - ({}^{w}C_{i1})({}^{w}C_{11}^{-1})({}^{w}C_{1j}) \tag{61}$$

This general form is valid for any triclinic anisotropic structure. The differential operator **A** for a TI elastically symmetric medium can be obtained by

substituting the elastic stiffness submatrices from Appendix A into equations (60),(60),100), and (100). The differential operator **A** is then expressed analytically for the case when the symmetry axis $\hat{s}$ is aligned with the Cartesian coordinate axes.

For $\hat{s}(\theta,\varphi) = \hat{s}(0°,0°) = \hat{z}$:

$$A^{11} = \begin{pmatrix} 0 & ik_y\frac{A-2N}{A} & -\frac{F}{A}\frac{\partial}{\partial z} \\ ik_y & 0 & 0 \\ -\frac{\partial}{\partial z} & 0 & 0 \end{pmatrix},$$

$$A^{12} = \begin{pmatrix} \frac{1}{A} & 0 & 0 \\ 0 & \frac{1}{N} & 0 \\ 0 & 0 & \frac{1}{L} \end{pmatrix},$$

$$A^{21} = \begin{pmatrix} -\rho\omega^2 & 0 & 0 \\ 0 & -\rho\omega^2 - \frac{\partial}{\partial z}\left(L\frac{\partial}{\partial z}\right) + {k_y}^2\left(\frac{4N(N-A)}{A}\right) & ik_y\frac{2NF}{A}\frac{\partial}{\partial z} + \frac{\partial}{\partial z}\left(ik_yL\right) \\ 0 & ik_yL\frac{\partial}{\partial z} + \frac{\partial}{\partial z}\left(ik_y\frac{2NF}{A}\right) & -\rho\omega^2 - \frac{\partial}{\partial z}\left(\frac{AC-F^2}{A}\frac{\partial}{\partial z}\right) + k_y^2L \end{pmatrix},$$

$$A^{22} = \begin{pmatrix} 0 & ik_y & -\frac{\partial}{\partial z} \\ ik_y\frac{A-2N}{A} & 0 & 0 \\ -\frac{\partial}{\partial z}\frac{F}{A} & 0 & 0 \end{pmatrix}, \tag{62}$$

This is the same result found by Park and Odom (1997).

For $\hat{s}(\theta,\varphi) = \hat{s}(90°, 0°) = \hat{x}$:

$$
\begin{aligned}
A^{11} &= \begin{pmatrix} 0 & ik_y\frac{F}{C} & -\frac{F}{C}\frac{\partial}{\partial z} \\ ik_y & 0 & 0 \\ -\frac{\partial}{\partial z} & 0 & 0 \end{pmatrix}, \\
A^{12} &= \begin{pmatrix} \frac{1}{C} & 0 & 0 \\ 0 & \frac{1}{L} & 0 \\ 0 & 0 & \frac{1}{L} \end{pmatrix}, \\
A^{21} &= \begin{pmatrix} -\rho\omega^2 & 0 & 0 \\ 0 & -\rho\omega^2 - \frac{\partial}{\partial z}\left(N\frac{\partial}{\partial z}\right) + {k_y}^2\left(\frac{AC-F^2)}{C}\right) & ik_y\left(\frac{AC-2CN-F^2}{C}\right)\frac{\partial}{\partial z} + \frac{\partial}{\partial z}\left(ik_yN\right) \\ 0 & ik_yN\frac{\partial}{\partial z} + \frac{\partial}{\partial z}\left(ik_y\frac{AC-2CN-F^2}{C}\right) & -\rho\omega^2 - \frac{\partial}{\partial z}\left(\frac{AC-F^2}{C}\frac{\partial}{\partial z}\right) + k_y^2N \end{pmatrix}, \\
A^{22} &= \begin{pmatrix} 0 & ik_y & -\frac{\partial}{\partial z} \\ ik_y\frac{F}{C} & 0 & 0 \\ -\frac{\partial}{\partial z}\frac{F}{C} & 0 & 0 \end{pmatrix},
\end{aligned}
\tag{63}
$$

For $\hat{s}(\theta,\varphi) = \hat{s}(90°, 90°) = \hat{y}$:

$$A^{11} = \begin{pmatrix} 0 & ik_y\frac{F}{A} & -\frac{A-2N}{A}\frac{\partial}{\partial z} \\ ik_y & 0 & 0 \\ -\frac{\partial}{\partial z} & 0 & 0 \end{pmatrix},$$

$$A^{12} = \begin{pmatrix} \frac{1}{A} & 0 & 0 \\ 0 & \frac{1}{L} & 0 \\ 0 & 0 & \frac{1}{N} \end{pmatrix},$$

$$A^{21} = \begin{pmatrix} -\rho\omega^2 & 0 & 0 \\ 0 & -\rho\omega^2 - \frac{\partial}{\partial z}\left(L\frac{\partial}{\partial z}\right) + {k_y}^2\left(\frac{AC-F^2)}{A}\right) & ik_y\left(\frac{2NF}{A}\right)\frac{\partial}{\partial z} + \frac{\partial}{\partial z}\left(ik_yL\right) \\ 0 & ik_yL\frac{\partial}{\partial z} + \frac{\partial}{\partial z}\left(ik_y\frac{2NF}{A}\right) & -\rho\omega^2 - \frac{\partial}{\partial z}\left(\frac{4N(N-A)}{A}\frac{\partial}{\partial z}\right) + k_y^2L \end{pmatrix},$$

$$A^{22} = \begin{pmatrix} 0 & ik_y & -\frac{\partial}{\partial z} \\ ik_y\frac{F}{A} & 0 & 0 \\ -\frac{\partial}{\partial z}\frac{A-2N}{A} & 0 & 0 \end{pmatrix}, \tag{64}$$

Additional symmetry, where the TI elastic symmetry reduces to isotropic symmetry may be considered. When $A = C$, $L = N$, $H = F$, and $F = A - 2L$, then all planes within medium are symmetry planes, and therefore

all directions are equivalent:

$$A^{11} = \begin{pmatrix} 0 & ik_y\frac{F}{A} & -\frac{F}{A}\frac{\partial}{\partial z} \\ ik_y & 0 & 0 \\ -\frac{\partial}{\partial z} & 0 & 0 \end{pmatrix},$$

$$A^{12} = \begin{pmatrix} \frac{1}{A} & 0 & 0 \\ 0 & \frac{1}{L} & 0 \\ 0 & 0 & \frac{1}{L} \end{pmatrix},$$

$$A^{21} = \begin{pmatrix} -\rho\omega^2 & 0 & 0 \\ 0 & -\rho\omega^2 - \frac{\partial}{\partial z}\left(L\frac{\partial}{\partial z}\right) + {k_y}^2\left(\frac{A^2-F^2)}{A}\right) & ik_y\left(\frac{AF-F^2}{A}\right)\frac{\partial}{\partial z} + \frac{\partial}{\partial z}\left(ik_yL\right) \\ 0 & ik_yL\frac{\partial}{\partial z} + \frac{\partial}{\partial z}\left(ik_y(\frac{AF-F^2}{A})\right) & -\rho\omega^2 - \frac{\partial}{\partial z}\left(\frac{F^2-A^2}{A}\frac{\partial}{\partial z}\right) + k_y^2L \end{pmatrix},$$

$$A^{22} = \begin{pmatrix} 0 & ik_y & -\frac{\partial}{\partial z} \\ ik_y\frac{F}{A} & 0 & 0 \\ -\frac{\partial}{\partial z}\frac{F}{A} & 0 & 0 \end{pmatrix}, \tag{65}$$

where $A = \lambda + 2\mu$, $L = \mu$, and $F = \lambda$.

This is the same result as reported by Park and Odom (1997) and Maupin (1988).

Consider the case where $\mu = 0$ and the isotropic medium becomes an isotropic fluid. As stated by Maupin (1988), the ${}^wC_{11}$ matrix becomes singular for a fluid layer. A simple solution is to define the ${}^wC_{11}$ matrix and its inverse ${}^wC_{11}^{-1}$ within a fluid as Kennett (1983) does in his monograph:

$$({}^wC_{11})_{fluid} = \begin{pmatrix} A & 0 & 0 \\ 0 & 0 & 0 \\ 0 & 0 & 0 \end{pmatrix} \quad ({}^wC_{11}^{-1})_{fluid} = \begin{pmatrix} \frac{1}{A} & 0 & 0 \\ 0 & 0 & 0 \\ 0 & 0 & 0 \end{pmatrix} \tag{66}$$

Therfore, a form of the differential operator and equation of motion for any

fluid layers may be formulated.

$$A^{11} = \begin{pmatrix} 0 & ik_y & -\frac{\partial}{\partial z} \\ ik_y & 0 & 0 \\ -\frac{\partial}{\partial z} & 0 & 0 \end{pmatrix},$$

$$A^{12} = \begin{pmatrix} \frac{1}{A} & 0 & 0 \\ 0 & 0 & 0 \\ 0 & 0 & 0 \end{pmatrix},$$

$$A^{21} = \begin{pmatrix} -\rho\omega^2 & 0 & 0 \\ 0 & -\rho\omega^2 & 0 \\ 0 & 0 & -\rho\omega^2 \end{pmatrix},$$

$$A^{22} = \begin{pmatrix} 0 & ik_y & -\frac{\partial}{\partial z} \\ ik_y & 0 & 0 \\ -\frac{\partial}{\partial z} & 0 & 0 \end{pmatrix}, \tag{67}$$

After some algebra, the system of equations can be reduced to a two component displacement-stress vector form.

$$A_{fluid} = \begin{pmatrix} 0 & -\frac{ik_y{}^2}{\rho\omega^2} + \frac{\partial}{\partial z}\frac{1}{\rho\omega^2}\frac{\partial}{\partial z} + \frac{1}{A} \\ -\rho\omega^2 & 0 \end{pmatrix}, \tag{68}$$

where u, w_2, w_3, and t are defined as:

$$\mathrm{u} = (\mathrm{w}_1, t)^T \tag{69}$$

$$\mathrm{w}_2 = \frac{ik_y}{\rho\omega^2} t \tag{70}$$

$$\mathrm{w}_3 = -\frac{1}{\rho\omega^2}\frac{\partial t}{\partial z} \tag{71}$$

$$t = t_{ii} \tag{72}$$

This is Maupin's (1988) result for a fluid layer. The fluid/solid coupling terms used in the main text are the same as those reported in Maupin (1988).

Tromp (1994) also has described fluid/solid coupling terms using a slightly different modal notation.

C Coupling Matrix $\mathbf{B}_{qr}$

The $\mathbf{B}_{qr}$ coupling matrix as described by Maupin(1988) and the main text is defined as:

$$\mathbf{B}_{qr} = \left(-\left\langle \mathbf{u}^q, \frac{\partial \mathbf{u}^r}{\partial x} \right\rangle + i \sum_n \dot{h}_n \mathbf{w}^{q*} [\mathbf{t}^r]_n \right) \exp\left(i \int_0^x (k^q - k^r) d\xi \right) \quad (73)$$

where the Hermitian scalar product is defined as

$$\langle \mathbf{u}^q, \mathbf{u}^r \rangle = i \int_0^\infty (\mathbf{w}^q \mathbf{t}^r - \mathbf{t}^q \mathbf{w}^r)\, dz \quad (74)$$

The traction $\mathbf{t}$ may be discontinuous across the interfaces, resulting in the evaluation of an improper integral. This leads to interface summation terms that include jumps across the boundary discontinuities. The coupling matrix for an unperturbed, deterministic structure has the expanded form:

$$\begin{aligned}
B_{qr} &= \frac{1}{k^q - k^r} \left(\int_0^{h(x)} \left(w_1^{q*} \dot{\rho} \omega^2 w_1^r + \mathbf{t}^{q*} \left(\frac{1}{\lambda} - \frac{\dot{p}^2}{\rho \omega^2} \right) \mathbf{t}^r - \frac{\partial \mathbf{t}^{q*}}{\partial z} \frac{\dot{1}}{\rho \omega^2} \frac{\partial \mathbf{t}^r}{\partial z} \right) dz \right. \\
&+ \int_{h(x)}^\infty \left(\mathbf{w}^{q*} \dot{\rho} \omega^2 \mathbf{w}^r - \frac{\partial \mathbf{w}^{q*}}{\partial z} \dot{Q}_{33} \frac{\partial \mathbf{w}^r}{\partial z} - \mathbf{w}^{q*} ip \dot{Q}_{23} \frac{\partial \mathbf{w}^r}{\partial z} + \frac{\partial \mathbf{w}^{q*}}{\partial z} \dot{Q}_{32} ip \mathbf{w}^r \right. \\
&- \mathbf{w}^{q*} \dot{Q}_{22} \mathbf{w}^r p^2 - \frac{\partial \mathbf{w}^{q*}}{\partial z} (C_{31} \dot{C}_{11}^{-1}) \mathbf{t}^r - \mathbf{w}^{q*} ip (C_{21} \dot{C}_{11}^{-1}) \mathbf{t}^r - \mathbf{t}^{q*} (\dot{C}_{11}^{-1} C_{13}) \frac{\partial \mathbf{w}^r}{\partial z} \\
&\left. + \mathbf{t}^{q*} (C_{11}^{-1} \dot{C}_{12}) ip \mathbf{w}^r + \mathbf{t}^{q*} \dot{C}_{11}^{-1} \mathbf{t}^r \right) dz \\
&+ \sum_n \dot{h}_n \left[-\mathbf{w}^{q*} \rho \omega^2 \mathbf{w}^r - \frac{\partial \mathbf{w}^{q*}}{\partial z} Q_{33} \frac{\partial \mathbf{w}^r}{\partial z} + \mathbf{w}^{q*} Q_{22} \mathbf{w}^r p^2 - \frac{\partial \mathbf{w}^{q*}}{\partial z} (C_{31} C_{11}^{-1}) \mathbf{t}^r \right. \\
&\left. - \mathbf{t}^{q*} (C_{11}^{-1} C_{13}) \frac{\partial \mathbf{w}^r}{\partial z} + \mathbf{t}^{q*} C_{11}^{-1} \mathbf{t}^r \right]_n \\
&- \dot{h} \left(-\frac{\partial t_{33}^{q*}}{\partial z} \frac{1}{\rho \omega^2} \frac{\partial t_{33}^r}{\partial z} - t_{33}^{q*} \left(\frac{1}{\lambda} - \frac{p^2}{\rho \omega^2} \right) t_{33}^r + w_1^{q*} \rho \omega^2 w_1^r \right)_{h(x)^-} \\
&\left. - i \dot{h} \left((k^q - k^r)(w_1^{q*} t_{33}^r + t_{33}^{q*} w_1^r) \right)_{h(x)^+} \right) \exp\left(i \int_0^x (k^q - k^r) d\xi \right) \quad (75)
\end{aligned}$$

When the material properties are constant within each layer of the model, then any derivative of the constants is zero. When the horizontal derivatives

of the elastic moduli are zero, then volume terms of the coupling matrix $\mathbf{B}_{qr}$ become zero, and only the interface terms of the $\mathbf{B}_{qr}$ matrix remain. The fluid-fluid interface terms have been neglected and their contribution to the coupling terms is assumed negligible. Therefore, in the absence of material property variations, the coupling matrix reduces to:

$$\begin{aligned}
\mathbf{B}_{qr} &= \frac{1}{k^q - k^r}\left(\sum_n \dot{h}_n \left[-\mathbf{w}^{q*}\rho\omega^2\mathbf{w}^r - \frac{\partial \mathbf{w}^{q*}}{\partial z}Q_{33}\frac{\partial \mathbf{w}^r}{\partial z} + \mathbf{w}^{q*}Q_{22}\mathbf{w}^r p^2\right.\right. \\
&\quad \left.\left. -\frac{\partial \mathbf{w}^{q*}}{\partial z}(C_{31}C_{11}^{-1})\mathbf{t}^r - \mathbf{t}^{q*}(C_{11}^{-1}C_{13})\frac{\partial \mathbf{w}^r}{\partial z} + \mathbf{t}^{q*}C_{11}^{-1}\mathbf{t}^r\right]_n \right. \\
&\quad - \dot{h}\left(-\frac{\partial t_{33}^{q*}}{\partial z}\frac{1}{\rho\omega^2}\frac{\partial t_{33}^r}{\partial z} - t_{33}^{q*}\left(\frac{1}{\lambda} - \frac{p^2}{\rho\omega^2}\right)t_{33}^r + w_1^{q*}\rho\omega^2 w_1^r\right)_{h(x)-} \\
&\quad \left. - i\dot{h}\left((k^q - k^r)(w_1^{q*}t_{33}^r + t_{33}^{q*}w_1^r)\right)_{h(x)+}\right)\exp\left(i\int_0^x (k^q - k^r)dx\right) \qquad (76)
\end{aligned}$$

We allow the material properties to vary with range within each layer. For this case all of the interface terms are zero, while the volume terms remain non-zero, giving the are the volume terms of the coupling matrix $\mathbf{B}_{qr}$

$$\begin{aligned}
B_{qr} &= \frac{1}{k^q - k^r}\left(\int_{h(x)}^{\infty}\left(\mathbf{w}^{q*}\dot{\rho}\omega^2\mathbf{w}^r - \frac{\partial \mathbf{w}^{q*}}{\partial z}\dot{Q}_{33}\frac{\partial \mathbf{w}^r}{\partial z} - \mathbf{w}^{q*}ip\dot{Q}_{23}\frac{\partial \mathbf{w}^r}{\partial z} + \frac{\partial \mathbf{w}^{q*}}{\partial z}\dot{Q}_{32}ip\mathbf{w}^r\right.\right. \\
&\quad - \mathbf{w}^{q*}\dot{Q}_{22}\mathbf{w}^r p^2 - \frac{\partial \mathbf{w}^{q*}}{\partial z}(C_{31}\dot{C}_{11}^{-1})\mathbf{t}^r - \mathbf{w}^{q*}ip(C_{21}\dot{C}_{11}^{-1})\mathbf{t}^r - \mathbf{t}^{q*}(\dot{C}_{11}^{-1}C_{13})\frac{\partial \mathbf{w}^r}{\partial z} \\
&\quad \left.\left. + \mathbf{t}^{q*}(\dot{C}_{11}^{-1}C_{12})ip\mathbf{w}^r + \mathbf{t}^{q*}\dot{C}_{11}^{-1}\mathbf{t}^r\right)dz\right.
\end{aligned}$$

D VTI Parameterization

The elastic stiffness constants in the elastic stiffness tensor, C_{iklj}, can be parameterized in a number of ways. Each parameterization results in the exact same elastic stiffness tensor. Love notation (1944), Backus notation (1965) and Takeuchi and Saito notation (1972) are each considered. The theory of Odom *et. al.* (1996) and Park *et. al.* (1997) use the Love parameterization where the five independent constants for a VTI medium are expressed as the elastic moduli A, C, F, L, N. Both relied on the Disper80 code which uses Takeuchi and Saito notation (1972) where the five independent constants are expressed as velocities α_H and β_V along with ratios of the elastic moduli χ, ϕ, η which are based on Love's notation. Park (1996) uses Backus notation (1965) where the five independent parameters of a VTI medium are the elastic moduli $\bar{A}, \bar{B}, \bar{C}, \bar{D}, \bar{E}$. The relationship between the three parameterizations is outlined below.

D.1 Love Parameterization

The ACFLN parameterization for a VTI medium can be described in terms of $\xi, \phi, \eta, \alpha_H, \beta_V$ and $\bar{A}, \bar{B}, \bar{C}, \bar{D}, \bar{E}$.

[Table 7 about here.]

D.2 Takeuchi and Saito Notation (Anderson Notation)

The anisotropy describe by Takeuchi and Saito (1972) is described by five parameters, a horizontal compressional velocity, a vertical shear velocity, a ratio of horizontal and vertical compressional velocities, a ratio of horizontal

and vertical shear velocities, and a fifth anisotropic parameter. The previous results can be substituted into the expressions given by Takeuchi and Saitio.

The Takeuchi and Saito notation can be described in terms of $ACFLN$, and $\bar{A}, \bar{B}, \bar{C}, \bar{D}, \bar{E}$.

[Table 8 about here.]

Notice that parameter ϕ is not to be confused with the angle φ in the xy-plane describing the orientation of the symmetry axis $\hat{s}$ of the TI medium.

D.3 Modified Backus Parameterization

The angular dependence of the compressional and shear velocities are treated in a similar manner to the formulas of Backus(1965), Crampin(1977), Shearer and Orcutt (1986), and Park(1996).

$$\begin{aligned} \rho\alpha^2(\xi) &= \bar{A} + \bar{B}\cos 2\xi + \bar{C}\cos 4\xi \\ \rho\beta^2(\xi) &= \bar{D} + \bar{E}\cos 2\xi \end{aligned} \tag{77}$$

The previous works related the five parameters $\bar{A}, \bar{B}, \bar{C}, \bar{D}, \bar{E}$ to the individual elastic stiffness tensor elements for a HTI, with a symmetry axis in the x-direction . These expressions are similar, except they describe the C_{iklj} elastic stiffness tensor for a VTI medium.

[Table 9 about here.]

Additional parameterizations of VTI media include the Thomsen parameterization (1986) and the alternate parameterization of Romanowicz and Snieder(1988) and Muyzert and Snieder(2000).

E Bond Transformation of TI Symmetric Structures

Any arbitrary tilt of a TI symmetric medium can be obtained by rotating through the two angles θ and φ. The Bond transformation matrices described by Auld(1990) are found below.

$$\mathbf{M} = \begin{bmatrix} a_{xx}^2 & a_{xy}^2 & a_{xz}^2 & 2a_{xy}a_{xz} & 2a_{xz}a_{xx} & 2a_{xx}a_{xy} \\ a_{yx}^2 & a_{yy}^2 & a_{yz}^2 & 2a_{yy}a_{yz} & 2a_{yz}a_{yx} & 2a_{yx}a_{yy} \\ a_{zx}^2 & a_{zy}^2 & a_{zz}^2 & 2a_{zy}a_{zz} & 2a_{zz}a_{zx} & 2a_{zx}a_{zy} \\ a_{yz}a_{zx} & a_{yy}a_{zy} & a_{yz}a_{zz} & a_{yy}a_{zz} + a_{yz}a_{zy} & a_{yz}a_{zz} + a_{yz}a_{zx} & a_{yy}a_{zx} + a_{yx}a_{zy} \\ a_{zz}a_{xx} & a_{zy}a_{xy} & a_{zz}a_{xz} & a_{xy}a_{zz} + a_{xz}a_{zy} & a_{xz}a_{zx} + a_{xx}a_{zz} & a_{xx}a_{zy} + a_{xy}a_{zx} \\ a_{xx}a_{yx} & a_{xy}a_{yy} & a_{xz}a_{yz} & a_{xy}a_{yz} + a_{xz}a_{yy} & a_{xz}a_{yx} + a_{xx}a_{yz} & a_{xx}a_{yy} + a_{xy}a_{yz} \end{bmatrix} \quad (78)$$

The Bond transformation matrix M is composed of the elements form the general transform matrix a.

$$\mathbf{a} = \begin{bmatrix} a_{xx} & a_{xy} & a_{xz} \\ a_{yx} & a_{yy} & a_{yz} \\ a_{zx} & a_{zy} & a_{zz} \end{bmatrix}$$

The general transformation matrices for rotation about the y and z axes are a^y and a^z respectively.

$$\mathbf{a}^y = \begin{bmatrix} \cos\theta & 0 & -\sin\theta \\ 0 & 1 & 0 \\ \sin\theta & 0 & \cos\theta \end{bmatrix}$$

$$\mathbf{a}^z = \begin{bmatrix} \cos\varphi & \sin\varphi & 0 \\ -\sin\varphi & \cos\varphi & 0 \\ 0 & 0 & 1 \end{bmatrix}$$

The corresponding Bond transformation matrices about the y and z axes are then M^y and M^z respectively.

$$\mathbf{M}^y = \begin{bmatrix} \cos^2\theta & 0 & \sin^2\theta & 0 & -\sin 2\theta & 0 \\ 0 & 1 & 0 & 0 & 0 & 0 \\ \sin^2\theta & 0 & \cos^2\theta & 0 & \sin 2\theta & 0 \\ 0 & 0 & 0 & \cos\theta & 0 & \sin\theta \\ \frac{1}{2}\sin 2\theta & 0 & -\frac{1}{2}\sin 2\theta & 0 & \cos 2\theta & 0 \\ 0 & 0 & 0 & -\sin\theta & 0 & \cos\theta \end{bmatrix} \tag{79}$$

$$\mathbf{M}^z = \begin{bmatrix} \cos^2\varphi & \sin^2\varphi & 0 & 0 & 0 & \sin 2\varphi \\ \sin^2\varphi & \cos^2\varphi & 0 & 0 & 0 & -\sin 2\varphi \\ 0 & 0 & 0 & 0 & 0 & 0 \\ 0 & 0 & 0 & \cos\varphi & -\sin\varphi & 0 \\ 0 & 0 & 0 & \sin\varphi & \cos\varphi & 0 \\ -\frac{1}{2}\sin 2\varphi & \frac{1}{2}\sin 2\varphi & 0 & 0 & 0 & \cos 2\varphi \end{bmatrix} \tag{80}$$

Applying the Bond transformation to the elastic stiffness matrix ${}^a\mathbf{C}$ to obtain a general rotation.

$${}^a\mathbf{C}'' = [\mathbf{R}][{}^a\mathbf{C}][\mathbf{R}]^T \qquad \text{where } \mathbf{R} = \mathbf{M}^z\mathbf{M}^y$$

The individual elements of the elastic-stiffness tensor for a TI elastically symmetric medium can be found by the following relation.

$$\begin{aligned} {}^aC''_{IJ} &= A(R_{i1}R_{j1} + R_{i2}R_{j2}) + H(R_{i1}R_{j2} + R_{i2}R_{j1}) \\ &+ F(R_{i1}R_{j3} + R_{i2}R_{j3} + R_{i3}R_{j1} + R_{i3}R_{j2}) + CR_{i3}R_{j3} \\ &+ L(R_{i4}B_{j4} + R_{i5}R_{j5}) + NR_{i6}R_{j6} \end{aligned} \tag{81}$$

The $\mathbf{R}$ transformation matrix for a general rotation of a VTI medium to any

arbitrary orientation is:

$$\mathbf{R} = \left[\begin{array}{ccc:ccc:ccc} \cos^2\theta cos^2\varphi & \sin^2\varphi & \sin^2\theta cos^2\varphi & - \sin\theta \sin 2\varphi & - \sin 2\theta \cos^2\varphi & \cos\theta \sin 2\varphi \\ \cos^2\theta \sin^2\varphi & \cos^2\varphi & \sin^2\theta \sin^2\varphi & \sin\theta \sin 2\varphi & - \sin 2\theta \sin^2\varphi & - \cos\theta \sin 2\varphi \\ \sin^2\theta & 0 & \cos^2\theta & 0 & \sin 2\theta & 0 \\ -\frac{1}{2}\sin 2\theta \sin\varphi & 0 & \frac{1}{2}\sin 2\theta \sin\varphi & \cos\theta \cos\varphi & - \cos 2\theta \sin\varphi & \sin\theta \cos\varphi \\ \frac{1}{2}\cos\theta \sin 2\varphi & 0 & -\frac{1}{2}\sin 2\theta \cos\varphi & \cos\theta \sin\varphi & \cos 2\theta \cos\varphi & \sin\theta \sin\varphi \\ -\frac{1}{2}\cos^2\theta \sin 2\varphi & \frac{1}{2}\sin 2\varphi & -\frac{1}{2}\sin^2\theta \sin 2\varphi & - \sin\theta 2\cos\varphi & \frac{1}{2}\sin 2\theta \sin 2\varphi & \cos\theta \cos 2\varphi \end{array}\right] \tag{82}$$

Once the rotated elastic moduli are determined for some symmetry axis $\hat{s}(\theta, \phi)$, they can be inserted into the elements of the differential operator A and the coupling matrix $\mathbf{B}_{qr}$. The elements of ${}^aC_{ij}$ need to be converted from abbreviated subscript notation into Woodhouse notation as done in Appendix A. It should be noted that the Bond Transformations that include rotations about both the y and z axes are best done numerically. Analytical results are not always insightful for most arbitrary symmetry axis orientations of $\hat{s}(\theta, \varphi)$.

The sensitivity of the elastic stiffness matrix to changes in θ and φ may also be considered.

$$\frac{\partial({}^a\mathbf{C})}{\partial\Delta} = \frac{\partial\mathbf{R}}{\partial\Delta}{}^a\mathbf{C}\mathbf{R}^T + \mathbf{R}{}^a\mathbf{C}\frac{\partial\mathbf{R}^T}{\partial\Delta} \qquad \text{where } \mathbf{R} = \mathbf{M}^z\mathbf{M}^y \tag{83}$$

The individual elements of the derivative of the elastic stiffness matrix with respect to the generic angle Δ is:

$$\begin{aligned}
\frac{\partial({}^{a}C_{IJ})}{\partial\Delta} &= A\left(\frac{\partial R_{i1}}{\partial\Delta}R_{j1}+R_{i1}\frac{\partial R_{j1}}{\partial\Delta}+\frac{\partial R_{i2}}{\partial\Delta}R_{j2}+R_{i2}\frac{\partial R_{j2}}{\partial\Delta}\right)\\
&+ H\left(\frac{\partial R_{i1}}{\partial\Delta}R_{j2}+R_{i1}\frac{\partial R_{j2}}{\partial\Delta}+\frac{\partial R_{i2}}{\partial\Delta}R_{j1}+R_{i2}\frac{\partial R_{j1}}{\partial\Delta}\right)\\
&+ F\left(\frac{\partial R_{i1}}{\partial\Delta}R_{j3}+R_{i1}\frac{\partial R_{j3}}{\partial\Delta}+\frac{\partial R_{i2}}{\partial\Delta}R_{j3}+R_{i2}\frac{\partial R_{j3}}{\partial\Delta}\right.\\
&+ \left.\frac{\partial R_{i3}}{\partial\Delta}R_{j1}+R_{i3}\frac{\partial R_{j1}}{\partial\Delta}+\frac{\partial R_{i3}}{\partial\Delta}R_{j2}+R_{i3}\frac{\partial R_{j2}}{\partial\Delta}\right)\\
&+ C\left(\frac{\partial R_{i3}}{\partial\Delta}R_{j3}+R_{i3}\frac{\partial R_{j3}}{\partial\Delta}\right)\\
&+ L\left(\frac{\partial R_{i4}}{\partial\Delta}R_{j4}+R_{i4}\frac{\partial R_{j4}}{\partial\Delta}+\frac{\partial R_{i5}}{\partial\Delta}R_{j5})+R_{i5}\frac{\partial R_{j5}}{\partial\Delta}\right)\\
&+ N\left(\frac{\partial R_{i6}}{\partial\Delta}R_{j6}+R_{j6}\frac{\partial R_{i6}}{\partial\Delta}\right)
\end{aligned}$$

$$\frac{\partial\mathbf{R}}{\partial\theta} = \left[\begin{array}{ccc:ccc:ccc}
-\sin 2\theta cos^2\varphi & 0 & \sin 2\theta cos^2\varphi & \cos\theta\sin 2\varphi & -2\cos 2\theta\cos^2\varphi & -\sin\theta\sin 2\varphi\\
-\sin 2\theta\sin^2\varphi & 0 & \sin 2\theta\sin^2\varphi & \cos\theta\sin 2\varphi & -2\cos 2\theta\sin^2\varphi & \sin\theta\sin 2\varphi\\
\sin 2\theta & 0 & -\sin^2\theta & 0 & 2\cos 2\theta & 0\\
\cos 2\theta\sin\varphi & 0 & \cos 2\theta\sin\varphi & -\sin\theta\cos\varphi & 2\sin 2\theta\sin\varphi & \cos\theta\cos\varphi\\
-\frac{1}{2}\sin\theta\sin 2\varphi & 0 & -\cos 2\theta\cos\varphi & -\sin\theta\sin\varphi & -2\sin 2\theta\cos\varphi & \cos\theta\sin\varphi\\
-\frac{1}{2}\sin 2\theta\sin 2\varphi & 0 & \frac{1}{2}\sin 2\theta\sin 2\varphi & -\cos\theta 2\cos\varphi & \cos 2\theta\sin 2\varphi & -\sin\theta\cos 2\varphi
\end{array}\right] \qquad (84)$$

$$\frac{\partial \mathbf{R}}{\partial \varphi} = \left[\begin{array}{ccc|ccc} -\cos^2\theta\sin 2\varphi & \sin 2\varphi & -\sin^2\theta\sin 2\varphi & -2\sin\theta\cos 2\varphi & \sin 2\theta\sin 2\varphi & 2\cos\theta\cos 2\varphi \\ \cos^2\theta\sin 2\varphi & -\sin 2\varphi & \sin^2\theta\sin 2\varphi & 2\sin\theta\cos 2\varphi & -\sin 2\theta\sin 2\varphi & -2\cos\theta\cos 2\varphi \\ 0 & 0 & 0 & 0 & 0 & 0 \\ -\frac{1}{2}\sin 2\theta\cos\varphi & 0 & \frac{1}{2}\sin 2\theta\cos\varphi & -\cos\theta\sin\varphi & -\cos 2\theta\cos\varphi & -\sin\theta\sin\varphi \\ \cos\theta\cos 2\varphi & 0 & \frac{1}{2}\sin 2\theta\sin\varphi & \cos\theta\cos\varphi & -\cos 2\theta\sin\varphi & \sin\theta\cos\varphi \\ -\cos^2\theta\cos 2\varphi & \cos 2\varphi & -\sin^2\theta\cos 2\varphi & 2\sin\theta 2\sin\varphi & \sin 2\theta\cos 2\varphi & -2\cos\theta\sin 2\varphi \end{array}\right] \tag{85}$$

F Equations of Motion and First Order Equations

Consider the equations of motion for elastic waves in anisotropic structures as described equation (3) of Maupin (1988).

$$\begin{aligned} -\rho\omega^2\mathbf{w} &= \frac{\partial bft_1}{\partial x} + \frac{\partial bft_2}{\partial y} + \frac{\partial bft_3}{\partial z} + \mathbf{F} \\ \mathbf{t}_i &= {}^wC_{ij}\frac{\partial \mathbf{w}}{\partial x_j} \end{aligned} \tag{86}$$

The characteristic equation can be expanded out for each individual traction vector.

$$\mathbf{t}_1 = {}^wC_{11}\frac{\partial \mathbf{w}}{\partial x} + {}^wC_{12}\frac{\partial \mathbf{w}}{\partial y} + {}^wC_{13}\frac{\partial \mathbf{w}}{\partial z} \tag{87}$$

$$\mathbf{t}_2 = {}^wC_{21}\frac{\partial \mathbf{w}}{\partial x} + {}^wC_{22}\frac{\partial \mathbf{w}}{\partial y} + {}^wC_{23}\frac{\partial \mathbf{w}}{\partial z} \tag{88}$$

$$\mathbf{t}_3 = {}^wC_{31}\frac{\partial \mathbf{w}}{\partial x} + {}^wC_{32}\frac{\partial \mathbf{w}}{\partial y} + {}^wC_{33}\frac{\partial \mathbf{w}}{\partial z} \tag{89}$$

Now consider the the derivative with respect to x of $\mathbf{w}$ and $\mathbf{t}_1$. The derivatives are chosen to be expressed only in terms of material properties and the vectors $\mathbf{w}$ and $\mathbf{t}_1$:

$$\frac{\partial \mathbf{w}}{\partial x} = {}^wC_{11}^{-1}\mathbf{t}_1 - {}^wC_{11}^{-1}{}^wC_{12}\frac{\partial \mathbf{w}}{\partial y} + {}^wC_{11}^{-1}{}^wC_{13}\frac{\partial \mathbf{w}}{\partial z} \tag{90}$$

$$\begin{aligned} \frac{\partial \mathbf{t}_1}{\partial x} &= -\rho\omega^2\mathbf{w} - \frac{\partial}{\partial y}\left(X_{22}\frac{\partial \mathbf{w}}{\partial y}\right) - \frac{\partial}{\partial y}\left(X_{23}\frac{\partial \mathbf{w}}{\partial z}\right) - \frac{\partial}{\partial y}\left({}^wC_{21}{}^wC_{11}^{-1}\mathbf{t}_1\right) \\ &\quad -\frac{\partial}{\partial z}\left(X_{32}\frac{\partial \mathbf{w}}{\partial y}\right) - \frac{\partial}{\partial z}\left(X_{33}\frac{\partial \mathbf{w}}{\partial z}\right) - \frac{\partial}{\partial z}\left({}^wC_{31}{}^wC_{11}^{-1}\mathbf{t}_1\right) - \mathbf{F} \end{aligned} \tag{91}$$

Now consider $\mathbf{w}$ and $\mathbf{t}_2$ and their derivative with respect to y. The derivatives are chosen to be expressed only in terms of material properties and the

vectors $\mathbf{w}$ and $\mathbf{t}_2$:

$$\frac{\partial \mathbf{w}}{\partial y} = {}^{w}C_{22}^{-1}\mathbf{t}_2 - {}^{w}C_{22}^{-1\,w}C_{21}\frac{\partial \mathbf{w}}{\partial x} + {}^{w}C_{22}^{-1\,w}C_{23}\frac{\partial \mathbf{w}}{\partial z} \tag{92}$$

$$\begin{aligned}\frac{\partial \mathbf{t}_2}{\partial y} = {} & -\rho\omega^2\mathbf{w} - \frac{\partial}{\partial x}\left(Y_{11}\frac{\partial \mathbf{w}}{\partial x}\right) - \frac{\partial}{\partial x}\left(Y_{13}\frac{\partial \mathbf{w}}{\partial z}\right) - \frac{\partial}{\partial x}\left({}^{w}C_{12}{}^{w}C_{22}^{-1}\mathbf{t}_2\right) \\ & -\frac{\partial}{\partial z}\left(Y_{31}\frac{\partial \mathbf{w}}{\partial x}\right) - \frac{\partial}{\partial z}\left(Y_{33}\frac{\partial \mathbf{w}}{\partial z}\right) - \frac{\partial}{\partial z}\left({}^{w}C_{32}{}^{w}C_{22}^{-1}\mathbf{t}_1\right) - \mathbf{F}\end{aligned} \tag{93}$$

Similarly the derivatives of $\mathbf{w}$ and $\mathbf{t}_2$ with respect to z may be considered. The derivatives are chosen to be expressed only in terms of material properties and the vectors $\mathbf{w}$ and $\mathbf{t}_3$:

$$\frac{\partial \mathbf{w}}{\partial z} = {}^{w}C_{33}^{-1}\mathbf{t}_3 - {}^{w}C_{33}^{-1\,w}C_{31}\frac{\partial \mathbf{w}}{\partial x} + {}^{w}C_{33}^{-1\,w}C_{32}\frac{\partial \mathbf{w}}{\partial y} \tag{94}$$

$$\begin{aligned}\frac{\partial \mathbf{t}_3}{\partial z} = {} & -\rho\omega^2\mathbf{w} - \frac{\partial}{\partial x}\left(Z_{11}\frac{\partial \mathbf{w}}{\partial x}\right) - \frac{\partial}{\partial x}\left(Z_{12}\frac{\partial \mathbf{w}}{\partial y}\right) - \frac{\partial}{\partial x}\left({}^{w}C_{13}{}^{w}C_{33}^{-1}\mathbf{t}_3\right) \\ & -\frac{\partial}{\partial y}\left(Z_{21}\frac{\partial \mathbf{w}}{\partial x}\right) - \frac{\partial}{\partial y}\left(Z_{22}\frac{\partial \mathbf{w}}{\partial y}\right) - \frac{\partial}{\partial y}\left({}^{w}C_{23}{}^{w}C_{33}^{-1}\mathbf{t}_3\right) - \mathbf{F}\end{aligned} \tag{95}$$

These three sets of equations can be reformulated into a single set of generalized equations of motion.

$$\frac{\partial \mathbf{w}}{\partial x_m} = {}^{w}C_{mm}^{-1}\mathbf{t}_m - {}^{w}C_{mm}^{-1\,w}C_{mi}\frac{\partial \mathbf{w}}{\partial x_i} + {}^{w}C_{mm}^{-1\,w}C_{mj}\frac{\partial \mathbf{w}}{\partial x_j} \tag{96}$$

$$\begin{aligned}\frac{\partial \mathbf{t}_m}{\partial x_m} = {} & -\rho\omega^2\mathbf{w} - \frac{\partial}{\partial x_i}\left(({}^{w}C_{ii} - {}^{w}C_{im}{}^{w}Cmm^{-1\,w}C_{mi})\frac{\partial \mathbf{w}}{\partial x_i}\right) \\ & -\frac{\partial}{\partial x_i}\left(({}^{w}C_{ij} - {}^{w}C_{im}{}^{w}Cmm^{-1\,w}C_{mj})\frac{\partial \mathbf{w}}{\partial x_j}\right) \\ & -\frac{\partial}{\partial x_i}\left({}^{w}C_{im}{}^{w}C_{mm}^{-1}\mathbf{t}_m\right) \\ & -\frac{\partial}{\partial x_j}\left(({}^{w}C_{ji} - {}^{w}C_{jm}{}^{w}Cmm^{-1\,w}C_{mi})\frac{\partial \mathbf{w}}{\partial x_i}\right) \\ & -\frac{\partial}{\partial x_j}\left(({}^{w}C_{jj} - {}^{w}C_{jm}{}^{w}Cmm^{-1\,w}C_{mj})\frac{\partial \mathbf{w}}{\partial x_j}\right) \\ & -\frac{\partial}{\partial x_j}\left({}^{w}C_{jm}{}^{w}C_{mm}^{-1}\mathbf{t}_m\right) - \mathbf{F}\end{aligned} \tag{97}$$

where $m = 1, 2, 3$ and $x_m = x, y, z$

An eigenvalue problem may be formulated from the generalized equations of motion, which results in a generalized firt order coupled equation.

$$\frac{\partial \mathbf{u}^m}{\partial x_m} = \mathbf{A}^m \mathbf{u}^m - \mathbf{F} \qquad \text{where } \mathbf{u}^m = (\mathbf{w}, \mathbf{t}_m)^T \tag{98}$$

$$\mathbf{A} = \begin{pmatrix} A_{11}^m & A_{12}^m \\ A_{21}^m & A_{22}^m \end{pmatrix} \tag{99}$$

For a solid triclinic anisotropic medium, the sub-operators for the generalized first order coupled equation are:

$$\begin{aligned}
A_{11}^m &= \left(-({}^wC_{mm}^{-1})({}^wC_{ii})\frac{\partial}{\partial x_i} + ({}^wC_{mm}^{-1})({}^wC_{jj})\frac{\partial}{\partial x_j} \right), \\
A_{12}^m &= \left({}^wC_{mm}^{-1} \right), \\
A_{21}^m &= \left(-\rho\omega^2 \mathbf{w} - \frac{\partial}{\partial x_i}\left(({}^wC_{ii} - {}^wC_{im}{}^wCmm^{-1}{}^wC_{mi})\frac{\partial}{\partial x_i} \right) \right. \\
&\quad -\frac{\partial}{\partial x_i}\left(({}^wC_{ij} - {}^wC_{im}{}^wCmm^{-1}{}^wC_{mj})\frac{\partial}{\partial x_j} \right) - \frac{\partial}{\partial x_i} \\
&\quad -\frac{\partial}{\partial x_j}\left(({}^wC_{ji} - {}^wC_{jm}{}^wCmm^{-1}{}^wC_{mi})\frac{\partial}{\partial x_i} \right) \\
&\quad \left. -\frac{\partial}{\partial x_j}\left(({}^wC_{jj} - {}^wC_{jm}{}^wCmm^{-1}{}^wC_{mj})\frac{\partial}{\partial x_j} \right) - \frac{\partial}{\partial x_j} \right), \\
A_{22}^m &= \left(-\frac{\partial}{\partial x_i}({}^wC_{im})({}^wC_{mm}^{-1}) - \frac{\partial}{\partial x_j}({}^wC_{jm})({}^wC_{mm}^{-1}) \right),
\end{aligned} \tag{100}$$

G Symmetry Planes and Wave Polarizations

The polarization of the modes composing the seismo-acoustic wavefield depend on the propagation direction through the anisotropic medium. The polarization of any mode will change if the propagation direction changes or the elastic stiffness matrix is rotated. Pure P-SV and SH polarization directions exist in a TI elastically symmetric medium for specific propagation directions. The polarization of the modes is determined by the proximity of the propagation direction to the symmetry axis direction.

The form of the elastic stiffness matrix indicates the amount of symmetry and the location of symmetry planes for an anisotropic medium. These symmetry planes, help predict when transverse particle motion may propagate independently of the P-SV particle motion, or when quasi-SH particle motions propagates independently of quasi-P-SV particle motions.

Auld(1990) discusses pure plane-wave mode propagation directions in relation to symmetry planes and symmetry axes. The modes of a shallow water waveguide follow these same principles with a little modification. P, SV, and SH plane waves propagate independently for pure mode directions of propagation. For the modes of a shallow water wave guide, the P and SV particle motions are always coupled, but the SH particle motions may propagate independently for some geometries of the symmetry axis and propagation directions. If the SH motions coupled with either SV or P particle motions, then the modes will have polarizations in all three coordinate directions.

[Table 10 about here.]

Whenever the propagation is within a symmetry plane, the single generalized mode family splits into two independent mode families, and the SH

modes will propagate independently of the P-SV modes. The propagation, in a sense will behave as quasi-isotropic. This is true regardless of whether the anisotropy is strong or weak. A VTI medium can be thought as a quasi-isotropic or quasi-orthorhombic medium. The wave propagation is similar to an isotropic medium, but the modes have slightly different shapes.

Consider rotating the elastic stiffness matrix, so that the symmetry axis $\hat{s}$ first aligns with the three coordinate axes. When $\hat{s} = \hat{x}, \hat{y}$, or $\hat{z}$ then the form of the elastic stiffness matrix remains in the *form* of a quasi-orthorhombic, with 12 non-zero matrix elements and the remainder having zero values:

$$ {}^{a}C_{IJ} = \begin{bmatrix} C_{11} & C_{12} & C_{13} & 0 & 0 & 0 \\ C_{21} & C_{22} & C_{23} & 0 & 0 & 0 \\ C_{31} & C_{32} & C_{33} & 0 & 0 & 0 \\ 0 & 0 & 0 & C_{44} & 0 & 0 \\ 0 & 0 & 0 & 0 & C_{55} & 0 \\ 0 & 0 & 0 & 0 & 0 & C_{66} \end{bmatrix} \quad \text{where } \hat{s} = \hat{x}, \hat{y}, \text{ or } \hat{z} \tag{101} $$

For a VTI medium, all elements of the elastic stiffness matrix ${}^{a}C_{IJ}$ are unaltered by rotations about the z-axis.

An orthorhombic medium has the xy, xz, and yz-planes as symmetry planes, and the quasi-orthorhombic elastic stiffness matrix will have these symmetry planes as well. Applying the symmetry principles from table 10 for $\hat{s}$ along any of the coordinate axes, the SH modes will propagate independently of the P-SV modes. The mode set is separated into two families of modes, the SH modes and the P-SV modes, when the $\hat{s}$ is aligned with any of the three coordinate axes.

Now consider tilting the symmetry axis $\hat{s}$ so that it remains in the xz-plane. The elastic stiffness matrix ${}^{a}C_{IJ}$ takes on the *form* of a monoclinic

medium where the single symmetry plane is orthogonal to the y-axis and parallel to the xz-plane.

$$ {}^{a}C_{IJ} = \begin{bmatrix} C_{11} & C_{12} & C_{13} & 0 & C_{15} & 0 \\ C_{21} & C_{22} & C_{23} & 0 & C_{25} & 0 \\ C_{31} & C_{32} & C_{33} & 0 & C_{35} & 0 \\ 0 & 0 & 0 & C_{44} & 0 & C_{46} \\ C_{51} & C_{52} & C_{53} & 0 & C_{55} & 0 \\ 0 & 0 & 0 & C_{64} & 0 & C_{66} \end{bmatrix} \qquad \text{where } \hat{s}(\theta, \varphi) = \hat{s}(all, 0°0102) $$

A monoclinic medium has a single plane of symmetry. Consider the form of the elastic stiffness matrix when the symmetry is parallel with the xz, yz, and xy-planes respectively. The tilted TI medium with the symmetry axis along one of the coordinate planes has the form of a monoclinic material, but with a higher degree of symmetry. A true monoclinic material has 13 independent parameters. The tilted TI medium only has five independent elastic moduli, even though the elastic stiffness matrix is populated the same as a monoclinic medium. The elastic stiffness tensor can be thought of exhibiting a quasi-monoclinic form, with higher symmetry due to a reduction in the number of independent elastic moduli.

For the symmetry axis in the xz-plane, the C_{22} element is insensitive to any variation in θ when $\varphi = 0°$. This is of little consequence, since the C_{22} element is not included in the equation of motion for 2-D propagation along the x-direction. The horizontally polarized shear modes will propagate independently of the P-SV modes for all orientations of the symmetry axis that lie in the xz-plane. The modes are split into two families of propagating modes: P-SV modes with polarizations in the xz-plane and SH modes with polarizations in the transverse coordinate direction.

Now consider tilting the symmetry axis so that it remains in the yz-plane. The elastic stiffness matrix again takes on the *form* of a quasi-monoclinic medium where the single symmetry plane is orthogonal to the x-axis and parallel to the yz-plane.

$$ {}^{a}C_{IJ} = \begin{bmatrix} C_{11} & C_{12} & C_{13} & C_{14} & 0 & 0 \\ C_{21} & C_{22} & C_{23} & C_{24} & 0 & 0 \\ C_{31} & C_{32} & C_{33} & C_{34} & 0 & 0 \\ C_{41} & C_{42} & C_{43} & C_{44} & 0 & 0 \\ 0 & 0 & 0 & 0 & C_{55} & C_{56} \\ 0 & 0 & 0 & 0 & C_{65} & C_{66} \end{bmatrix} \qquad \text{where } \hat{s}(\theta,\varphi) = \hat{s}(all, 90°)(103) $$

The C_{11} element of the stiffness tensor is insensitive to any variations of θ when $\varphi = 90°$.

The symmetry plane and symmetry axis principles indicate that no pure horizontally polarized modes should be expected when the elastic stiffness matrix is in this form, unless the symmetry axis $\hat{s}$ is vertical or horizontal in the yz-plane. The principles indicate that the quasi-shear modes will have polarizations parallel to the symmetry axis, having both transverse and vertical components. The modes will likely consist of a single family of generalized P-SV-SH modes with polarizations in all three coordinate directions. The quasi-monoclinic elastic stiffness matrix has a higher degree of symmetry than a true monoclinic medium.

Next consider tilting the symmetry axis $\hat{s}$ so that it remains in the xy-plane. The elastic stiffness matrix again takes on the *form* of a quasi-monoclinic medium with the single symmetry plane orthogonal to the z-axis

and parallel to the xy-plane.

$$ {}^{a}C_{IJ} = \begin{bmatrix} C_{11} & C_{12} & C_{13} & 0 & 0 & C_{16} \\ C_{21} & C_{22} & C_{23} & 0 & 0 & C_{26} \\ C_{31} & C_{32} & C_{33} & 0 & 0 & C_{36} \\ 0 & 0 & 0 & C_{44} & C_{45} & 0 \\ 0 & 0 & 0 & C_{54} & C_{55} & 0 \\ C_{61} & C_{62} & C_{63} & 0 & 0 & C_{66} \end{bmatrix} \qquad \text{where } \hat{s}(\theta, \varphi) = \hat{s}(90°, all) \quad (104) $$

The C_{33} element of the elastic stiffness matrix is insensitive to any variations of φ for $\theta = 90°$.

Now consider tilting the symmetry axis to a general orientation that excludes the coordinate axes directions and the xy, xz, and yz coordinate planes. The general *form* of the rotated ${}^{a}C_{IJ}$ elastic stiffness matrix is quasi-triclinic in nature with a higher degree of symmetry than a true triclinic elastic stiffness matrix. Similar to the monoclinic comparison, a ture triclinic material has 21 independent elastic moduli. The rotated elastic stiffness matrix in equation (105) still only has 5 independent elastic moduli. Each element remains a linear combination of the five elastic moduli. So the rotated elastic stiffness matrix can be thought of being quasi-triclinic, with a higher degree of symmetry due to the reduction in the number of independent elastic moduli.

$$ {}^{a}C_{IJ} = \begin{bmatrix} C_{11} & C_{12} & C_{13} & C_{14} & C_{15} & C_{16} \\ C_{21} & C_{22} & C_{23} & C_{24} & C_{25} & C_{26} \\ C_{31} & C_{32} & C_{33} & C_{34} & C_{35} & C_{36} \\ C_{41} & C_{42} & C_{43} & C_{44} & C_{45} & C_{46} \\ C_{51} & C_{52} & C_{53} & C_{54} & C_{55} & C_{56} \\ C_{61} & C_{62} & C_{63} & C_{64} & C_{65} & C_{66} \end{bmatrix} \qquad \text{where } \hat{s}(\theta, \varphi) \quad (105) $$

Except when the symmetry axis $\hat{s}$ is aligned with the x-axis or y-axis, the mode set consists of quasi-P-SV, quasi-SH, or generalized P-SV-SH modes.

The *form* of the elastic stiffness tensor may change as a TI medium rotates from a general orientation to more specific orientations. The elastic stiffness tensor of a TTI medium would be described as quasi-triclinic, the elastic stiffness tensor for a symmetry axis within any of the coordinate planes would be described as quasi-monoclinic, and the elastic stiffness tensor when the symmetry axis is aligned with any of the three coordinate axes would be quasi-orthorhombic.

Figure 27 shows the *form* the elastic stiffness matrix takes for orientations of the symmetry axis $\hat{s}(\theta, \varphi)$ in the first quadrant. The vertical axis is the angle φ in 10° increments and the horizontal axis is the angle θ in 10° increments. Each matrix represents the form of the elastic stiffness matrix ${}^{a}\mathbf{C}_{IJ}$ for a specific symmetry axis $\hat{s}$ orientation. The first row shows the form of ${}^{a}\mathbf{C}_{IJ}$ for $\varphi = 0°$ and $\theta = 0° - 90°$. This represents the symmetry axis within the sagittal plane and the elastic stiffness matrix has the *form* of a quasi-monoclinic medium. The first column shows the elastic stiffness matrix for $\hat{s} = \hat{z}$, with the form of a quasi-orthorhombic medium or VTI. The corner matrices of figure 27 in the tenth column also have the quasi-orthorhombic form and correspond to HTI media with the symmetry axis $\hat{s}$ aligned parallel to the $\hat{x}$ and $\hat{y}$ axes. The tenth column shows the form of ${}^{a}\mathbf{C}_{IJ}$ for $\theta = 90°$ and $\varphi = 0° - 90°$. This represents the symmetry axis within the xy-plane and the matrices have the form of a quasi-monoclinic medium. This also is a HTI medium where $\hat{s}(\theta, \varphi) = \cos\varphi\hat{x} + \sin\varphi\hat{y}$. The tenth row shows the form of the elastic stiffness matrices for $\phi = 90°$ and $\varphi = 0° - 90°$. The matrices for $\hat{s}$ in the yz-plane also have a quasi-monoclinic form. All other orientations

of the symmetry axis for ${}^{a}C_{IJ}$ produce the form of a quasi-triclinic medium. Okaya and McEvilly (2003) noticed similar results for rotations of hexagonal symmetry about the x, y, and z axes, and mentioned the appearance of monoclinic symmetry for rotations about the y-axis. Shoenberge and Costa (1991) also state that hexagonal anisotropy behaves as monoclinic when the symmetry axis is within the sagittal plane.

[Figure 27 about here.]

Contents

List of Figures

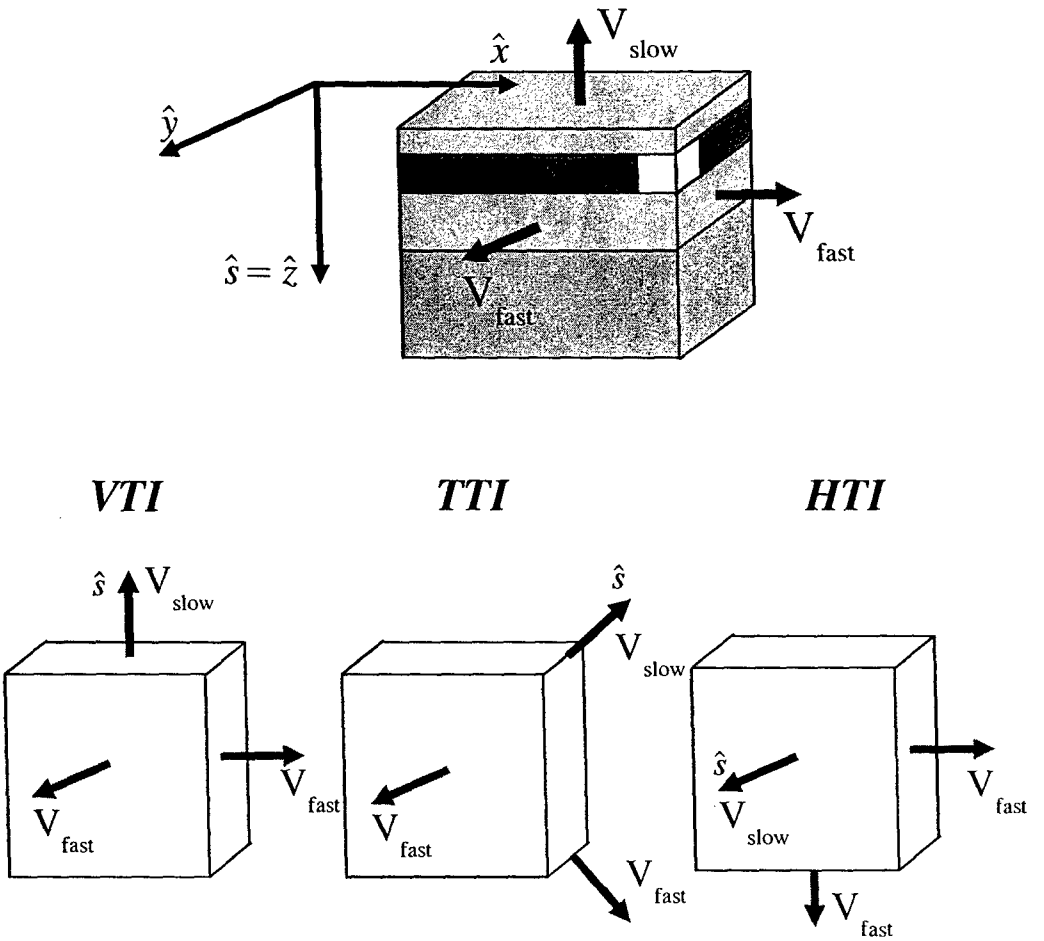

Figure 1: A representative elastically symmetric transversely isotropic structure (TI) due to compositional layering with a vertical symmetry axis $\hat{s}$. The fast velocity directions $\mathbf{V}_{fast}$ are normal to the symmetry axis direction and parallel to the bedding plane, the xy-plane for this instance. The slow velocity direction $\mathbf{V}_{slow}$ is parallel to the vertical symmetry axis. A TI structure with a vertical symmetry axis is often referred to as vertical transverse isotropy (VTI) or as azimuthally isotropic. The geometrical orientation of the anisotropy in a plane layered homogeneous anisotropic model, depends on the orientation of the symmetry axis $\hat{s}$. The white block of material from the plane layered structure on the right is expanded on the left to show the importance of symmetry axis direction on velocity properties of the medium. A structure can be transversely isotropic with a vertical, tilted (neither vertical nor horizontal), or horizontal symmetry axis and be classified as VTI, TTI, or HTI respectively. For a VTI orientation, the fast velocity direction is in the horizontal plane. A TTI orientation results in the fast velocity direction being contained to an oblique plane and the HTI orientation restricts the fast velocity directions to a vertical plane normal to the symmetry axis $\hat{s}$. Note that the slow velocity direction ($\mathbf{V}_{slow}$) always corresponds with the symmetry axis direction $\hat{s}$.

Fixed Cartesian Coordinate System

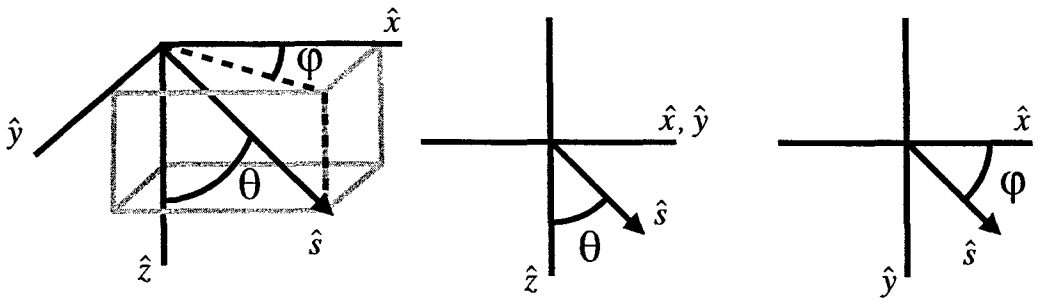

coordinate system full view | *xy and yz plane view* | *xy plane view*

Figure 2: The Cartesian coordinate system is defined with the x-direction corresponding with the direction of propagation, the z-direction is positive downwards, and thee y-direction is free of any lateral variations. The symmetry axis $\hat{s}$ is defined in reference to the fixed Cartesian coordinate system by the Spherical coordinate angles θ and φ. The angle between the z-axis and the symmetry axis $\hat{s}$ is described by θ. The angle between the projection of the symmetry axis $\hat{s}$ onto the horizontal plane and the x-direction is described by φ.

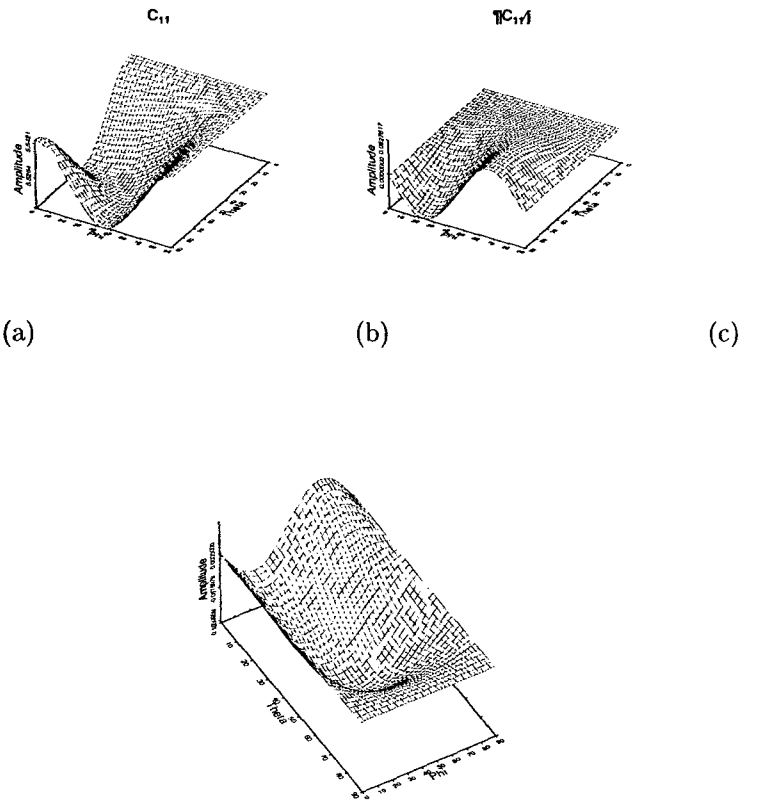

Figure 3: The C_{11} element of the elastic stiffness matrix ${}^{a}C_{IJ}$ is shown in Figure 3(a) for various angles of θ and φ. This is a numerical plot of equation 11. Figures 3(b) and 3(c) plot the sensitivity of the C_{11} element to the angles φ and θ respectively.

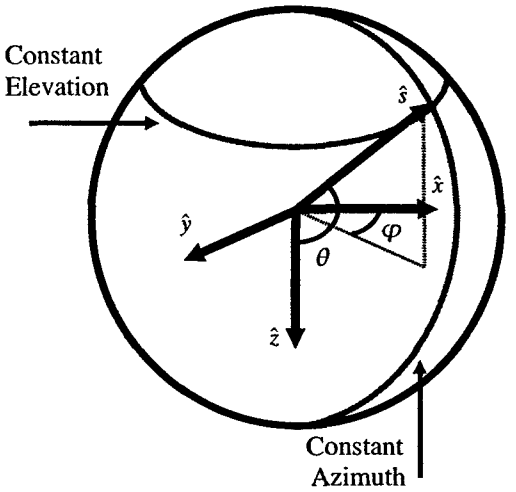

Figure 4: Any tilt of the symmetry axis with respect to the fixed coordinate system results in an azimuthal, elevational, or a combination of azimuthal and elevational change in anisotropy. The red line in the horizontal plane represents changes of azimuth φ of the symmetry axis and the red line in the vertical plane represents changes in elevation θ of the symmetry axis.

1–D Plane Layered Homogeneous Anisotropic Structure

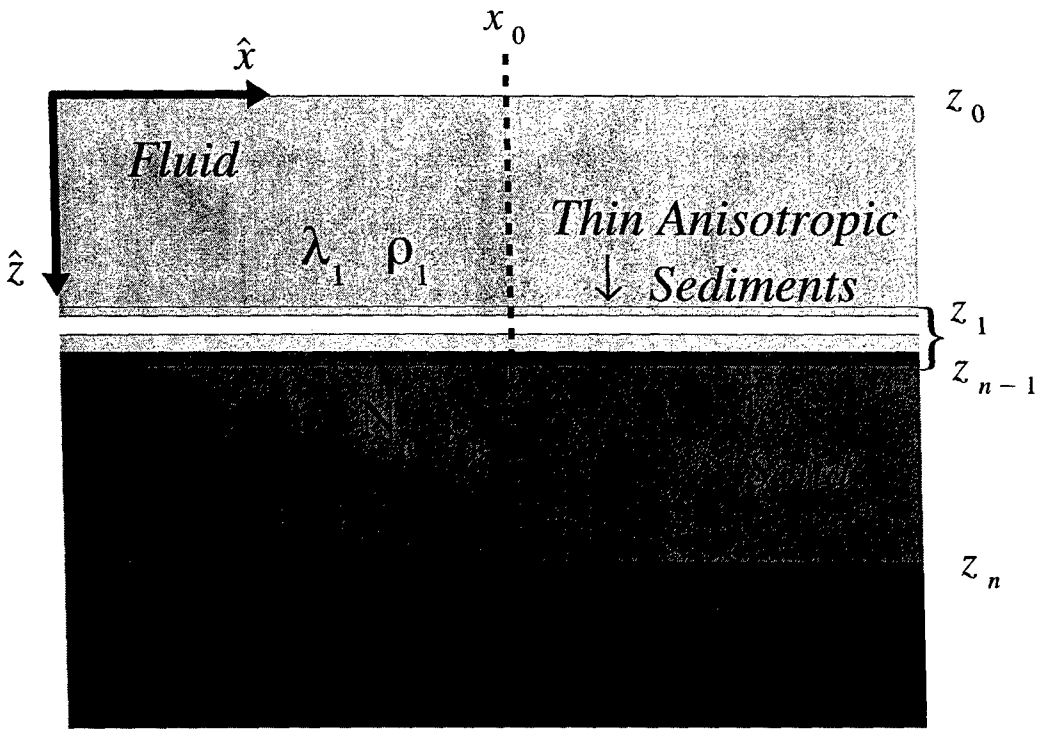

Figure 5: A 1-D plane layered homogeneous anisotropic structure representation of shallow water environments. The model contains fluid layers over thin anisotropic and/or isotropic sediments, additional sediment and/or basement layers, and is terminated by an isotropic halfspace. There is no lateral variations in the structure, and thee elastic parameters only vary with depth. The anisotropy is restricted to elastically symmetric transverse isotropy, but the symmetry axis $\hat{s}$ may have any arbitrary orientation.

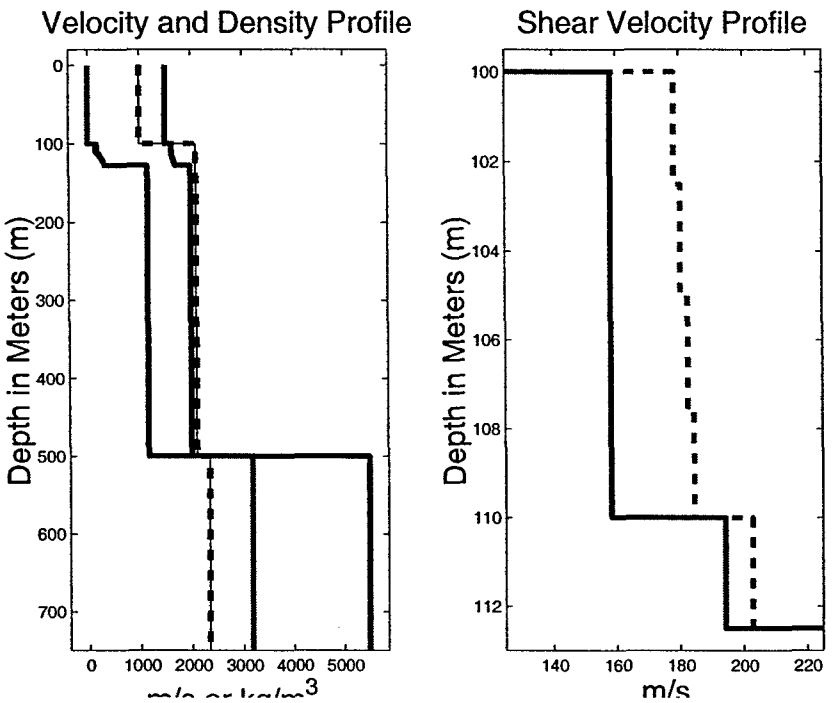

Figure 6: The velocity and density profile of the starting VTI medium. The red, blue, and dotted black lines represent the shear velocity, compressional velocity, and density respectively with depth. The profile on the right is an enlargement of the thin sediment region to show the shear wave velocity splitting within the anisotropic layers. The solid red line represents the vertical shear speed β_V and the dotted red line represents the horizontal shear speed β_H. Note that the velocity profile lacks any compressional anisotropy

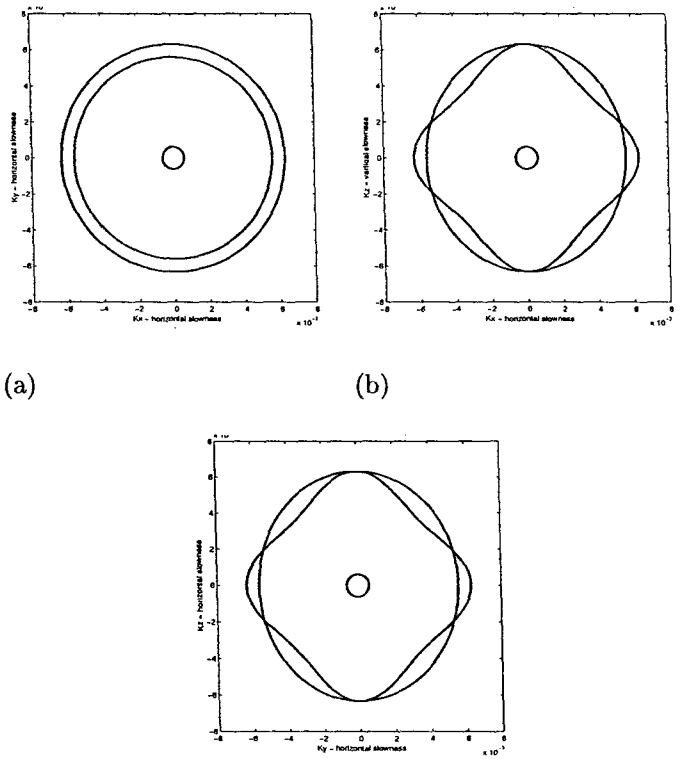

(a) (b) (c)

Figure 7: The slowness curves for the xy, xz, and yz-planes for a VTI anisotropic sediment layer, where $\hat{s} = \hat{z}$. The inner circle is the compressional slowness, indicating the absence of any anisotropy in the compressional velocity. The outer paths represent the vertical and horizontal shear slownesses. In Figure (a) there is complete shear velocity splitting. Both Figures (b) and (c) reveal shear velocity singularities at $\theta = 0°, 180°$ and $\theta \approx 70°, 110°$.

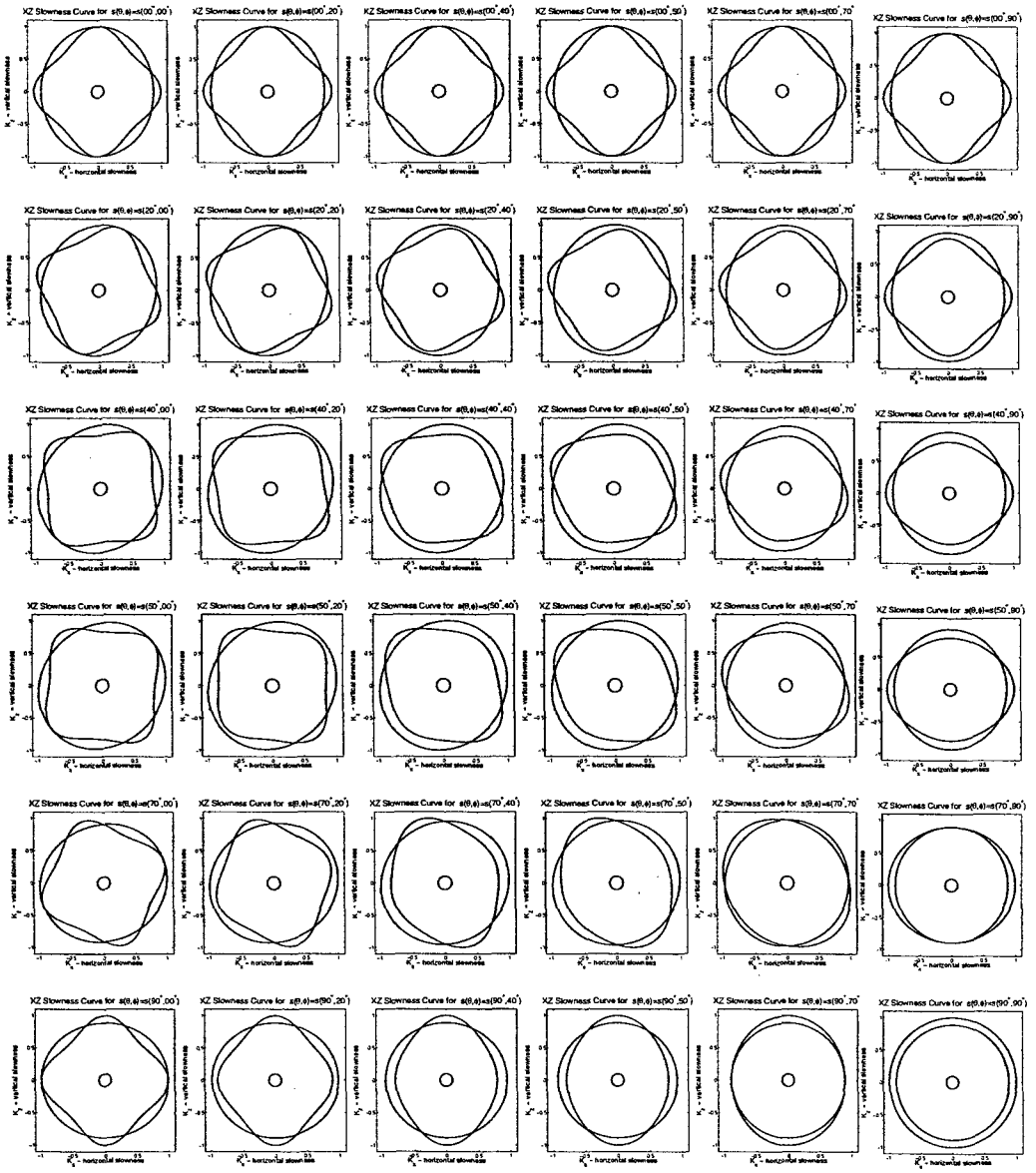

Figure 8: The Figure shows the slowness curves for orientations of the symmetry axis $\hat{s}$ within the first quadrant. Each slowness figure indicates a change in azimuth or elevation of symmetry axis of 10°. The horizontal row represents variations of θ and the vertical column represents variations of φ. The slowness curves are shown for the xz-plane for an anisotropic marine sediment layer.

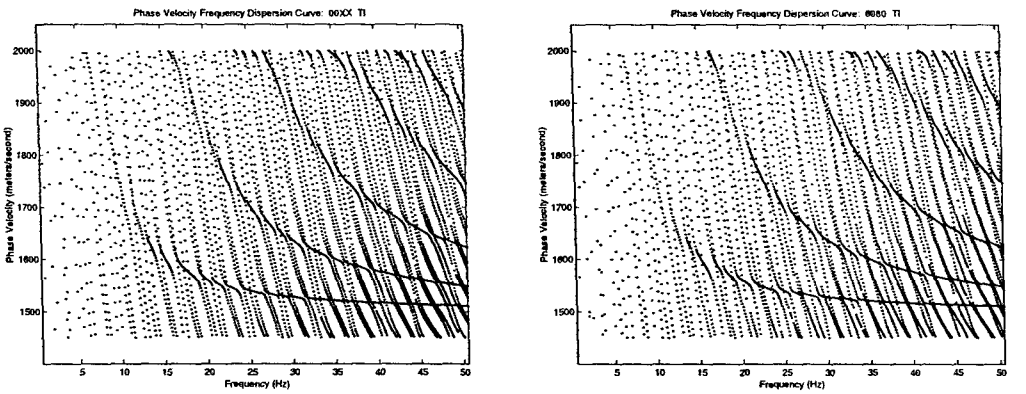

(a) (b)

Figure 9: Frequency dispersion curves for modal phase velocities between $1500m/s$ and $2000m/s$, for the VTI ($\hat{s}(\theta,\varphi) = \hat{s}(0°, 0°)$ and a TTI ($\hat{s}(\theta,\varphi) = \hat{s}(60°, 80°)$. The dispersion curves for the VTI symmetry in (a) and TTI symmetry (b) are very similar. Both figures clearly show the "solotone" effect, the dark bands in both figures (a) and (b). The modal phase velocities trace out vertical paths that are nearly parallel in figure (a). The even parallel nature is disrupted when the phase velocities approach the value of an "invariant" mode. The modal phase velocities in figure (b) also trace out vertical paths, but a braiding effect can be seen to occur between adjacent phase velocity traces. The dark bands that represent the phase velocities of the "invariant" modes are frequency dependent, but they vary more slowly than for the non-invariant modes.

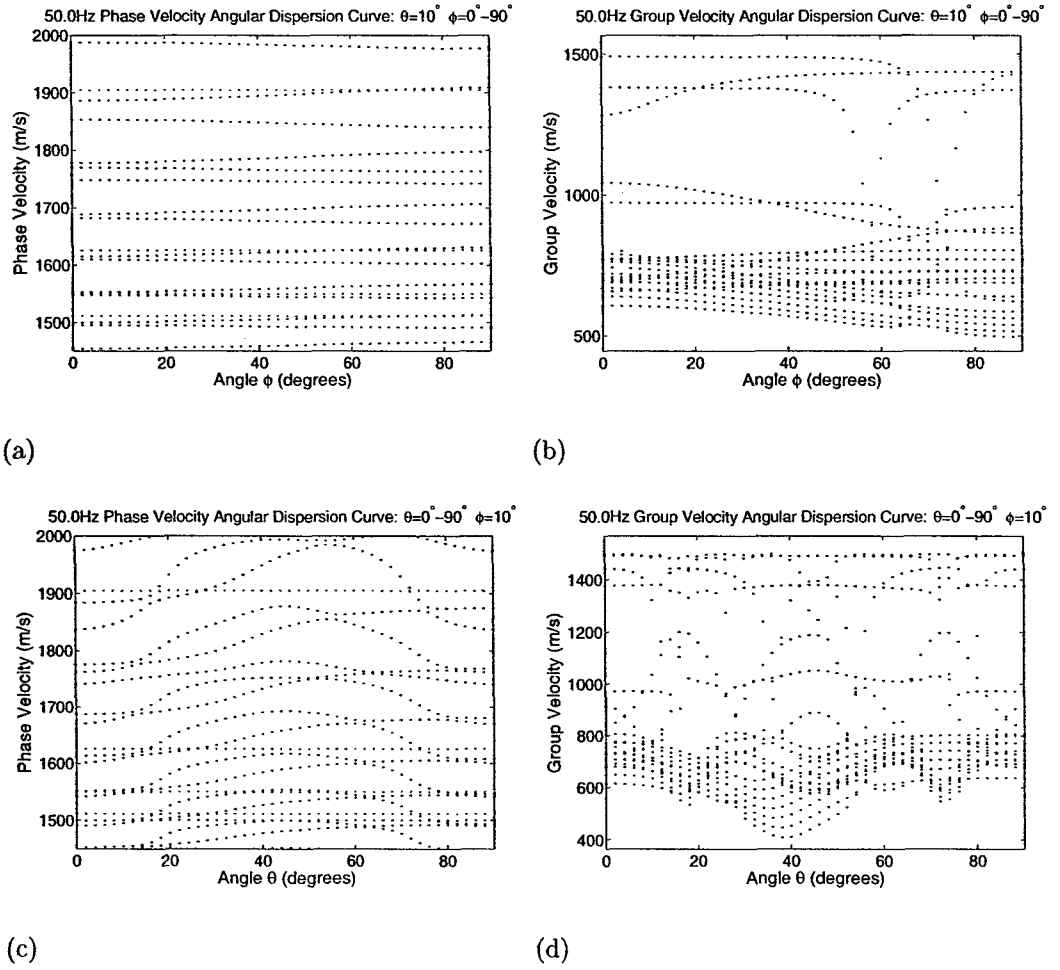

Figure 10: Angular dispersion curves for both phase and group velocities. Figure (a) and (b) show the angular dispersion curves for the phase and group velocities respectively for $\hat{s}(\theta, \varphi) = \hat{s}(10°, 0° - 90°)$. Figure c) and (d) represent the angular dispersion curves for the phase and group velocities respectively for $\hat{s}(\theta, \varphi) = \hat{s}(0° - 90°, 10°)$. In general, changes in elevation (θ) have a larger affect on the phase and group velocities than changes in azimuth (φ).

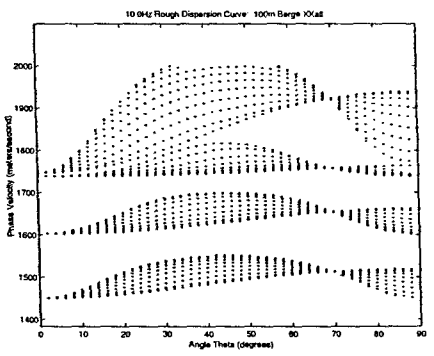

(a)

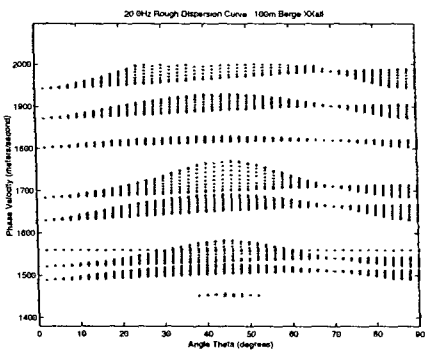

(b)

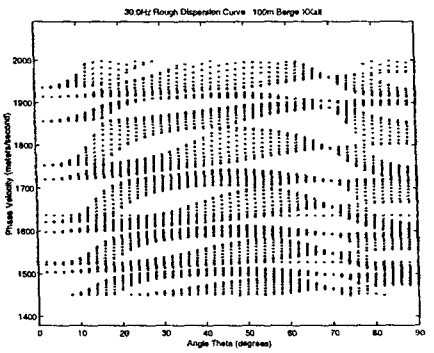

(c)

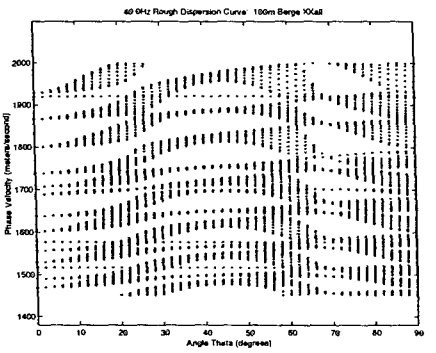

(d)

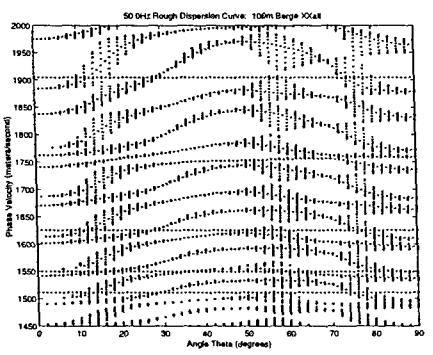

(e)

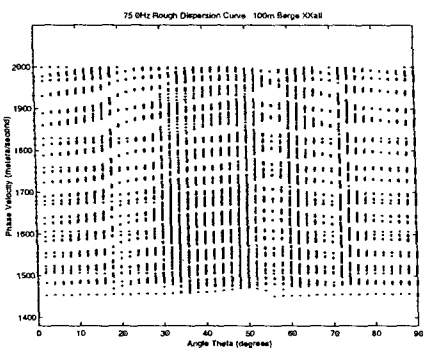

(f)

Figure 11: The stacked angular dispersion curves show the dependence and sensitivity of the dispersion branches on variations of the angles θ and φ for a range of frequencies. The thickness of an envelope indicates the sensitivity of a particular mode to changes in azimuth (φ). Note the convergence of the phase velocities at 0° and approximately 70°. This is where the shear velocities become degenerate.

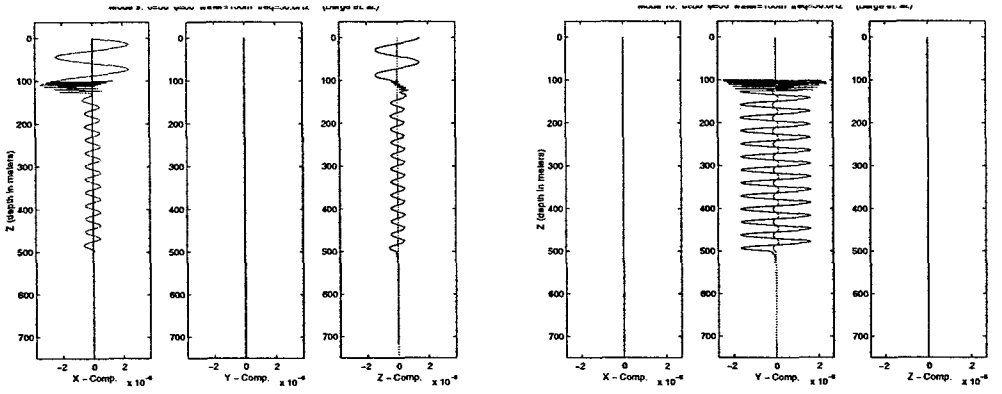

(a) (b)

Figure 12: This is an example of P-SV and SH modes for $\hat{s}(\theta, \varphi) = \hat{s}(80°, 0°)$. This is an instance where the elastic stiffness matrix is quasi-monclinic and the pure P-SV and SH modes have completely separate polarizations. The P-SV mode has particle motion in the sagittal plane and the SH mode has particle motion in the y-coordinate-direction of the horizontal plane.

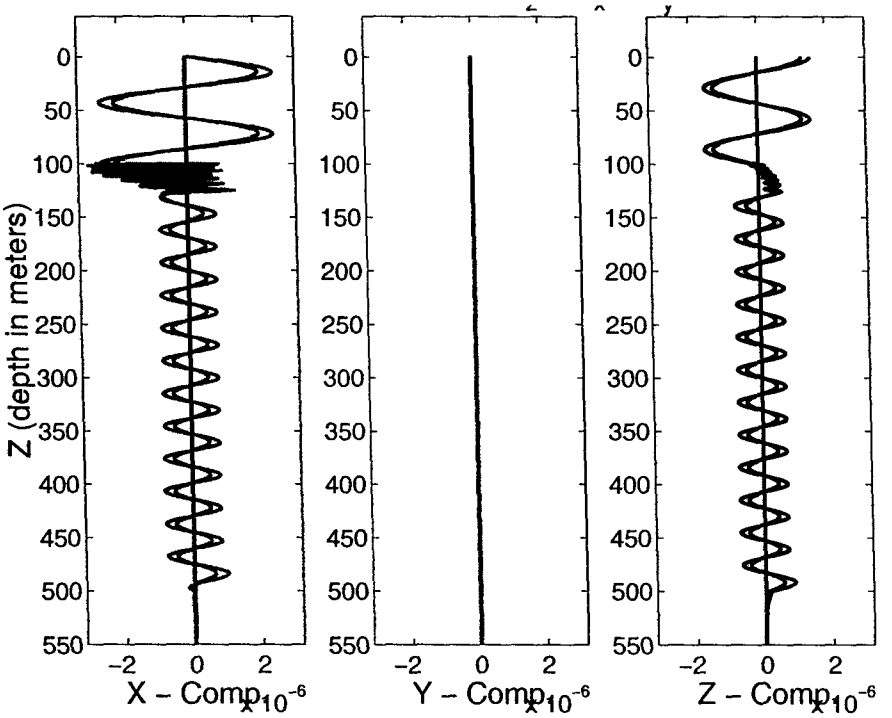

Figure 13: The P-SV mode remains polarized in the sagittal plane when the symmetry axis $\hat{s} = \hat{x}, \hat{y}, \hat{z}$. The mode shapes are similar when the symmetry axis is aligned parallel to any of the three coordinate axis directions.

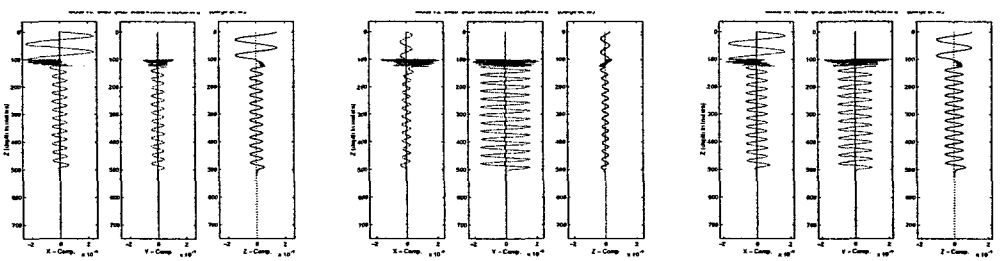

(a) (b) (c)

Figure 14: The quasi-P-SV mode in figure (a) has gained some particle motion in the y-direction, but still has particle motion predominantly in the sagittal plane. The quasi-SH mode in figure (b) has gained particle motion in the sagittal plane, but the mode remains predominantly polarized along the y-direction. The P-SV-SH mode in figure (c) has polarizations in all three coordinate directions and attributes of both P-SV and SH modes.

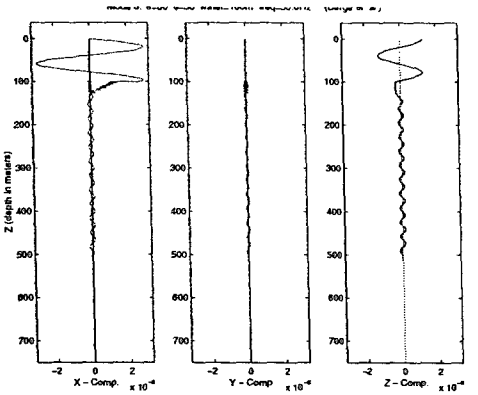

Figure 15: An example of an "invariant acoustic mode" at 50.0Hz for $\hat{s}(\theta, \varphi) = \hat{s}(80°, 30°)$. The mode only gains a very small portion of particle motion in the y-direction.

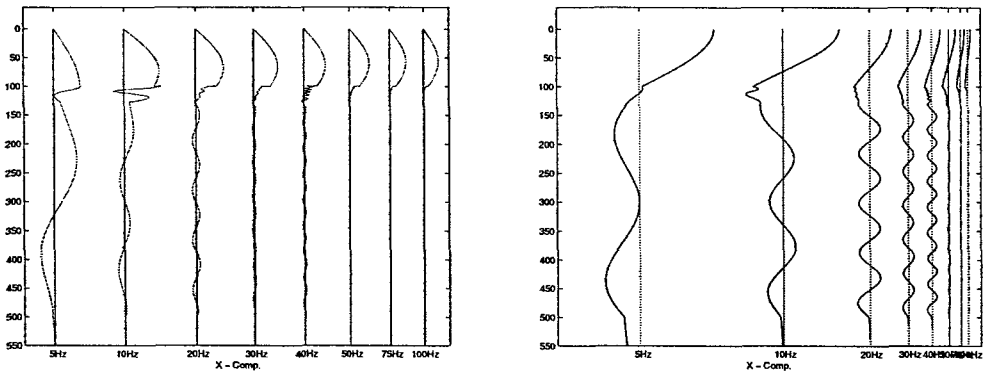

(a) (b)

Figure 16: The characteristics of an acoustic mode changes with frequency. Figure (a) shows the x-component of displacement and figure (b) shows the z-component of displacement. The acoustic mode shown has a single zero crossing in the z-component particle displacement within the fluid layer at higher frequencies.

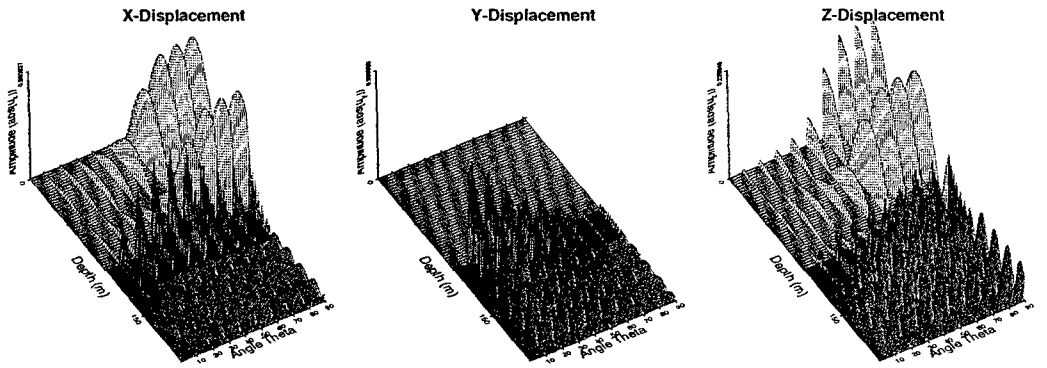

(a) (b) (c)

Figure 17: The x,y, and z particle displacements of a mode switches characteristics with another mode due to a near degeneracy. The near degeneracy occurs a the symmetry axis $\hat{s}$ is varied in θ. In this case the quasi-SH mode becomes a quasi-P-SV mode as $\theta = 0° - 90°$.

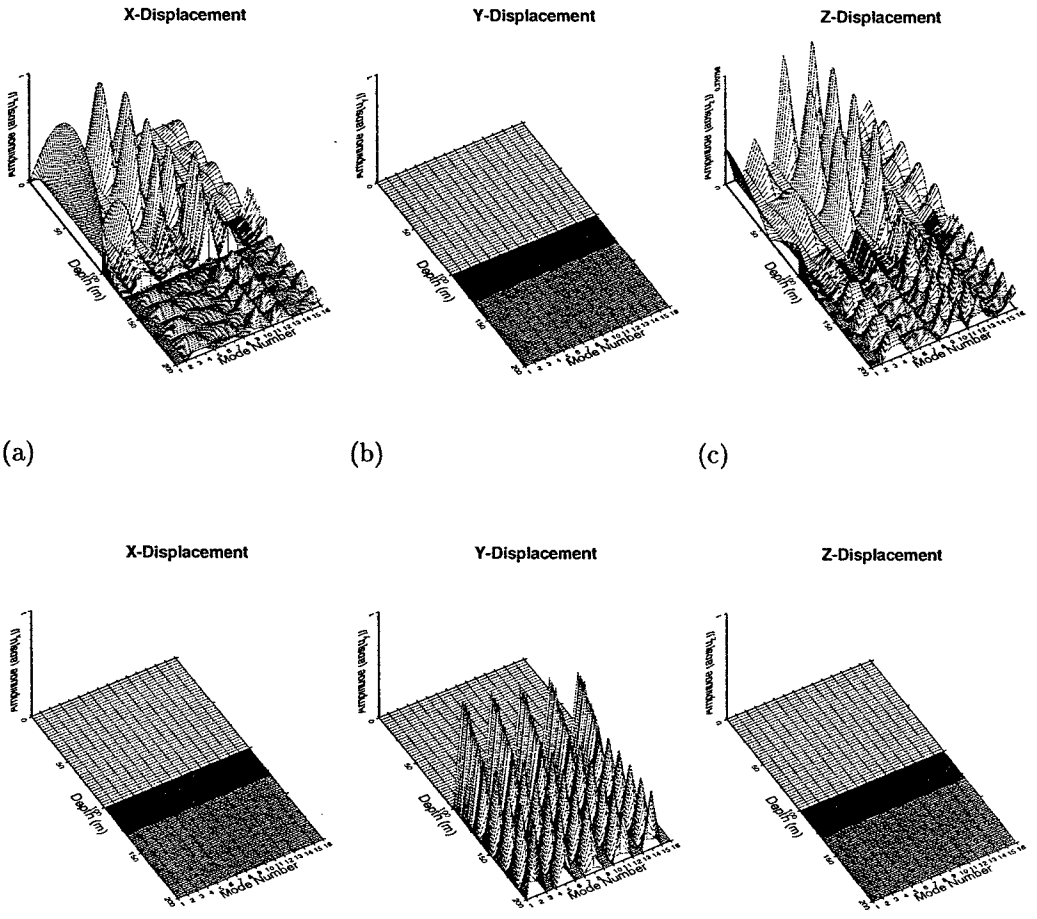

Figure 18: The figures (a), (b), and (c) show the x, y, and z displacement components for an explosive source respectively. The figures (d), (e), and (f) show the x, y, and z displacement component for a double couple source respectively. An explosive source only excites modes with particle motion in the sagittal plane. A double couple in the horizontal plane only excites modes with particle motion in the y-direction. These modes reflect a geometrical orientation of the symmetry axis $\hat{s}$ when the P-SV and SH particle motions propagate independently. The modes of this quasi-monoclinic medium are similar to modes of an isotropic or VTI medium.

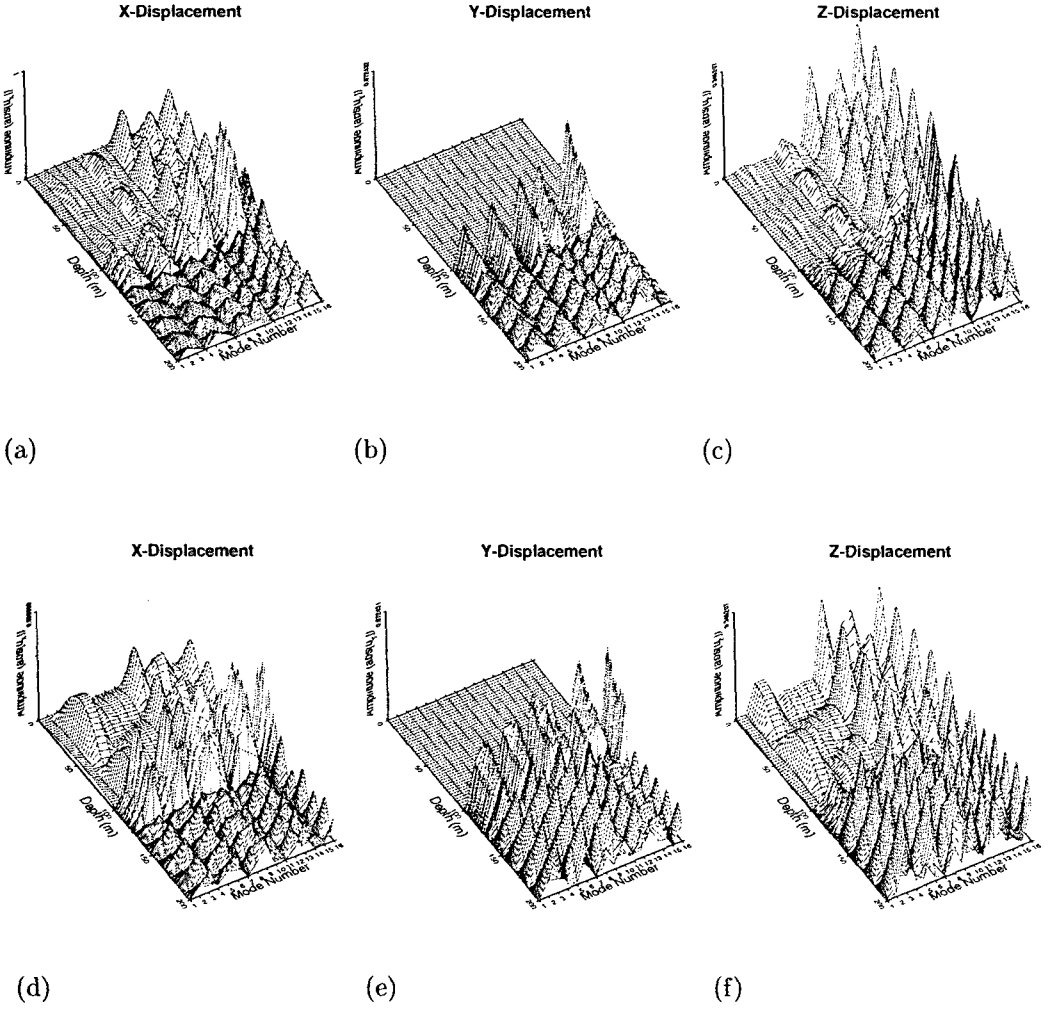

Figure 19: Both explosive and double couple sources are effective at exciting modes with 3-D particle motion. This is purely a result of the introduction of anisotropy into the sediments, which results in the coupling of the x, y, and z particle displacements. Note that the double couple source is more effective at exciting the lower order modes, than the explosive source. The figures show the displacement of all the modal eigenfunctions with phase velocities between the of 1500m/s and 2000m/s. The x, y and z-components of displacement are shown in figures (a) & (d), (b) & (e), and (c) & (f) respectively. P-SV-SH modes are clearly evident with energy in all three coordinate directions.

2–D Layered Laterally Heterogeneous Anisotropic Structure

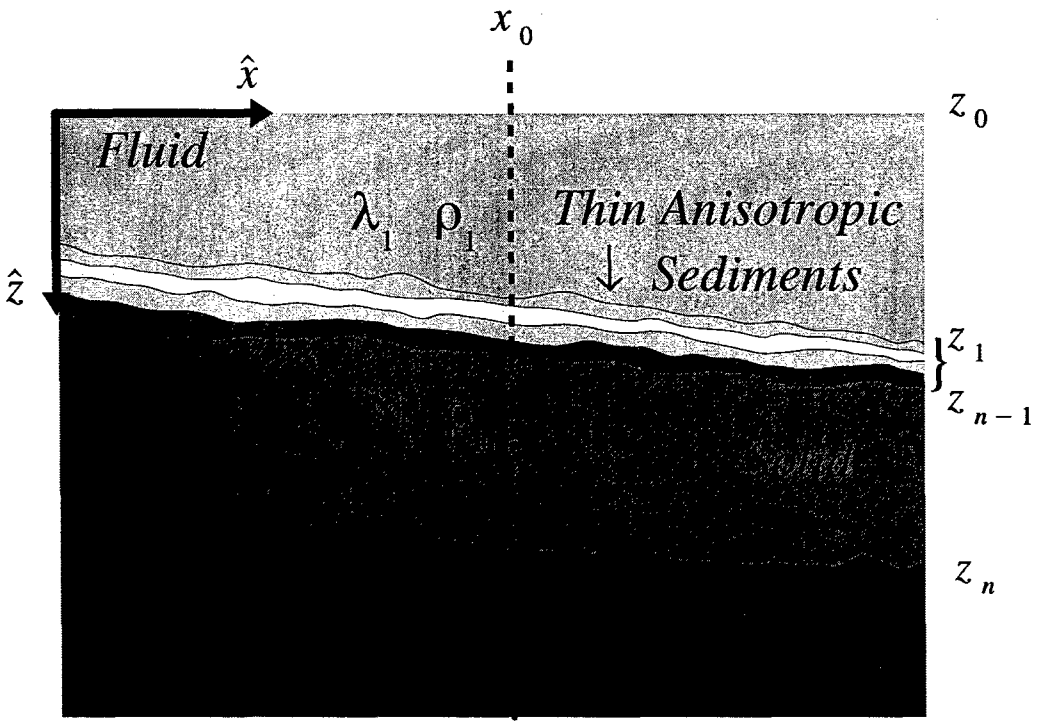

Figure 20: A 2-D laterally heterogeneous anisotropic structure. The structure contains fluid layers over thin range-dependent anisotropic and/or isotropic sediments, additional range-dependent sediments and/or basement layers, and is terminated by an isotropic halfspace. The elastic moduli may vary in both range and depth. The local equivalent of this 2-D model at x_0 is the plane-layered homogeneous anisotropic model in figure 5.

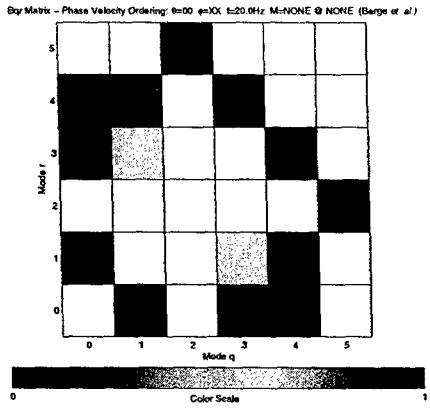

(a)

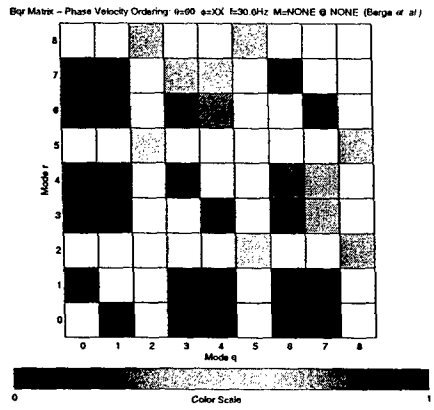

(b)

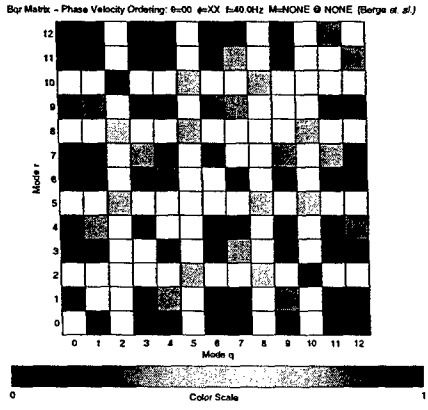

(c)

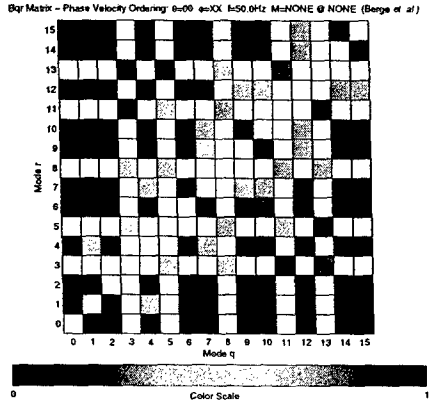

(d)

Figure 21: $\mathbf{B}_{qr}$ coupling matrices for P-SV and SH modes at 20.0Hz-50.0Hz when $\hat{s}(\theta, \varphi) = \hat{s}(0°, 0°)$. The coupling is restricted to P-SV/P-SV and SH/SH coupling. The white spaces indicate that there is no P-SV/SH coupling for this symmetry axis orientation.

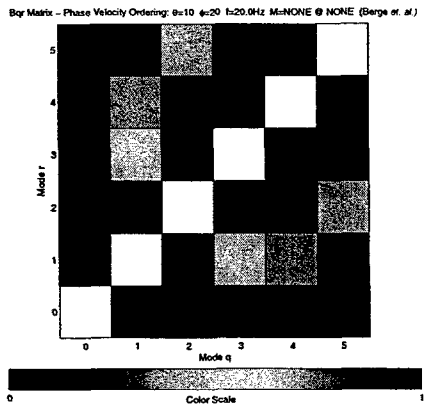

(a)

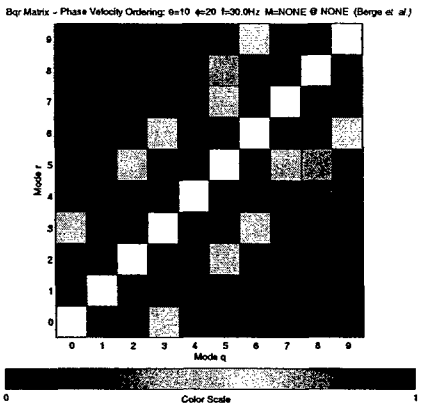

(b)

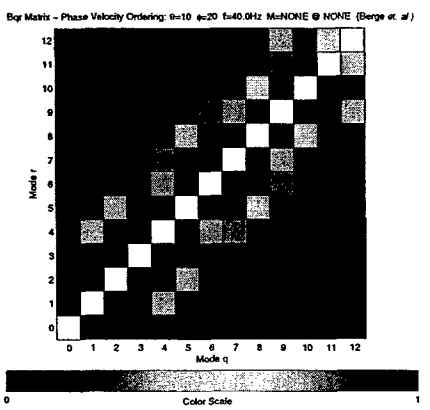

(c)

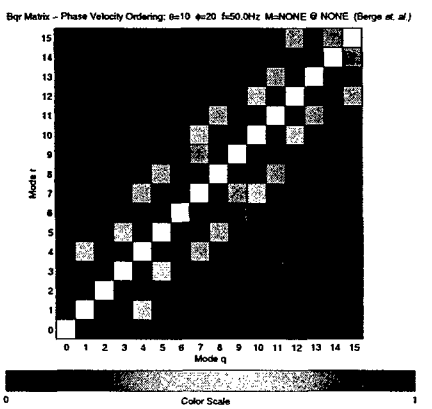

(d)

Figure 22: $\mathbf{B}_{qr}$ coupling matrices for quasi-P-SV, quasi-SH, and P-SV-SH modes at 20.0Hz-50.0Hz. Any mode may coupling into any other mode without the restrictions to the quasi-monoclinic symmetries.

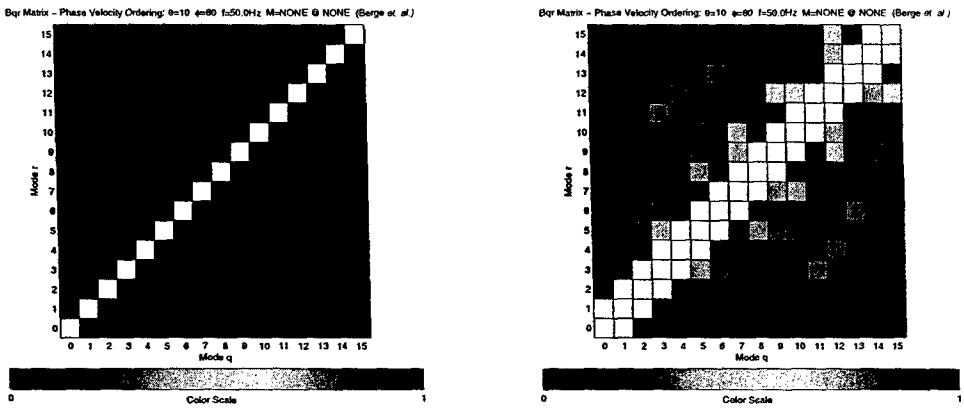

(a) (b)

Figure 23: Coupling matrices showing the effects of near degeneracy. Near a degeneracy in phase velocity, two modes may strongly couple and dominate the appearance of the coupling matrix. When the nearest-neighbor coupling terms are removed, the coupling matrix resembles those of 22

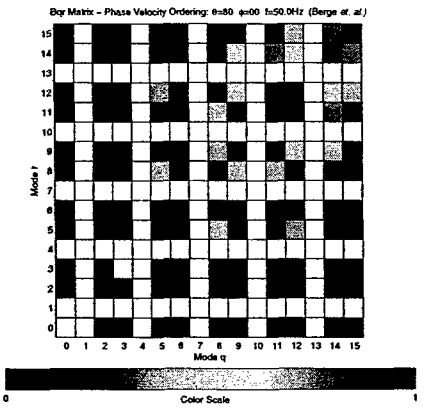

(a)

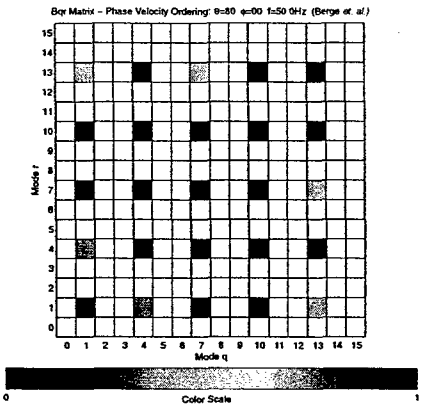

(b)

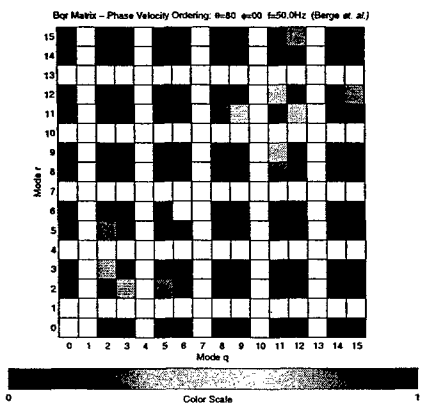

(c)

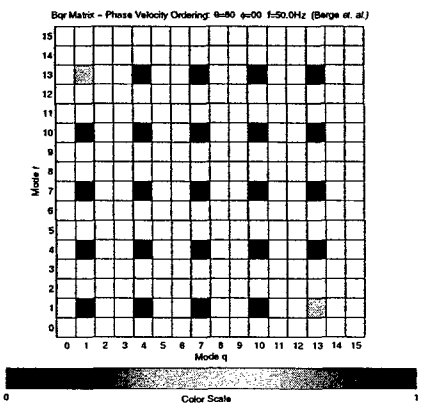

(d)

Figure 24: The excitation of P-SV and SH modes by explosive and double couple sources for $\hat{s}(\theta, \varphi) = \hat{s}(80°, 0°)$.

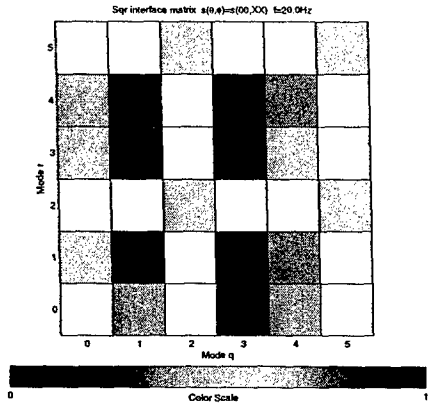

(a)

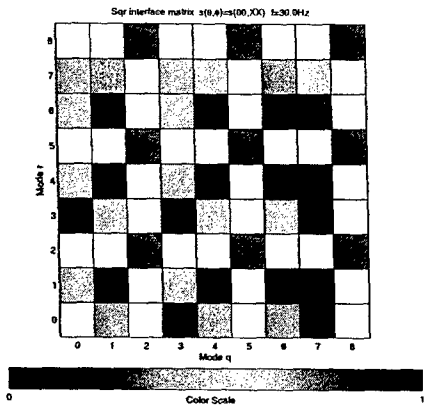

(b)

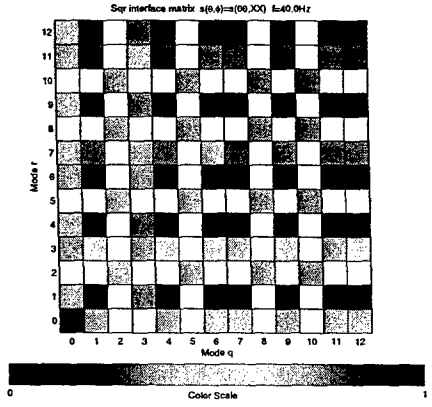

(c)

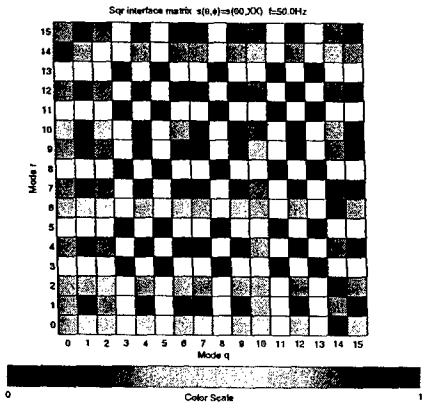

(d)

Figure 25: $\mathbf{S}_{qr}$ coupling matrices for P-SV and SH modes at 20.0Hz-50.0Hz. The rows represent modes from the primary wavefield, and the columns represent the modes from the scattered wavefield.

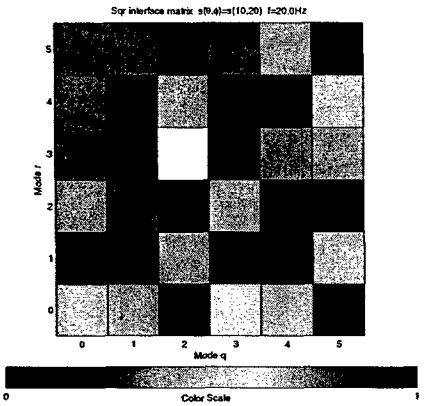

(a)

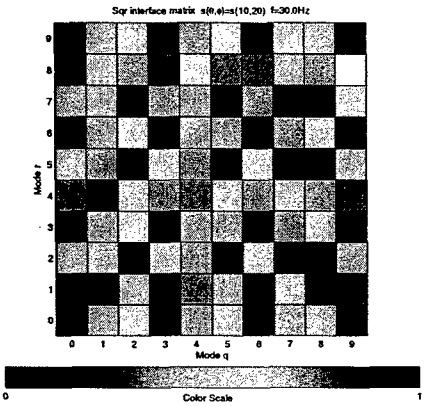

(b)

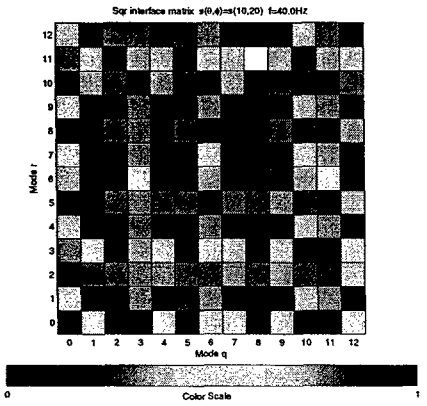

(c)

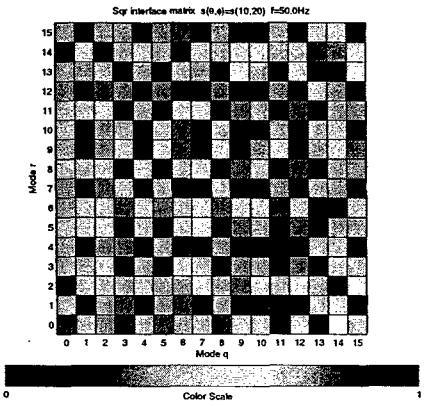

(d)

Figure 26: $\mathbf{S}_{qr}$ coupling matrices for quasi-P-SV, quasi-SH, and P-SV-SH modes at 20.0Hz-50.0Hz. The rows represent modes from the primary wavefield, and the columns represent the modes from the scattered wavefield.

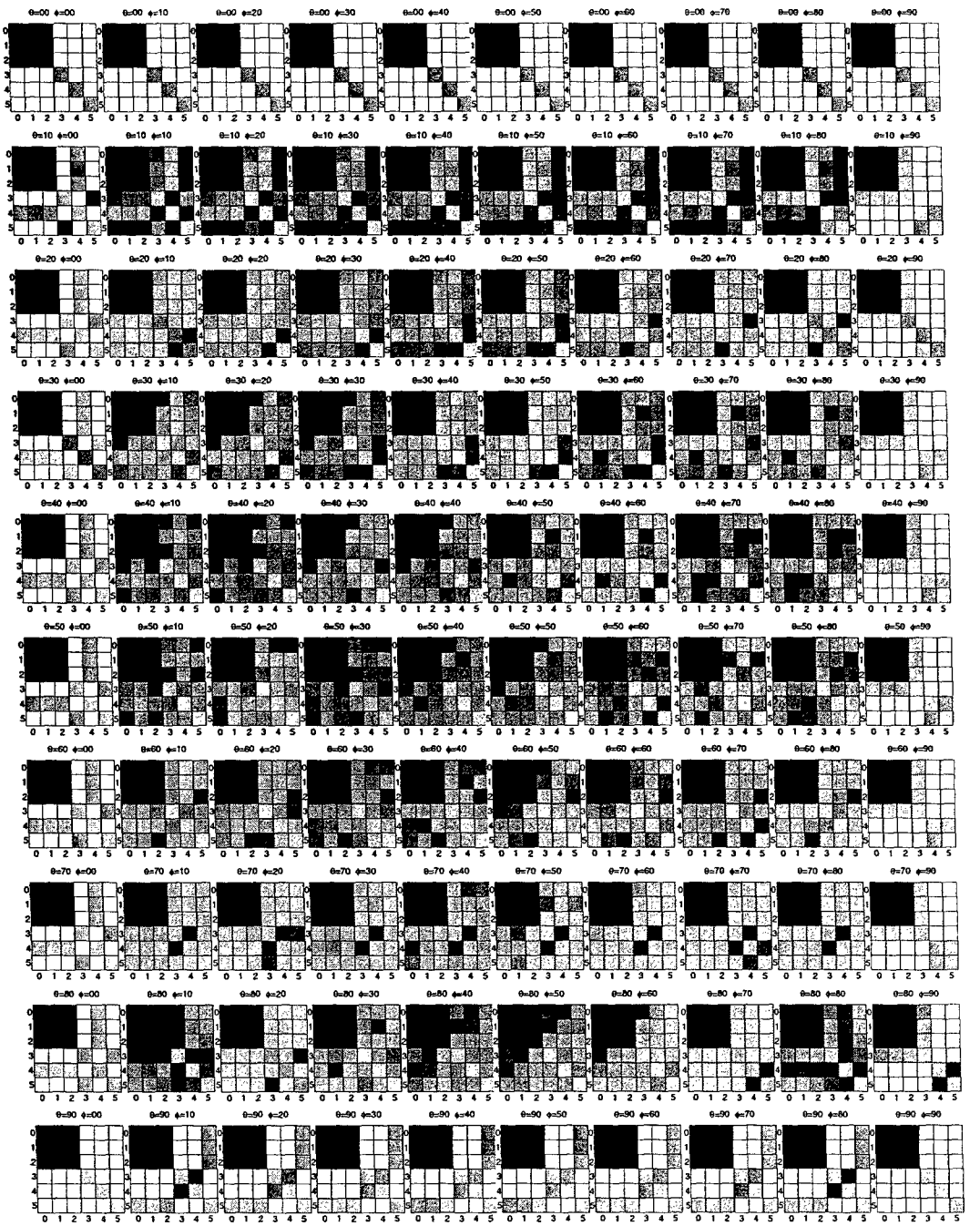

Figure 27: Each matrix in the figure represents the *form* of the elastic stiffness matrix ${}^{a}\mathbf{C}_{IJ}$ for specific orientations of the symmetry axis $\hat{s}$. The matrices graphically reveal how the elastic stiffness matrix ${}^{a}\mathbf{C}_{IJ}$ is populated as the symmetry axis is rotated. Each matrix in a horizontal row represents a 10° increments in φ for a fixed value of θ. Likewise, each matrix in a vertical column represents a 10° increment of θ for a fixed value of φ. The first row represents rotations about the y-axis, the last row represents rotations about the x-axis, and the last column represents rotations about the z-axis when $\hat{s}$ is within the xy-plane. All of the matrices on the outside edges of the figure represent the elastic stiffness matrix being rotated about a coordinate axis and have a quasi-monoclinic form. More general rotations of the symmetry axis $\hat{s}$ results in a quasi-triclinic form of ${}^{a}\mathbf{C}_{IJ}$.

List of Tables

Table 1: Mode Wavelength Ranges

Phase Velocity	10.0Hz	20.0Hz	30.0Hz	40.0Hz	50.0Hz	75.0Hz
1500.0m/s	150.00m	75.00m	50.00m	37.50m	30.0m	40.00m
2000.0m/s	200.00m	100.00m	66.67m	50.00m	40.00m	26.67m

Table 2: Velocity/Density Profile

DEPTH	$A = {}^aC_{11}$	$C = {}^aC_{33}$	$F = {}^aC_{13}$	$L = {}^aC_{44}$	$N = {}^aC_{66}$	ρ
100.00	2.250	2.2	2.2	0.0000	0.0000	1000
2.50	5.544	5.544	5.376	0.0526	0.0669	2100
2.50	5.544	5.544	5.376	0.0526	0.0683	2100
2.50	5.544	5.544	5.376	0.0526	0.0700	2100
2.50	5.544	5.544	5.376	0.0526	0.0714	2100
2.50	5.586	5.586	5.376	0.0792	0.0864	2100
2.50	5.586	5.586	5.366	0.1100	0.1100	2100
2.50	5.649	5.649	5.383	0.1330	0.1330	2100
2.50	5.754	5.754	5.438	0.1580	0.1580	2100
2.50	5.859	5.859	5.495	0.1820	0.1820	2100
2.50	5.964	5.964	5.550	0.2070	0.2070	2100
2.50	6.069	6.069	5.607	0.2310	0.2310	2100
372.50	8.400	8.400	2.798	2.8010	2.8010	2100
1000.00	70.634	70.634	23.528	23.5530	23.5530	2335

Table 3: Invariant Acoustic Modes

Frequency	Mode 1	Mode 2	Mode 3	Mode 4	Mode 5	Mode 6
10.0Hz						
20.0Hz	1560m/s					
30.0Hz	1528m/s	1637m/s				
40.0Hz	1517m/s	1577m/s	1920m/s			
50.0Hz	1511m/s	1550m/s	1626m/s	1905m/s		
75.0Hz	1506m/s	1524m/s	1556m/s	1606m/s	1679m/s	1757m/s

Table 4: P-SV and SH Particle Motion Independence

Coordinate Axes:
$\hat{s}(\theta,\varphi) = \hat{s}(90°, 0°) = \hat{x}$
$\hat{s}(\theta,\varphi) = \hat{s}(90°, 90°) = \hat{y}$
$\hat{s}(\theta,\varphi) = \hat{s}(0°, 0°) = \hat{z}$
Sagittal Plane:
$\hat{s}(\theta,\varphi) = \hat{s}(all°, 0°)$

Table 5: Symmetry Axis Orientation and Coupling

Coordinate Axes:
SH/SH
P-SV/P-SV
Arbitrarily Oriented $\hat{s}$:
quasi-P-SV/quasi-SH
quasi-P-SV/quasi-P-SV
quasi-P-SV/P-SV-SH
quasi-SH/quasi-SH
quasi-SH/P-SV-SH
P-SV-SH/P-SV-SH

Table 6: Abbreviated Subscript Notation

ik or lj	I or J
11	1
22	2
33	3
23,32	4
13,31	5
12,21	6

Table 7: Love Notation

Love Notation	Backus Notation	Takeuchi and Saito Notation	Isotropy
$A =$	$\bar{A} - \bar{B} + \bar{C}$	$\rho\alpha_H^2$	$\lambda + 2\mu$
$C =$	$\bar{A} + \bar{B} + \bar{C}$	$\rho\alpha_H^2\phi$	$\lambda + 2\mu$
$F =$	$\bar{A} - 3\bar{C} - 2(\bar{D} + \bar{E})$	$\rho\eta(\alpha_H^2 - 2\beta_V^2)$	λ
$L =$	$\bar{D} + \bar{E}$	$\rho\beta_V^2$	μ
$N =$	$\bar{D} - \bar{E}$	$\rho\beta_V^2\xi$	μ

Table 8: Takeuchi and Saito Notation

Takeuchi and Saito Notation	Love Notation	Backus Notation	Isotropy
$\alpha_H =$	$\sqrt{\frac{A}{\rho}}$	$\sqrt{\frac{\bar{A}-\bar{B}+\bar{C}}{\rho}}$	$\sqrt{\frac{\lambda+2\mu}{\rho}}$
$\beta_V =$	$\sqrt{\frac{L}{\rho}}$	$\sqrt{\frac{\bar{D}+\bar{E}}{\rho}}$	$\sqrt{\frac{\mu}{\rho}}$
$\xi =$	$\frac{N}{L}$	$\frac{\bar{D}-\bar{E}}{\bar{D}+\bar{E}}$	1
$\phi =$	$\frac{C}{A}$	$\frac{\bar{A}+\bar{B}+\bar{C}}{\bar{A}-\bar{B}+\bar{C}}$	1
$\eta =$	$\frac{F}{A-2L}$	$\frac{\bar{A}-3\bar{C}-2(\bar{D}+\bar{E}}{\bar{A}-\bar{B}+\bar{C}-\bar{D}-\bar{E}}$	1

Table 9: Backus Notation

Backus Notation	Love Notation	Takeuchi and Saito Notation	Isotropy
$\bar{A} =$	$\frac{3(A+C)+2(F+2L)}{8}$	$\frac{\alpha_H^2(3(1+\phi)+2\eta)+2\beta_V^2(1-\eta)}{8}$	$\lambda + 2\mu$
$\bar{B} =$	$\frac{4(C-A)}{2}$	$\frac{4\alpha_H^2(\phi-1)}{8}$	0
$\bar{C} =$	$\frac{A+C-2(F+2L)}{8}$	$\frac{\alpha_H^2(1+\phi-2\eta)-4\beta_V^2(1-\eta)}{8}$	0
$\bar{D} =$	$\frac{L+N}{2}$	$\rho{\beta_V}^2\left(\frac{1+\xi}{2}\right)$	μ
$\bar{E} =$	$\frac{L-N}{2}$	$\rho{\beta_V}^2\left(\frac{1-\xi}{2}\right)$	0

Table 10: Propagation Principles

Symmetry Plane Principles
propagation direction within symmetry plane:
shear motion polarized normal to symmetry plane
propagation direction normal to TI symmetry axis $\hat{s}$:
shear motion polarized parallel to TI symmetry axis $\hat{s}$
propagation direction parallel to TI symmetry axis $\hat{s}$: